THE DEVELOPMENT OF AN ARTIFICIAL HAND USING NICKEL-TITANIUM AS ACTUATORS

MAKUSUDI LONGELA SIMON

Elastic Modulus in X (75 GPa (A) 40 GPa (M))

Poisson's Ratio in XY 0.33

Initial Yield Stress (Tensile Loading)
Final Yield Stress (Tensile Loading)

Initial Yield Stress (Tensile Unloading)
Initial Yield Stress (Tensile Unloading)

~~Final Yield Stress~~
Initial Yield Stress (Compressive Loading)
Final Yield Stress (Compressive Loading)

Initial Yield Stress (Compressive Unloading)
Final Yield Stress (>> >>)

Ultimate Plastic Strain Measure (Tension)

Mass Density | 6.45 g/cm³ (A) 6.45 g/cm³ (M) Kg/m³

Thermal Expansion Coefficient in X 11.10⁻⁶ /°C (A) 6.6.10⁻⁶ /°C (M) /K

12V

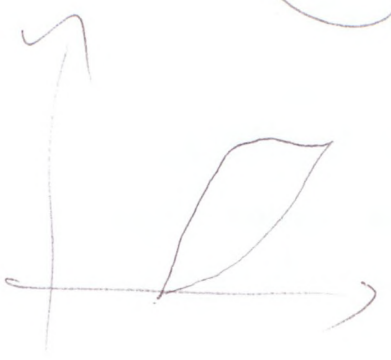

I Motivation
- State of Art
- Actuation Principle
- Hydraulics
- Polymer actuators
- Today and Future.

II SMA Fundamental Characterisation NiTi

Stress
↓↓ Force applied
Strain

III Concept & Design of The working Model

Object distortion [in percentage]
(Shrink, expanding
Stretching, twisting
Compressing)

IV Rapid Prototype and Manufacturing.

V Analysing ....

Elastic Modulus of NiTi = in X
Poissons Ratio in XY
~~Shear Modulus~~
Initial Yield Stress

INTRODUCTION AND MOTIVATION

Technical Challenges & Considerations

1. Smoothness [during Camber]
2. Type, The size, and position of wings spars in the wing.
3. Number and Location of Actuators.
4. Type and properties of wing skin materials.

Main Spar Location

↳ 1. To The A.Center.

2. Strong (Aluminum + Wood Inside) for not flexibility.
3. Actuators must be Strong enough to ~~althere~~. alter the wing shape, and To HOLD the wing shape against aerodynamic Loads. Install ~~in drive~~ inside the Wing.

Cape Peninsula
University of Technology

THE DEVELOPMENT OF AN ARTIFICIAL HAND USING NICKEL-TITANIUM AS ACTUATORS

by

MAKUSUDI LONGELA SIMON

Thesis submitted in fulfilment of the requirements for the degree

Master of Technology: Mechanical Engineering

in the Faculty of Engineering

at the Cape Peninsula University of Technology

Supervisor: Oscar Philander
Co-supervisor: Mornay Riddles

Bellville Campus
Date of submission: March 2013

DECLARATION

I, Makusudi Longela Simon, declare that the contents of this thesis represent my own unaided work, and that the thesis has not previously been submitted for academic examination towards any qualification. Furthermore, it represents my own opinions and not necessarily those of the Cape Peninsula University of Technology.

Signed

03/03 2013

Date

ABSTRACT

This thesis outlines a proposed mechanical design, prototyping and testing of a five fingered artificial hand made of 15 articulated joints actuated by Shape Memory Alloys (SMAs) mimicking muscular functions. SMAs Artificial muscles were incorporated in the forearm and artificial tendons made of nylon wires passing through a hollow palm transmit the pulling force to bend the fingers. Torsion springs set in each joint of the fingers create enough restoring force to straighten the finger when the actuators are disengaged.

Nickel-Titanium (NiTi) wires were intrinsically embedded within the hand structure allowing significant movements mimicking human hand-like gestures.

A control box made of switches connected to the artificial hand helps to control each gesture.

A modular approach was taken in the design to facilitate the manufacture and assembly processes. Nickel-Titanium wires were used as actuators to perform the artificial muscle functions by changing their crystallographic structures due to Joule's heating.

Rapid prototyping techniques were employed to manufacture the hand in ABS plastic.

Keywords: Shape Memory Alloys, Shape Memory Effect, Actuator, Nickel-Titanium

ACKNOWLEDGEMENTS

I wish to thank:

- My God, Jehovah Jireh, source of all intelligence and knowledge.
- Dr Oscar Philander, my supervisor, for letting me work under the auspices of his notoriety, I mean, prestige. He introduced to me this exciting research environment free of boundaries. He not only introduced a high level of technology of Adaptronics, but he also monitored the progress of my research regularly, reminding me each time to "think out of the box and be crazy in your imagination".
- Mr Mornay Riddles, my co-supervisor, without whose generous help, interest, and resources, I could have never done this research.
- Georgia P. Longela, my dear wife, for the colours of happiness she brings to my life.
- Yvonne S., my mother, for her constant prayers.
- Cathy L., my sister, for her unremitting encouragements.
- The AMTL members: Matshoba L., Sam M., Michael P., Nsenda P., André D., Majiet M., Nanga M., Cyprian O., Nebese F. and Lorenzo B., for their support and encouragements.
- A special thank to Humphreys S, Bannister H and Michael S who preceded investigating on artificial fingers at the Cape Peninsula University of Technology.

The financial assistance of the Adaptronics Advanced Manufacturing Technology Laboratory (AMTL) and the Cape Peninsula University of Technology (CPUT) towards this research is acknowledged.

TABLE OF CONTENTS

Chapter One

Introduction

In this chapter, the motivation, objectives and work conducted with similar prosthetic models will be discussed. Four previously manufactured prosthetic hands will be discussed and disadvantages will be delineated. Other actuators considered for potential actuation will be compared to human muscle capabilities, and the process of elimination of these actuators will be discussed. Finally, an overview of all the chapters will be presented.

This thesis presents the development of a prototype of an articulated artificial hand using Nickel-Titanium wires as actuators to best mimic the movement of a human hand.

1.1 Motivation

Humans are social beings by nature and being part of a group is immensely important to most. The psychological and physical trauma caused by the loss of a human limb can severely affect the quality of life of a person who has had a limb removed by amputation rendering even the most basic of tasks very difficult. A prosthetic device can be of great benefit to the amputee in the performance of everyday human tasks and thus makes it easier for them to fit into a specific group by being able to do what others do and appear to look the same. This poses an important challenge for the engineering discipline and designers specifically with the prosthetic of today.

Previous models and prosthetic devices were big and movement did not mimic the natural hand movement efficiently as seen from studies by Banks (2001). Studies into previous models also showed that movements of prosthesis were not smooth and the drive assemblies were big. The drive assembly can be defined as the device that provides power to the components of the prosthetic fingers causing displacement.

An actuator is any component that is used to generate the motion in a mechanism. All actuators use energy, usually created by the flow of fluids or electricity, and convert

this energy into mechanical motion, a motion which can be a linear, rotary or oscillatory motion. Traditional means of actuation mainly include electromagnetic motors and hydraulic/pneumatic actuators. These actuators have been utilised extensively in the previous century for applications in a variety of industries ranging from automotive, manufacturing, robotics, power plants, etc. Yet some of the novel applications, specifically in the biomedical field, require compact set-up and reduced weight; such onerous applications necessitate new components for actuation such as Shape Memory Alloys (**SMAs**), piezoelectric actuators and electro-active polymers. Actuation using these means is dependent on the properties and the behaviour of the materials under specific conditions (Lederlé, 2002:17-20). Unlike traditional actuators, these newer actuators are not available ready-made. The specific design of the application is needed and therefore these ways are very good for miniaturisation. Some of these materials, in particular the SMAs, show the change of the electric resistance along with a change in the physical shape. Therefore, by monitoring the resistance, both actuation (strain change) and sensing (resistance measurement) can be simultaneously imposed.

Due to the actuation-sensing characteristics of SMAs, this material is often referred to as a 'smart material'. When this actuation-sensing capability of a smart actuator is embedded in a structure, it becomes a 'smart structure'.

This thesis outlines a proposed mechanical design and the manufacture of an articulated artificial hand actuated by SMAs. It is proposed that the SMA wires be embedded intrinsically within the prosthetic hand structure, allowing for significant flexibility for use either as a prosthetic hand solution, or even as part of a complete lower arm prosthetic solution. A bio-mimetic approach will be applied in the design process as the artificial hand should reproduce anatomically the functioning of an actual human hand as far as mechanically possible.

1.2 Objectives

As mentioned, SMAs will be used as actuators in this project, with a thermal field generated by an electric current to activate them. The specifically selected actuator for this project will be the Nickel-Titanium alloy, which will be trained to mimic the human muscle. Other materials could have been selected for actuation, such as Piezopolymer, magnetic SMAs, and both low and high strain Piezoelectric. These materials will be discussed in the current state-of-the-art section.

The main objectives of this project were:

- to manufacture a prototype artificial hand;
- to model the shape and size according to the human hand, with movements mimicking the human hand as accurate as possible;
- to model the actuator positioning as similarly to the human anatomy as possible; and
- to mimic human fingers' uniform motion.

1.3 Study Background

Prosthetic devices have existed for centuries. Originally, prostheses were simply replacements for missing limbs, but nowadays limbs are creatively devised to assist people and animals in living extremely active lives. Vast improvements have been made possible because of improved surgical techniques, the advancement of components required to make prostheses, and intelligent creative engineering ideas.

1.3.1 Historical Timeline

Below is a timeline recounting the significant dates and developments for prostheses.

In mythology: (Britt *et al.,* 2010:1)

- Aia Paec, a Peruvian deity, was missing one of his arms.
- Tezcatlitoca, the Aztec deity of creation and revenge, was missing the right leg.
- New Hah, an Irish deity, was an 'arm amputee' with a four-fingered silver prosthesis.
- Pelops, the grandson of Zeus, killed by his father Tantalus, was to be eaten by the gods, but Demeter, the Greek goddess of agriculture, devoured Pelops' shoulder. When she realised what she had done, she brought him back to life, giving him an ivory shoulder.

In 3500 BC:

- An Indian poem, Rig-Veda, is the first recorded text about prostheses. The poem tells the tragic story of Queen Vishpla, a warrior, who lost her leg in battle. After the battle, she had an iron prosthesis made, and she was able to go back to battle.

In the 5th century BC:

- A Greek dramatist, Aristophanes, included a character with a prosthetic leg in his comedy "Birds".

In 218 BC:

- The Roman general, Marcus Sergius, lost his right arm in the Second Punic War. He received an iron prosthetic hand so that he could return to the battle field. However, because of his amputation, he was prohibited from becoming a priest.

In the 1st century BC:

- Archaeologists discovered bronze leg prosthesis. Although it was rusted, it is the oldest usable man-made prosthetic.

In 1508:

- The hands of the German knight, Gotz von Berlichingen (1480-1562), were amputated and he received two prosthetic iron hands following the battle of Landshut.

In 1529:

- An innovative French surgeon, Ambroise Pare, who served as royal surgeon for a number of French kings, introduced amputation to the medical community. He is considered to be the 'father of the prosthetics'. In 1536, he made an artificial arm and elbow and created other limbs later as well.

In 1696:

- A Dutch Surgeon, Pieter Andriannszoon Verduyn, developed the first non-locking prosthesis, forming the basis for the current joint and corset prosthesis.

In 1843:

- An English physician, James Syme, introduced conservative alternatives to major amputations. Theses amputations bore his name, as he replaced a portion of below-knee amputation which was standard practice at that time.

In 1858:

- In Capri, Italy, the oldest known copper and wood leg was discovered, dated 300 B.C.

1861-1865:

- The American Civil War was largely responsible for initiating the prosthetic field in America. It is reported that there were at least 30,000 amputations on the Union side alone.

1914-1918:

- Because the United States entered World War I late, not as many Americans suffered as did the European nations.

1939-1945:

- In contrast to the relatively low number of amputees during World War I, there were no significant prosthetic developments during and after World War II. World War II veterans found the current technology insufficient and those in the medical field recognised the need for necessary advancements.

In the 1960's:

- The development of Externally Powered Prosthetic Hands (EPPH) controlled by muscle contraction in the residual limb started in the 1950s. Later, the so-called "Heidelberg Pneumatic Arm prosthesis", (Kargov *et al.*, 2008:550) was driven by pressurised carbon dioxide stored in pressure tanks (Figure 1.1).

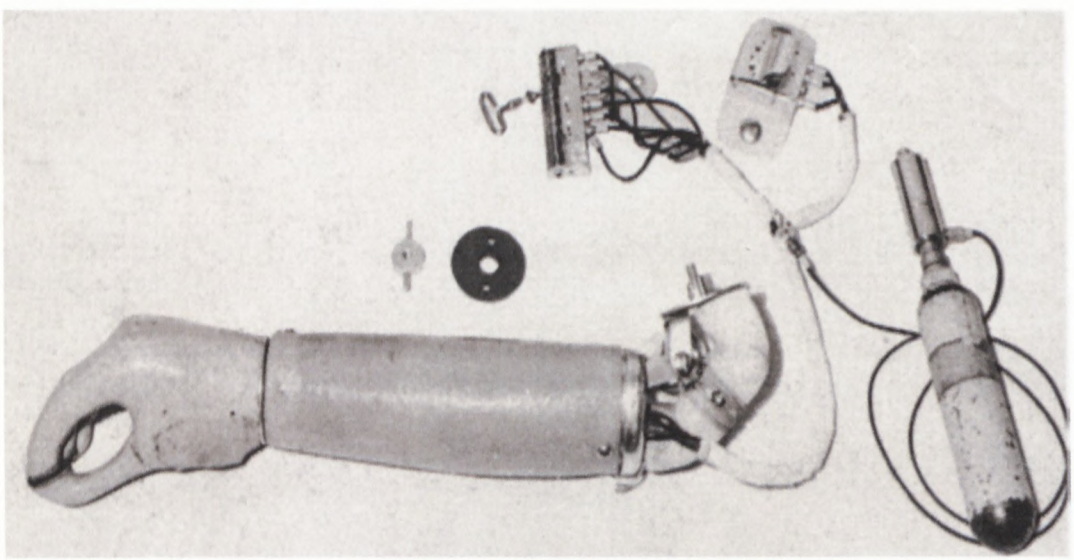

Figure 1.1: Heidelberg pneumatic arm prosthesis of 1956 (Kargov, *et al.*, 2008:550)

This prototype allowed active flexion of the elbow joint, hand rotation, and separate control of thumb and index finger. Several prototypes of hydraulically driven hands were developed in the 1970s. Concurrently, new small-sized, powerful DC motors and rechargeable batteries became available and electrically driven hands have since set a new standard. Since 1960, thousands of patients worldwide have been fitted with electrically driven prostheses. Because of their compactness, reliability, and simplicity of recharging the energy source, this actuation principle has been superior to all others when designing an EPPH that allows for a single grasping pattern.

- In the meantime, modern manufacturing technologies and materials have allowed for the development of hydraulic prosthetic hands, meeting the demands for a compact design, increased safety, increased controllability, simplicity of use, and autonomy from external mechanisms. Adaptive grasping is an additional criterion in the design of prosthetic hands (Warwick *et al.*, 2005: 1663-1668). Its implementation requires an increase in the degrees of freedom that extends the range of motion and allows for different grip types for prosthetic hands.

1.3.2 Today and Future

- Within the scientific community, there has been consideration given to using advanced prostheses to replace healthy body parts with artificial mechanisms and systems for improving function. Currently, the morality and desirability of such technologies are being debated. Limbs such as legs, arms, hands, feet, can, more readily than in the past, be replaced if desired.

  The first experiment with a healthy individual appears to be that by the British scientist Warwick (2003). In 2002, an implant was interfaced directly into Warwick's nervous system. The electrode array, containing approximately a hundred electrodes, was placed on his median nerve. The signals produced were detailed enough that a robot arm was able to mimic the actions of Warwick's own arm and provide a form of touch feedback again via the implant.

- In early 2008, Oscar Pistorius, the 'Blade Runner' of South Africa, was briefly ruled ineligible to compete in the 2008 Summer Olympics because his prosthetic limbs purportedly gave him an unfair advantage over runners who had ankles. One researcher found that Pistorius' limbs used twenty-five percent less energy than those of an able-bodied runner moving at the same speed (Warwick *et al.*, 2009:212-218).

- Currently, engineers are attempting to develop prostheses for human beings and animals that suffer from disease and damaged body parts using implants of smart materials and nanotechnology devices: MEMS (Micro-Electro-Mechanical Systems).

1.4 Related Works

In this section, works conducted in the field of prosthetics (the branch of medicine dealing with the production and implementation of artificial body parts) and robotics will be discussed. The four types of robotic hands examined will be as follows: 1) the Stanford hand, 2) the Utah dexterous hand, 3) the Hitachi robotic hand, and 4) the DLR hand. However, only the 'designs' of these respective hands will be discussed.

1.4.1 Stanford /JPL (Salisbury) Hand

This system consists of 3 degrees-of-freedom digits. Four flexible Teflon-coated steel cables, originating from a remotely situated DC servo motor assembly are connected to the joints of the three digits. The simple assembly makes manufacturing straightforward, but a lumbering drive assembly makes push/pull flexible cables limited in both reliability and power transmission (Banks, 2001:21-23).

1.4.2 Utah/MIT Dexterous Hand

Circumduction motion is defined as the rotating motion around the respective joint, and unfortunately in this model the circumduction motion of the digits is absent. Independent actuators and tension cables control each finger. The 'tendon-cables' form part of a complex cable drive system propelled by 32 specially design pneumatic glass cylinders and jet-pipe valves. Another disadvantage of this model is that the drive system degrades finger control and kinematics due to the unreliably long cables. Yet another disadvantage is the large motor apparatus (Banks, 2001:21-23).

1.4.3 Hitachi Robot Hand

This robotic hand establishes smooth joint movement and compact design with SMA actuation. Each of the three digits has four joints individually actuated and built into the forearm of the model. The pulling force of a drive wire bends the digit, and the return of the finger is accomplished by the shrinking of the drive wire against the force of a spring set into each joint. This system has a good power/weight ratio and is capable of high speeds and load capacity. However, the major disadvantage of this hand is its tendency to malfunction because of the performance deprivation after a number of performing cycles (Banks, 2001:21-23).

1.4.4 Deutches Zentrum für Luft-und Raumfahrt (DLR) Hand

Designed by the German Aerospace Centre (DLR), this hand is multi-sensorial with four digits controlled through data gloves. Linear actuators are either integrated into the palm, or the proximal finger links manipulate the finger. This hand is capable of flexion, extension, adduction and abduction. The distal joint is controlled secondarily by the inter-joint coupling. But a disadvantage of this system is the secondary control of the actual finger by the data glove (Banks, 2001:21-23).

1.5 Current State of Art

Though the selected actuator for this project's artificial hand was the SMA, other actuators were given consideration for this research project: pneumatic and hydraulic, Piezopolymer, Magnetostrictive, Magnetic SMAs and Voice Coil Transducers. The principles of these five different options for actuation will be explained, and elimination of each will be substantiated. The process of elimination was mainly due to the lack of compatibility between the actuators and the human muscle characteristics. The quantitative comparison between other actuators and the human muscle can be seen in Table 1.1 on page 11. The process of elimination of each potential actuator will be discussed in the following paragraphs.

1.5.1. Pneumatic and Hydraulic Actuators

These particular actuators were eliminated without much prolonged consideration because of the size of the equipment to be used when modified to smart structures. Smart structures require external sensors, actuators and control mechanisms. SMAs are unlike the above mentioned smart structures and have the feature of sensors, actuators and control mechanisms being part of the structure of the material itself, making it considerably smaller than conventional pneumatic and hydraulic systems. The main reasons for elimination resulted from a comparison between actuator and human hand characteristics, characteristics which included volumetric stroke work, specific stroke work and driving frequency (Lederlé, 2002:9-12).

1.5.2. Piezopolymer Actuators

An electric field applied to the piezopolymer actuator produces an elastic strain which causes an external force. The functional dependence of the strain on the applied electric field is predominantly linear but can also be non-linear. The strain produced by this particular material is rather small and generally lacks stiffness, but can be highly flexible and easily manufactured. The stress of this actuator (2 - 2.5 MPa) is quite high compared to the human muscle (0.4 - 0.5 MPa) and compares favourably,

but the actuation strain is too low compared to that of the human muscle, at 80 % – 90 % (Lederlé, 2002:9-12).

1.5.3. Magnetostrictor Actuators

When subjected to an external magnetic force, some ferromagnetic material undergoes elastic strain. A magnetic field is applied by a coil along the length of the magnetostrictive material. The compound Tb.3Dy.7Fe2, commercially known as Terfenol-D, exhibits the largest magnetostriction, producing strains up to a few tenths of 1%. These actuators can produce a large force output while only needing a relatively small power supply. Obtaining optimum performance from this actuator requires a stress to be applied to the magnetostrictor prior to actuation. Again the actuation strain (0.1% - 0.2 %) is too small compared to the actual capability of the human muscle. The actuation strain, the volumetric stroke work and the specific stroke work are lower numerical values compared to the human muscle driving frequency (Lederlé, 2002:9-12).

1.5.4. Voice Coil Transducer Actuators

The resistivity of the wire used for winding the solenoid's armature determines the DC resistance of the solenoid. The positioning of the windings and materials used to construct the actuator contribute to the inductance of the solenoid. Because the solenoid is resistive, any current through the windings produces heat, and excessive heat may damage the actuator *and* consume unnecessary power. This actuator has low actuation strain, volumetric stroke work output and driven frequency (Lederlé, 2002:9-12).

1.5.5. Magnetic Shape Memory Alloys Actuators

A magnetic field induced strain is exerted on an SMA. The discovery of this actuator started with a single crystal of Ni_2MnGa (Di-Nickel-Manganese-Gallium) showing a strain of 0.2%. The new material, a single crystal of NiMnGa (Nickel-Manganese-Gallium), produced an incredible 5% sheer strain at room temperature. The magnetic SMA is capable of giving high strains, but this alloy is actuated by heating or cooling, which is a relatively slow and inefficient process that produces little work. The disadvantage of this actuator is that the actuation strain (5% - 6%) is small compared to the human muscle value. The only characteristic comparison that is not too small is the power output per unit volume. The remainder of the characteristics is too small, including actuation stress and strain, volumetric stroke work, specific stroke, work output and driving frequency (Lederlé, 2002:9-12).

1.6 Active Material Selection

Active materials are a class of materials that can be deformed upon the application of a control signal, which may be a good alternative to traditional actuators such as pumps and motors for some shape-deformation applications. Indeed, they are more space-efficient and can lead to low weight actuation systems. A benefit they also offer is a simplification of the actuation system, as they can be embedded in structures.

It is possible to split active materials in different categories with respect to the actuating principle involved in driving them. Most active materials are activated by one or three types of fields:

1. *Electric field:* electrostrictive and piezoelectric ceramics and polymers (PZT, PZNPT) are driven by a voltage applied to the samples, and/or can provide a voltage when they are deformed;
2. *Magnetic field:* magnetostrictive materials and magnetic SMAs are driven by a magnetic field, allowing for non-contact actuation. However, they have the major drawback of occasionally requiring massive coils to perform the control; and,
3. *Thermal field:* SMAs are actuated by a change in temperature with speed depending on the dimension (length, thickness or diameter). Nickel-Titanium alloy, a compound of Nickel and Titanium plus minority species, is the most widespread of such alloy. Heating is often achieved by Joule's effect (resistive), that is, by passing an electric current [0-10A] through the wires; cooling is a more subtle issue that will be addressed later in this project.

1.6.1. Choice of Nickel-Titanium as Actuators

Lederlé (2002) compared the different performances of active materials, summarised in Table 1.1. This table presents the comparison of the characteristics of different actuation systems. For the purpose of this project, SMAs are suitable active materials to provide work due to their better actuation stress and work output per unit volume. Such alloys are indeed known for their ability to provide large strain and stress.

In the present project, certain advantages shown by this comparison led to the selection of Nickel-Titanium wires as actuators. It was expected that SMAs would simplify the design of the actuation system by requiring less amplification.

Table 1.1: Comparison of different performances of active materials (Lederlé, 2002:17)

Actuator	Stress (MPa)	Strain (%)	Efficiency (%)	Bandwidth (Hz)	Work (J/cm^3)	Power (W/cm^3)
SMAs	200	10	3	3	10	30
Human muscle	0.35	20	30	10	0.035	0.35
Hydraulic	20	50	80	4	5	20
Pneumatic	0.7	50	90	20	0.175	3.5
Piezoceramic	35	0.2	50	5000	0.035	175
Single crystal piezoelectric	300	1.7	90	5800	2.55	15000

For the same work output, much less mass of material is required to perform the actuation. Only hydraulic systems are expected to be better with respect to this metric. However, the use of pumps and tubes and such is expected to complicate the implementation of hydraulic systems as compared to SMAs.

An important point appears in the Table 1.1 above. Active materials undeniably have both benefits and drawbacks. For instance, SMAs are able to provide much more work, yet they cannot be actuated at high frequency, so they can only be expected to provide little power as compared to piezoelectric ceramics. Therefore, the field of active materials would benefit from materials research (and characterisation efforts) in order to search for even better performing materials. Such a high performance material is presented here--the single crystal piezoelectric--although the cost of such material is likely to be high. Another issue to consider in the selection of actuation technology is its maturity. Active materials have not been widely adopted in commercial applications due to their relatively low technical maturity.

As a result of such comparisons, SMAs were selected to perform the required actuation for this research. Issues related to this choice are the main points addressed by this project, and arguably lead to the main contribution.

Listed below, are alloys of metals having the memory effect at different temperatures and at different percentages of their solid solution contents.

- Ag-Cd (44/49 weight at % Cd);
- Au-Cd (46.5/50 weight at % Cd);
- Cu-Al-Ni (14/14.5 weight % Al and 3/4.5 % Ni);

- Cu-Sn (~15% Sn);
- Cu-Zn (38.5/41.5 weight at % Zn);
- Cu-Zn-X (X = Si, Al, Sn);
- Fe-Pt (~25% Pt);
- Mn-Cu (5/35 at % Cu);
- Fe-Mn-Si;
- Pt alloys;
- Co-Ni-Al;
- Co-Ni-Ga;
- Ni-Fe-Ga;
- Ti-Pd (in various concentrations);
- Ni-Ti (~55% Ni);
- Ni-Ti-Nb;
- Ni-Mn-Ga.

After selecting SMAs as the active material, it was necessary to select the appropriate alloy to perform efficient actuation of an artificial hand. The properties of SMAs depend on and are very sensitive to the concentration of different compounds inside the alloy. Hence, the most common practice is to consider only a limited number of compounds, thus limiting the variety of performances offered.

Some major characteristics are presented in performance charts by Lederlé (2002), in a way that can be compared to selection charts for engineering materials. With respect to such metrics as output volumetric work per unit of mass, resistive heating capacity, and characteristic variations with cycling, Nickel-Titanium (Ni-Ti) has been identified as the most suitable of the SMAs, while there is only a slight difference in cost.

In summary, the choice of Nickel-Titanium as actuators for this work is based on:

• Tight places utilisation– Nickel-Titanium actuator wires are smaller by far than alternatives. At least 1000 times smaller than solenoids for the same work done.

• Design simplification– Nickel-Titanium actuator wires can often be used "as is", eliminating gearboxes, housings, bearings, and so on. Their flexible forgiving performance is easier to work with.

• In corrosive environments– Nickel-Titanium actuator wires' high corrosion resistance really pays off.

• For noise levels reduction– Nickel-Titanium actuator wires' movement by molecular restructuring is acoustically quiet.

• Lower costs – Nickel-Titanium actuator wires are inexpensive and cost less to use in many applications[1].

• Actuation longevity: Nickel-Titanium actuator wires will permanently stretch out or strain with large cycles strokes and high stresses. At stresses below 103MPa, permanent strain will remain less than 0.5% strain even after hundreds of thousands of cycles. At 138MPa, 1% permanent strain will occur after 100,000 cycles, and with higher stresses proportionally more will occur.

These above listed facts justify the choice of Nickel-Titanium actuators.

1.7 Scope

Chapter Two examines the characteristics of SMAs, the purpose of which is to fully understand, both on microscopic and macroscopic levels, the special characteristics of SMAs. In fact, SMAs are compared to Stainless Steel, traditionally used in prosthetic devices, to show the performance of SMAs in the application.

Chapter Three describes the investigation into the anatomy of the human hand. This chapter includes investigation into the bones, muscle, tendons and movement of the human hand. A comprehensive study of the human hand was required as a basis for the model for the prototype. This chapter also investigates the thermo-electro-mechanical analysis of the Nickel-Titanium actuators.

Chapter Four introduces the concept formation of the prosthetic hand, the prototype of which was formed based on the anatomy of a human hand. The 3D Fused Deposition Modelling (FDM) process was used to manufacture, a process which will be discussed in detail in this chapter. Assembly and gesture testing of the prototype will be discussed as well.

Chapter Five presents conclusions drawn from the research and suggested recommendations for further work.

([1]):http://www.dynalloy.com/PriceGuide.php [Downloaded on March 15th, 2010]

Chapter Two

Fundamental Characterisation of Nickel-Titanium Shape Memory Alloys

2.1 Introduction

A background on SMAs will start this chapter and two special characteristics--Shape Memory Effect and Pseudo-elastic Effect--will be discussed. The two temperature dependant phases along with their crystal structures will be described. The thermo-mechanical properties of SMAs will be analysed to form a basic understanding of the thermodynamic constitutive model of this alloy.

2.2 Background of SMAs

In order to use the Nickel-Titanium as an actuator for the application of the artificial hand, a complete understanding of the behaviour of the alloy must be established. SMAs are comprised of two metallurgical phases: Martensite and Austenite (Lagoudas *et al.,* 2003:8). The Austenitic phase is a high-temperature phase and Martensite a low-temperature phase. The Martensitic phase can be in one of two forms: twinned (atoms are set in parallel configuration) and de-twinned (atoms are set in parallel but slanted position). The transformation between these phases can occur upon heating or cooling and temperature induction can occur with or without loading (Lagoudas *et al.*, 2003:8). The two phases of SMAs can be seen in Figure 2.1.

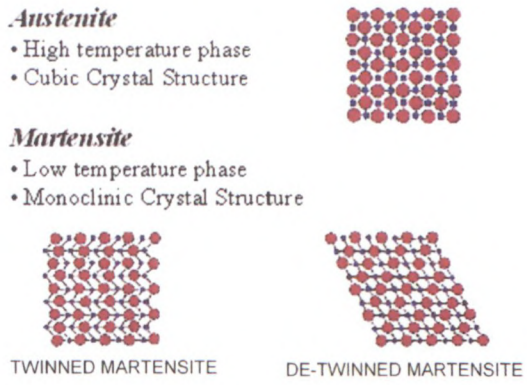

Figure 2.1: Two phases of SMAs (Lagoudas *et al.*, 2003:8)

SMAs have the remarkable property of forward and reverse thermo-elastic Martensitic transformation. When cooled to the critical temperature, the SMA will mainly consist of Martensite and can easily be manipulated to produce very large strain. When heated above a critical temperature, the alloy will revert to Austenitic phase, hence the previous elastic strain recovers and the alloy resumes the shape it normally has at high temperatures: this is the Shape Memory Effect (SME). At high temperature, the applied stress may cause Martensitic transformation and the SMA may deform somewhat 'plastically', both of which changes may be recovered as the applied stress is removed. These two phases can be obtained from temperature-induced or stress-induced transformation. Both of these two unique characteristics--the Shape Memory Effect and the Pseudo-elastic Effect—are exhibited in Figure 2.2.

2.3 General Characteristics of SMAs

SMAs are highly adaptive, compact, lightweight and have high force-to-weight ratios. Cost and size requirements are low while reliability is high. Another advantage of this alloy is that it is biocompatible and transparent to magnetic resonance tomography, making it extremely useful in the medical field (Thompson, 2000:303).

2.4 Special Characteristics of SMAs

The Shape Memory Effect refers to the alloy's ability to be mechanically deformed (seemingly permanently) at a temperature below a certain transition temperature. The material will then return to its original shape when heated above the transition temperature (Shaw, 1997:25). This characteristic will be used in the application of the artificial hand.

Pseudo-Elasticity refers to the material's ability to be strained significantly and yet return to its unstrained state when the load is removed (Shaw, 1997:25).

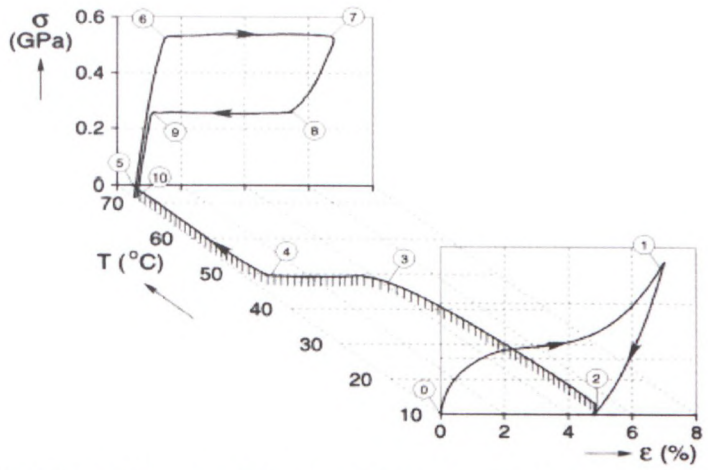

Figure 2.2: The Shape Memory Effect and Pseudo-elastic characteristics of SMAs (Shaw, 1997:25)

2.5 SMAs vs. Stainless Steel

In suggesting that SMAs could be used or replace conventional stainless steel actuators in the medical field of prosthetics, the mechanical characteristics of both metal and alloy need to be explored. Therefore, in the following subsections, the mechanical properties of SMAs and stainless steel will be compared.

2.5.1 Slip/Dislocation

As defined in the section of the background of SMAs, the super-elasticity (pseudo-elasticity) characteristic refers to the ability of Nickel-Titanium to return to its original shape after the applied load has been removed and substantial deformation has occurred (Schuerch, 1968:8-9). Most metals, including stainless steel, can be deformed, but slip or dislocation may occur and the metal does not return to its original shape. Stainless steel has an elastically recovered strain (linear portion) lower than 0.5%. Once the elastic limit is exceeded, the material yields (dislocates) and considerable increase in strain is achieved. During the increase in strain, the metal appears to flow like a viscous liquid and is called 'plastic deformation'. The material then acquires a permanent set that cannot be recovered after the stress is released. Nickel-Titanium responds to stress by simply changing the orientation of its crystal structure through the movement of twin boundaries. This process can be seen in Figure 2.3.

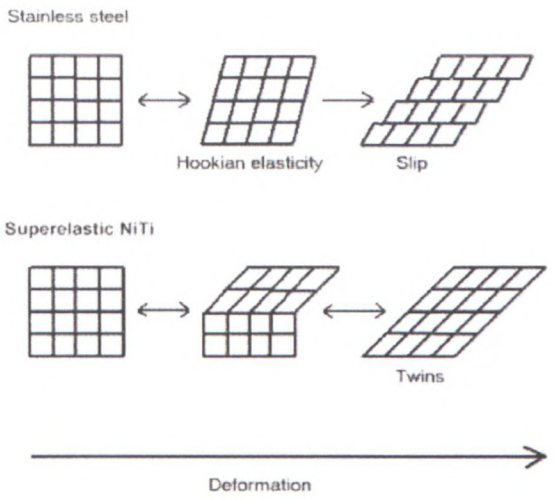

Figure 2.3: Schematic presentation of lattice structure changes caused by outer stress in stainless steel and Nickel-Titanium (Shaw, 1997:2)

Figure 2.3 shows the schematic presentation of lattice structure changes caused by outer stress in stainless steel or super-elastic Nickel-Titanium alloy. In stainless steel, outer stress first causes *reversible* changes in the elastic area (following Hook's Law of Elasticity). In the plastic area, deformation takes place through a mechanism called 'slip'. This deformation is *irreversible*. In super-elastic Nickel-Titanium alloy, outer stress causes a twinning type of accommodation which is recovered when outer stress is removed.

2.5.2 Flexibility

The flexibility of Nickel-Titanium is 10-20 times greater than that of stainless steel and can absorb strains as high as 11% (Shaw, 1997:18).

2.5.3 Wear Resistance

This characteristic is one of the most important to consider with regard to implants and prosthetics. Under abrasive conditions, the elastic limit is not exceeded and the alloy shows no damage to itself and no wear loss is experienced in the case of SMAs. For stainless steel, however, plastic strain is generated during the wear process as a result of the small elastic strain. When the plastic strain accumulates and the material reaches the critical strain for fracture, it will break. During a comparative study between the Cobalt-Chromium-Molybdenum alloys [Co-Cr-Mo], a component of hip joints, scratch-like damage is evident after two million loading-unloading cycles. The SMAs did not reveal any damage even after two million cycles (Shaw, 1997:18).

2.5.4 Mechanical Scratch Resistance

Tests conducted by Shaw (1997) with a ceramic stylus on electro-polished Nickel-Titanium showed superior healing ability compared to stainless steel.

2.5.5 Corrosion

Corrosion behaviour under stress tests showed that stainless steel loaded even within the elastic limits, resulted in an enhanced ion release (Shaw, 1997:18).

2.5.6 Mechanical Requirements for the Design Criterion

Generally there are two basic mechanical demands for material and design of mechanisms: 1) service stresses must be safely under the yield strength of the material, and 2) in the cyclic loading of the device, the service stress must be kept below the fatigue limit.

2.6 Setting the Shape Memory Properties

The use of the one-way shape memory or super-elastic property of Nickel-Titanium for a specific application requires a piece of Nickel-Titanium to be moulded into the desired shape. The characteristic heat treatment is then done to set the specimen to its final shape. The heat treatment methods used to set shapes in both the shape memory and the super-elastic forms of Nickel-Titanium are similar. Adequate heat treatment parameters (temperature and suitable time) are needed to set the shape and the properties of the item (Zhang *et al.*, 1987:353-362). The heat parameters must usually be determined experimentally for the requirements of each desired part. Rapid cooling of some kind is preferred, such as water quenching or rapid air cooling.

The two-way shape memory training procedure can be made by Shape Memory Effect training or SIM training (Stress Induced Martensite). In SME training, the specimen is cooled below Mf and bent to the desired shape. It is then heated to a temperature above the austenite finish temperature (A_f) and allowed freely to take its Austenite shape. The procedure is repeated 20-30 times, which completes the training. The sample now assumes its programmed shape upon cooling under M_f and to another shape when heated above A_f.

In SIM training, the specimen is bent just above the martensite start temperature (M_s) to produce the preferred variants of stress-induced martensite and then cooled below the martensite finish temperature (M_f). Upon subsequent heating above the A_f

temperature, the specimen takes its original austenitic shape. This procedure is repeated 20-30 times.

2.7 Training of Artificial Muscles

The training of artificial muscles of Nickel-Titanium wires used for this research conducted at the Adaptronics Advanced Manufacturing Technology Laboratory was aimed at obtaining SMA artificial muscles capable of contracting into spring coiled-shape by the application of heat and expansion after cooling. Equipment required: Electric oven (Figure 2.4), water boiler (kettle), water recipient (5 litre bucket) and a threaded steel bolt [Ø: 18mm] (see Figure 2.15).

Figure 2.4: Electric oven

The oven was set at ±400°C, which is the Curie point of Nickel-Titanium (Shaw, 1997:25).

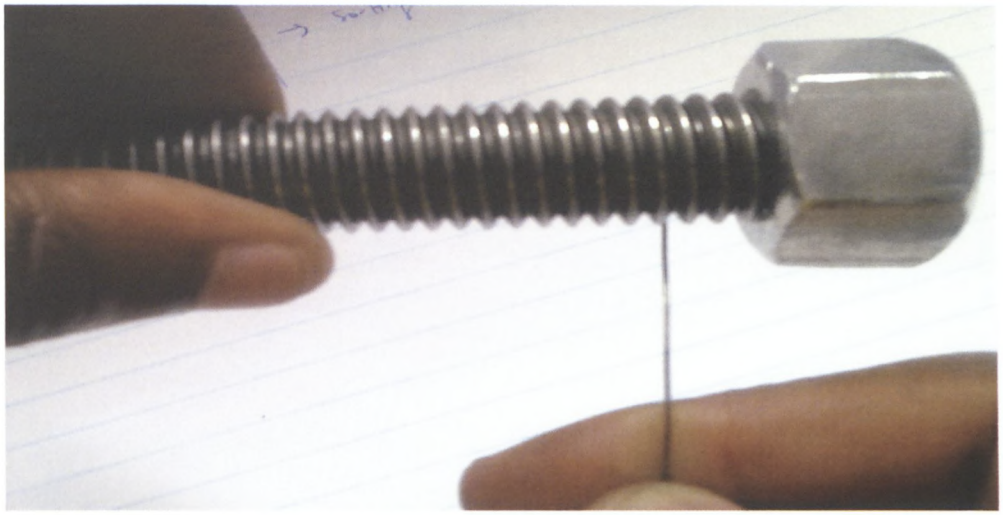

Figure 2.5: Wrapping the SMA wire around the threads of a bolt (Ø: 18mm)

The experiment consisted of the training of a straight Nickel-Titanium wire to remember a spring-coiled shape. The Nickel-Titanium wire had been wrapped around an Ø: 18mm bolt, clamped at each end (see Figure 2.5), and placed into the electric oven for 5 minutes, then suddenly removed from the oven and quenched in fresh water for three times consecutively.
Shaw (1997) suggested that when heated close to its Curie point of 400°C for 5 to 10 minutes, Nickel-Titanium wired is annealed to shape set.

If the trained specimen is deformed and heated again, the thermal motion causes the atoms to form the Austenite lattice, thus restoring the trained shape of the specimen.

Figure 2.6: Straightening a trained Nickel-Titanium wire before immersion in hot water

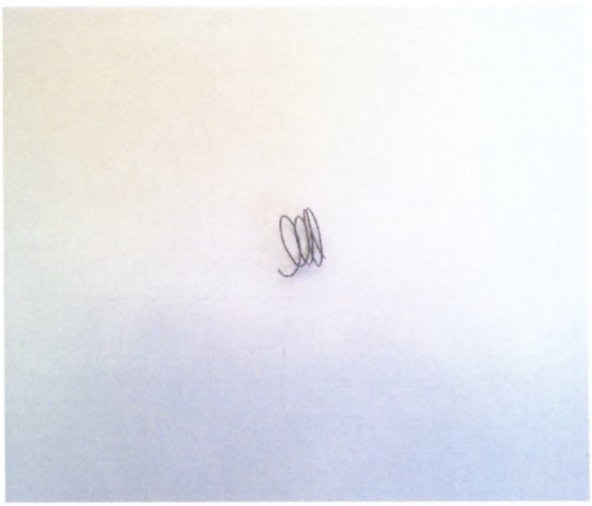

Figure 2.7: Helical shape recovery of trained Nickel-Titanium

After quenching in cool water, the specimen is straightened, and then immersed into hot water to verify its shape recovery memory. The annealing and quenching temperatures, as well as other properties, depend strongly on the alloy composition and additives used. Total shape memory recovery was observed; the wire returns *completely* into the helical spring shape (Figure 2.7).

2.8 Summary

In this chapter, special characteristics of SMAs have been discussed, with a depiction of the artificial muscle of Nickel-Titanium appointed as the actuator to develop the artificial hand. A comparison of SMAs and stainless steel was presented as well as the training of Nickel-Titanium wire to a helical spring shape.

This unique characteristic of SMAs to distort and regain their original shape will be exploited in actuating the fingers in an artificial hand. The following chapter will investigate the anatomy of the human hand and explain how this will be applied in the conceptualisation and manufacture of the artificial hand.

Chapter Three

Conceptual Design of the Working Model

3.1 Introduction

The purpose of this section is to propose a set of design variables, corresponding to the different functions of the proposed artificial hand. After identifying the variables; power, response time, and temperature range; they will be set within the constraints at the actuation of the fingers in the artificial hand.

The model is partitioned into four basic modules: 1) the mechanical, 2) the electrical, 3) the thermal, and finally, 4) the motion control unit. Each module ensures a function in the design process as shown in Figure 3.1 below:

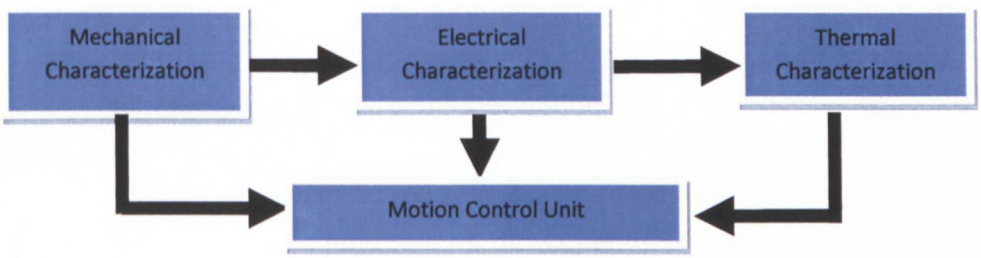

Figure 3.1: Schematic representation of the working model

1. **The mechanical characterisation** accesses the design and the performance of the actuator from a strictly mechanical point of view (force generated and movement obtained).
2. **The electrical characterisation** computes the resistance of the wires, the maximum current intensity that is allowed through those wires with respect to the available power.
3. **The thermal characterisation** is used to estimate the response time of actuation. This module identifies the transfer function between the heat source and the

resulting phase transformation and also captures the relation between the dimension of the wires and their heating and cooling times.

4. **The motion control unit** is constructed of a set of switches that control the actuation of fingers following an actuation logic algorithm.

3.2 Anatomy of a Human Hand

An understanding of the skeletal and joint structures of the human hand is a starting point for the development of an artificial hand.

A study of a human hand undergirds the design of the entire prosthetic hand as the human hand consists of a complex muscle structure, bones, joints and tendons. The muscle distribution, movement and composition of fingers will thus form the basis for the design and manufacture of the prosthetic hand.

3.2.1 Bones of Fingers

Each finger consists of two sets of bones: the Phalangeal and the Metacarpal bones. The Phalangeal bones are the Proximal Phalangeal, Middle Phalangeal and Distal Phalangeal bones, and the Index Metacarpal connects the finger to the wrist. The Proximal and Middle Phalangeal bones are concave (curved inward) and considered long bones. The Distal Phalangeal bone is concave on the dorsal (the back of the hand) side of the hand. The front and ends of all bones are known as heads and bases. The configuration of the bones can be seen in Figure 3.2 (Banks, 2001:26).

3.2.2 Joints of Fingers

The three joints of each finger are the Metacarpal Phalangeal (MCP) joint, Proximal Phalangeal (PIP) joint and Distal Phalangeal (DIP) joints (see Figure 3.2 on page 24).

3.2.2.1 Metacarpal Phalangeal Joint (MCP)

This joint is rounded at the protruded surface of the bone and has 2 degrees-of-freedom, meaning it can move in two distinct directions (up and down and side to side).

3.2.2.2 Proximal Phalangeal Joint (PIP)

This joint is hinged and has 1 degree-of-freedom (up and down).

3.2.2.3 Distal Phalangeal Joint (DIP)

This joint is hinged and has 1 degree-of-freedom (up and down).

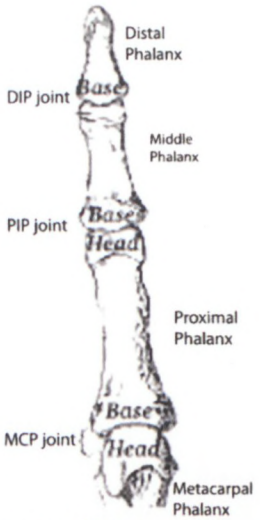

Figure 3.2: Joints and bones of the index finger - palmer view (Banks, 2001:26)

3.2.3 Tendons/Ligaments

Each finger is tightly bound by connecting tissue called tendons or ligaments. Tendons can be defined as an inelastic cord or band of tough white fibrous connecting tissue and can either be lateral (side of the finger) or anterior (palmer side of the digit).

3.2.3.1 Lateral Ligaments

These ligaments are tightly connected to each phalange bone and unite loosely at the MCP joint and more tightly at the interphalangeal joints. These tendons are strong rounded cords placed on each side of the joint (Banks, 2001:29).

3.2.3.2 Anterior Ligaments

The anterior ligaments are thick structures on the palmer side of the joint placed between the lateral ligaments. A groove in the anterior ligament is present for the passing of the flexor tendon. Figure 3.3 shows the white, cord-like structures (tendons) in the human wrist that move the fingers.

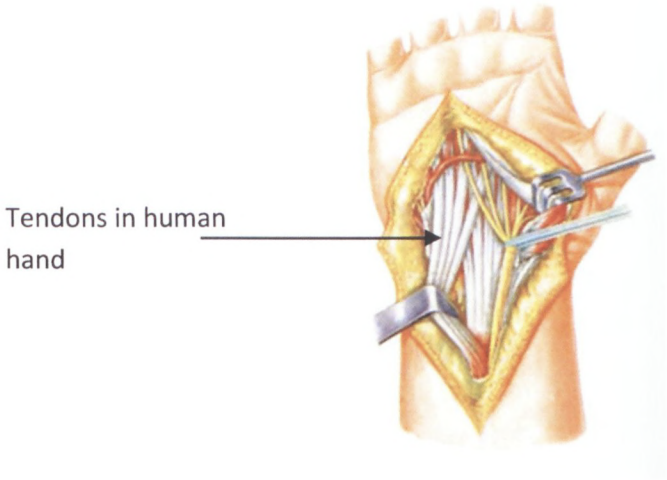

Figure 3.3: Tendons in wrist (Nelson, 2010:1)

Figure 3.4 below shows the connection of tendons to each bone of the finger.

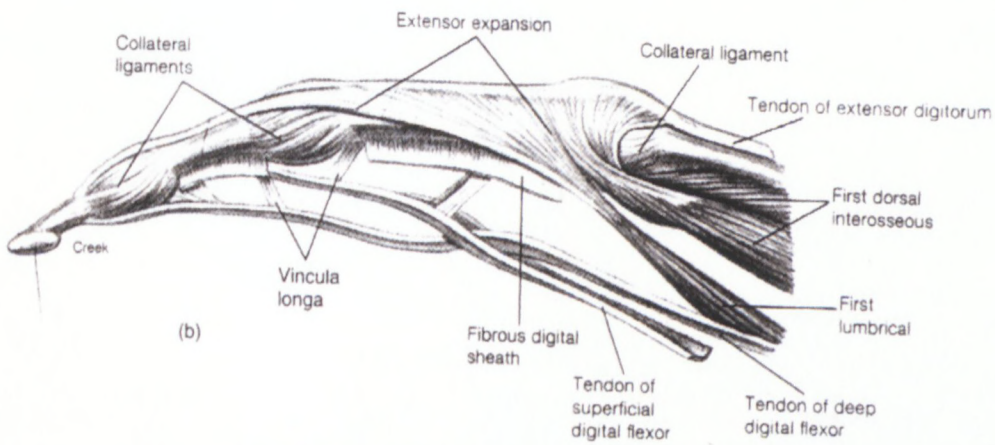

Figure 3.4: The tendon distribution of the index finger (Banks, 2001:26)

3.2.4 Movement Capability

The movement capability of the hand is demonstrated in Figure 3.5 below:

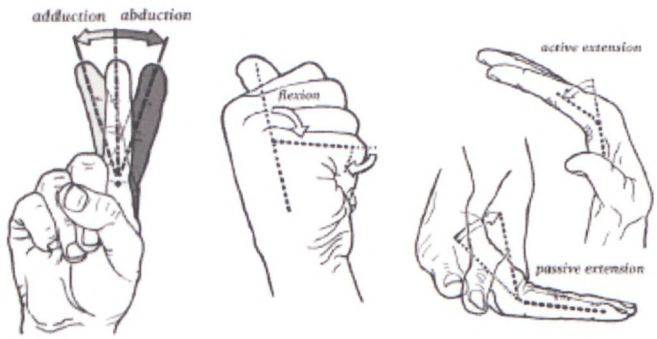

Figure 3.5: Movement capability of the hand (Banks, 2001:29)

3.2.4.1 Extension

The two tendons responsible for the extension of the index finger are the Extensor Digitorum Communis (EDC) and the Extensor IndicisPropius (EI). The EDC, located on the palmer side of the hand, is named for the fact that the same muscle belly (shape of the muscle) sprouts a separate tendon to each of the four digits. The EDC separates to attach to the base of the proximal phalanges. The main member then continues down the finger merging with the EI and splitting into three parts (see figure 3.6).

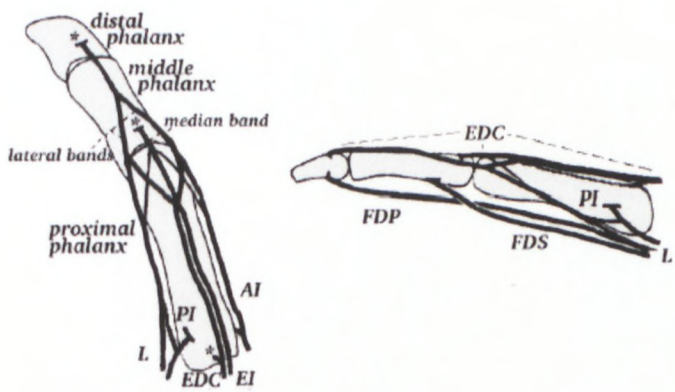

Figure 3.6: Muscle and tendons of each finger (Banks, 2001:29)

The EI is divided into three parts, a centre part and two outside sections. The centre part inserts as the median band into the base of the middle phalanx. The two outside parts of the lateral bands extend the length of the middle phalanges and finally unite at the base of the distal phalanx.

3.2.4.2 Flexion

The Flexor Digitorum Profundus (FDP) and the Flexor Disterum Sublimes (FDS) are responsible for most of the flexion of both the DIP and PIP joints of the index finger. The PIP joint flexes slightly beyond 90^0 and DIP can flex just under 90^0 (see Figure 3.6).

3.2.4.3 Adduction and Abduction

The Anterior (Dorsal) Interossei (AI), Palmer Interossei (PI) and the Lubricales (L) muscles are all muscles in the hand primarily responsible for adduction and abduction of each finger.

3.2.4.4 Passive Flexion and Passive Extension

The range of the Metacarpal Phalangeal joint for passive flexion is between 30^0–40^0. The DIP joint can passively extend up to 5^0. Active extension of the Metacarpal Phalangeal joint is up to 90^0. The DIP joint can passively extend to approximately 30^0. The PIP cannot actively extend.

The apparent coupling of the two DIP and PIP joints is, according to Banks (2001): "Flexion of the DIP joint is shortly followed by the flexion of the PIP joint, as there is no extensor to antagonize the flexion in the joint. Conversely, after the FDS has contracted to bend the Middle Phalanx, the FDP flexes pulling at the same time the distal phalanx. The result of the function is a part coupling." This movement will be simulated by the prototype artificial hand.

The joints of the finger have different connecting muscles responsible for the different movement of the finger.

The finger consists of the Metacarpal Phalangeal (connected to the wrist), Proximal Phalangeal, Middle Phalangeal and Distal Phalangeal bone and joints. These joints are the Metacarpal Phalangeal (MCP) connecting the wrist and Metacarpal Phalangeal bone, the Proximal Phalangeal (PIP) and the Distal Phalangeal joints (DIP).

The DIP and MCP joints have the capacity of flexion at 90^0. The PIP joint can obtain a maximum flexion angle of 135^0. When in full extension, all joints are restricted to 0^0. The DIP and PIP joints do not have abduction and adduction motion ability, but the MCP joint has a 30^0 angle of motion in both directions.

The concept of the prototype is formulated on the bones, joints, movement and the degrees-of-freedom of the human finger.

The SolidWorks (Release 2010), a Computer-Aided Design software package will be used to design the working model, to simulate and to mimic the movement of the human hand prior to manufacturing the prototyped hand.

3.3 Design of the Artificial Hand

The overall design concept of the prosthetic hand presented here is described in mechanical terms and related to human anatomy. The hand prototype is designed to allow the SMAs actuation mechanism to provide, to extend as much as possible, the functionality of an actual hand, such as coarse and fine grasping, and to avoid complexity in hand design and control.

The prosthetic hand will consist of five fingers (the thumb, the index, the middle finger, the ring finger and the pinkie finger). Each finger composed of links: distal phalanx, middle phalanx and proximal phalanx except the thumb which has only the proximal phalanx and the distal phalanx (Figure 3.7). The fingers are connected to a hollow palm routing nylon cables which represent tendons. The palm is connected to a forearm housing Nickel-Titanium wires.

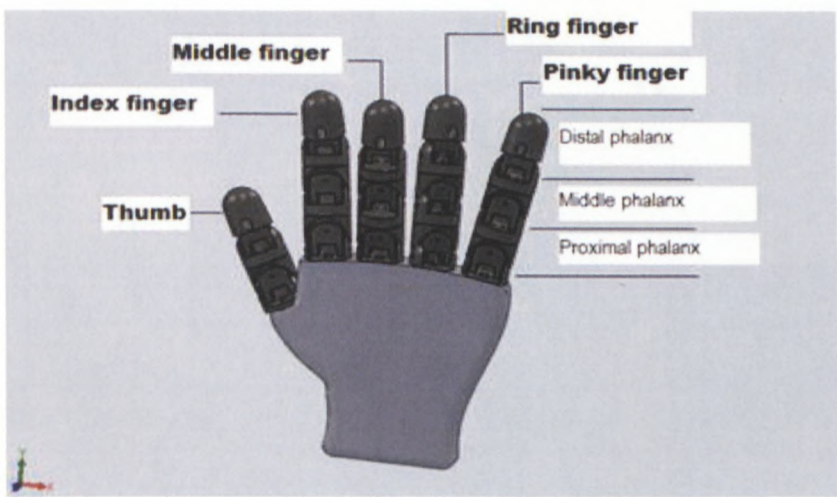

Figure 3.7: Conceptual assembly of the hand (SolidWorks, Release 2010)

The joints of the artificial hand are actuated by nylon cables, or "tendons", routed within the structure of the finger. The distal and middle links are coupled so that actuation of the distal link also moves the middle link, similar to the natural movement of an actual human finger. This coupling is done by running the cables from the distal

joint through the connecting channel of the middle joint, so that when the distal joint is actuated, the middle follows (Figure 3.8).

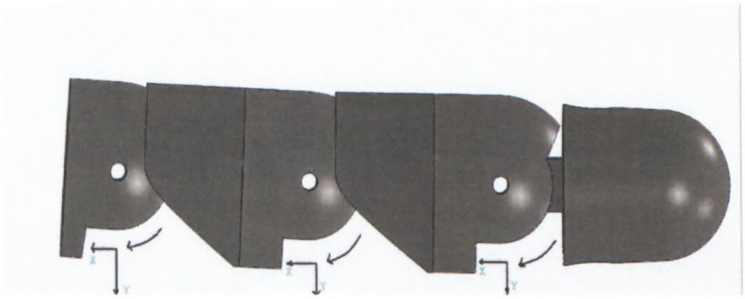

Figure 3.8: Extension and possible flexion of a finger (SolidWorks, Release 2010)

Figure 3.8: shows that the range of motion for the joints of a finger is 90^0 in both flexion and extension.

The goal is to develop a prosthetic hand for an adult. Hence, the prosthetic is designed to reproduce as closely as possible the size of an adult hand with a proposed finger design that mimics the kinematics and functionality of the human hand making a fist or grasping an object.

3.4 Dimensions of the Prototype

For simplicity, in the prototype hand the five fingers are all the same size, connected to the actuators of the same dimensions thus generating the same grasping force.

To provide a human-like sight of the prototype hand, four fingers (index, middle, ring and pinky fingers) are set on the curved edge of the palm while the thumb is separately fixed on the side edge of the palm (Fig. 3. 7).

Detail Drawings showing dimensions of each part of the hand are found in Appendix A of this thesis.

3.5 Kinematic Model

The kinematic model of the hand is designed to form the basis of a controller rather than be a comprehensive anatomical model. A compromise is required between

accuracy of the model and computational complexity, particularly regarding the inverse kinematics solution.

As stated above, all fingers except the thumb, have the same size (same size of the distal phalanx, proximal phalanx and middle phalanx), thus this kinematic study applied to one finger, will be the same for others. The thumb made of two components (distal phalanx and proximal phalanx) follows the same kinematic rule though the middle phalanx is to be disregarded (it does not exist on the thumb).

The kinematic model plays an important role in the work as it provides the geometric constraints on the X-Y plane positions of hand features. Using the D-H (Denavit-Hartenberg) representation, we start by solving the forward kinematic problem where individual link transforms are concatenated to yield a single transform that fully describes the position and orientation of the fingertip with respect to the base reference frame (finger palm housing). After that, the inverse kinematics equations are analysed from the quadrilateral (Guey, 2009:43).

The purpose of the finger kinematic analysis is to determine the final fingertip position in relationship to the angular positions of each joint. The finger design can be modelled as a robot hand fixed to the finger's palm housing. The schematic of a robot hand lying in the X-Y plane based on a prosthetic finger is shown in Figure 3.9.

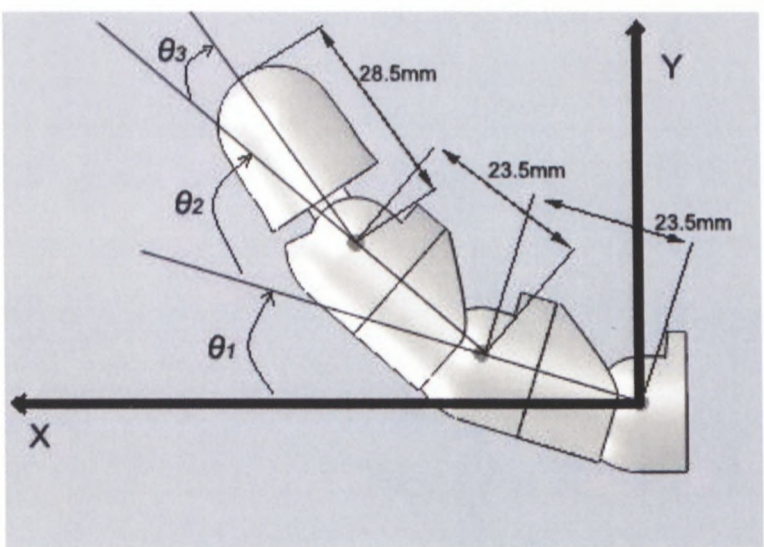

Figure 3.9: Kinematic study of the finger (SolidWorks, Release 2010)

For the kinematic analysis of the finger, there are two fundamental components to evaluate the fingertip position:

1. Given the desired position and orientation of the end-effectors of the manipulator, and the geometric link parameters with respect to a reference coordinate system, the desired joint angles can be calculated.

2. The second fundamental problem contrasts with the first. Given to each joint angle and the geometric link parameters, one can find the position and orientation of the end-effectors of the manipulator with respect to a reference coordinate system (Guey, 2009:44).

3.5.1 Forward Kinematics

In our kinematic model, four prosthetic fingers consist of three links (each corresponding to the three phalanges of the human finger) while the thumb is made of two links or phalanges (see Figure 3.7 on page 28).

Guey (2009:43-48) showed that the Denavit-Hartenberg's theorem is the most commonly used method to solve the forward kinematics problem, where the transformations of links connected in series are used to produce a single transformation showing the position or direction of the fingertip with respect to the palm or to the reference base. The finger kinematics can be considered in 2D kinematics and lying in the X-Y plane, as shown in Figure 3.9, because the abduction-adduction movement of the MCP joint was ignored, as previously explained.

Guey (2009:43-48) also showed that the Denavit-Hartenberg's theorem consists of four kinematic parameters; in the case of this study, these parameters are the joint angle θ_i, the link/phalanx offset d_i, the link/phalanx length L_i, and the link/phalanx twist α_i.

These four variables are used to calculate the position or direction of the fingertip.

The abduction-adduction movement of the MCP joint was ignored and makes no movement in the z-axis (Figure 3.9 on page 30) to cause the link/phalanx offset d_i and the link/phalanx twist α_i can be eliminated. The finger link/phalanx coordinate parameters are shown in Table 3.1.

Table 3.1: Finger joints and links/phalanges coordinate parameters

Joint (*i*)	Twist (α_i)	Angle (θ_i)	Length (L_i)	Offset (d_i)	Joint Angle Range
1	0	θ_1	23.5mm	0	$0 - 90^0$
2	0	θ_2	23.5mm	0	$0 - 90^0$
3	0	θ_3	28.5mm	0	$0 - 90^0$

Once the Denavit-Hartenberg's coordinate system has been established for each link, a homogeneous transformation matrix can easily be developed relating the *i*-th coordinate frame to the (*i-1*)-th coordinate frame.

$$^{i-1}T_{\,i} = T_{z,\theta}T_{z,d}T_{z,l}T_{z,\alpha} \tag{3.1}$$

$$^{i-1}T_{\,i} = \begin{bmatrix}1&0&0&0\\0&1&0&0\\0&0&1&0\\0&0&0&1\end{bmatrix}\begin{bmatrix}cos\theta i & -sin\theta i & 0 & 0\\ sin\theta i & cos\theta i & 0 & 0\\ 0 & 0 & 1 & 0\\ 0 & 0 & 0 & 1\end{bmatrix}\begin{bmatrix}1&0&0&Li\\0&1&0&0\\0&0&1&0\\0&0&0&1\end{bmatrix}\begin{bmatrix}1&0&0&0\\0&cos\,\alpha i&-sin\alpha i&0\\0&sin\,\alpha i&cos\,\alpha i&0\\0&0&0&1\end{bmatrix} \tag{3.2}$$

Since the link/phalanx offset d_i and the link/phalanx twist α_i are zero, then equation (3.2) can be simplified to equation (3.1).

$$^{i-1}T_{\,i} = \begin{bmatrix} cos\theta i & -sin\theta i & 0 & Li\,cos\,\theta i\\ 0 & cos\theta i & 0 & Li\,sin\,\theta i\\ 0 & 0 & 1 & 0\\ 0 & 0 & 0 & 1\end{bmatrix} \tag{3.3}$$

$$^{0}T_{\,i} = {}^{0}T_{\,1}.{}^{1}T_{\,2}.{}^{2}T_{\,3}\ldots{}^{i-1}T_{\,i} \tag{3.4}$$

Equation (3.4) is used to connect each individual link to a single transform that shows the position or direction of the fingertip with respect to the palm or reference base. In this case, equation (3.5) will be derived from equation (3.4).

$$^{0}T_{\,3} = {}^{0}T_{\,1}.{}^{1}T_{\,2}.{}^{2}T_{\,3} \tag{3.5}$$

$$^{0}T_{\,3} = \begin{bmatrix}C123 & -S123 & 0 & L1\,C1 + L2C12 + L3C123\\ S123 & C123 & 0 & L1\,S1 + L2S12 + L3S123\\ 0 & 0 & 1 & 0\\ 0 & 0 & 0 & 1\end{bmatrix} \tag{3.6}$$

$$^{0}T_{\,3} = \begin{bmatrix}Xi & Yi & Zi & Pi\\ 0 & 0 & 0 & 1\end{bmatrix} \tag{3.7}$$

Where:

$C123 = cos\,(\theta_1+\theta_2+\theta_3);$ (3.8)

$S123 = \sin(\theta_1+\theta_2+\theta_3)$; (3.9)

$C12 = \cos(\theta_1+\theta_2)$; (3.10)

$S12 = \sin(\theta_1+\theta_2)$; (3.11)

$C1 = \cos(\theta_1)$; (3.12)

$S1 = \sin(\theta_1)$; (3.13)

[Xi, Yi, Zi] = Orientation matrix of the *i-th* coordinate system established at link *i* with respect to base coordinate system. Upper left [3x3] partitioned matrix of ${}^0T_i$.

Pi: Position vector pointing from origin of the base coordinate system to the origin of the *i-th* coordinate system. Upper right [3x1] partitioned matrix of ${}^0T_i$.

Substituting parameter values given in Table 3.1 into equation (3.5), together with equation (3.7) to equation (3.9), the solution for the fingertip position can be found as given in equations (3.14), (3.15), (3.16) and (3.17).

$$P_{XFingertip} = L_1 \cos\theta_1 + L_2 \cos(\theta_1 + \theta_2) + L_3 \cos(\theta_1 + \theta_2 + \theta_3) \quad (3.14)$$

$$P_{YFingertip} = L_1 \sin\theta_1 + L_2 \sin(\theta_1 + \theta_2) + L_3 \sin(\theta_1 + \theta_2 + \theta_3) \quad (3.15)$$

$$P_{ZFingertip} = 0 \quad (3.16)$$

$$\emptyset = \theta_1 + \theta_2 + \theta_3 \quad (3.17)$$

Where:

$P_{X\ Fingertip}$, $P_{Y\ Fingertip}$, and $P_{Z\ Fingertip}$: Position of fingertip in x, y and z coordinate, (mm). L_1: lengths of 1st link MCP (28.5mm), L_2: 2nd link PPI (23.5mm) and L_3: 3rd link [DPI] (23.5mm). Ø: Angle between reference or orientation frame and fingertip.

On finger's mechanism design, all angles θ_1, θ_2 and θ_3 have been standardised, and have the same maximum value equalled to 90^0.

On extreme conditions, when $\theta_1 = \theta_2 = \theta_3 = 0$

$$P_{XFingertip}max = L_1 + L_2 + L_3 = 75.5mm \quad (3.18)$$

$$\theta 1max + \theta 2max + \theta 3max = 270^0 \quad (3.19)$$

By equation (3.15), (3.16) and (3.17) together with equation (3.19), the working envelope for the fingertip position can be plotted as in Figure 3.10 below. The plot shows all the X-Y data points generated by cycling through different combinations of θ_1, θ_2 and θ_3 and predicting the fingertip position in X and Y co-ordinates for each.

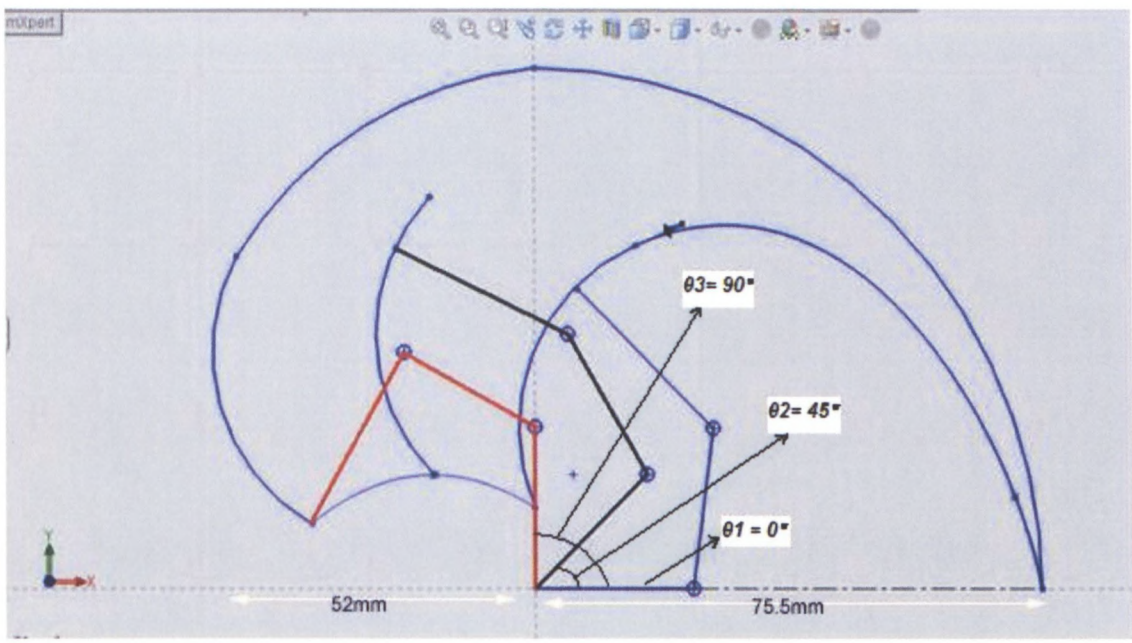

Figure 3.10: Fingertip working envelope (SolidWorks, Release 2010)

Figure 3.10 illustrates that Y position ranges from 0mm ≤$P_{YFingertip}$≤75.5mm, while X position ranges from -52mm ≤$P_{XFingerTip}$ ≤75.5mm. The difference between $P_{YFingertip}$ max and $P_{YFingertip}$ min (75.5mm-52mm) is the stroke of actuation, equalling to 23.5mm. The range of functionality of the articulated finger is summarised in Table 3.2.

An important conclusion is that the prosthetic fingertip working envelope has the same range of movement as an actual human finger, upon which the finger design was based (in this case, the small movement of abduction/adduction of the MCP joint is neglected). Therefore, it can be claimed that the artificial fingers provide a level of functionality very close to that of actual human fingers.

Table 3.2: Range of functionality of the articulated finger

Position	$P_{XFingerTip}$	θ_1	θ_2	θ_3
Min	-52mm	90^0	45^0	45^0
Max	75.5mm	0	0	0
Position	$P_{YFingerTip}$	θ_1	θ_2	θ_3
Min	0	0	0	0
Max	75.5mm	90^0	0	0

A bio-mimetic artificial hand designed to mimic the kinematic architecture of the human hand has been presented in this chapter. This finger design is in accordance with a natural human hand and finger anatomy in order to allow the hybrid actuation mechanism to be able to increase the number of active degrees-of-freedom.

The prosthetic fingers have 1 degree-of-freedom in contrast to the 2 degrees-of-freedom human fingers, since the movement of abduction/adduction in the MCP joint is not necessary for the middle finger to accomplish grasping functionality.

This fingertip working envelope shows all the X-Y data points generated by cycling through different combinations of joint angles and predicts the fingertip position in X and Y co-ordinates for each of them. It also illustrates the fingertip position range.

3.6 Actuation Mechanism

The SMA actuator design is the most challenging factor in order to have the smallest length possible, while yet producing enough grasping force and achieving a large linear stroke or displacement for large angular motion. The SMA actuator formed as a spring is used to control the flexion-extension of joints.

Nylon cables (1mm in diameter and 200mm long) are housed inside the palm pass through different fingers. When pulled, the cables drag the fingers to bend. As the SMA wires produce excessive heat when subjected to Joule's effect, they are far removed from the palmer region in the forearm where they can easily heat and cool without damage to other parts. The cables run through the middle of the wrist spherical joint and are attached to the artificial muscles, placed parallel to each other, in a position similar to the position of the radius and ulna in a human arm.

Once heated, the SMA wire will contract, thus pulling the cable anchored inside the finger, resulting in the finger clenching. Subsequently, when cooled off with a fan, the

SMA wire softens and expands. The springs inside the fingers, playing the role of restoring force, pull back the finger to its extended position.

3.6.1 Linear Displacement of Actuators

The displacement/stroke of the Nickel-Titanium actuator is very important and challenging, as it serves to pull the PIP joint sufficiently from 0^0 to 90^0. Before designing the SMA actuator, the limited dimension in which to place the SMA actuator is the crucial issue to be considered. The linear displacement (full flexion-deflexion) of the SMA actuator is then calculated as follows, taking to account the maximum and minimum positions of the fingertip (confer figure 3.10 on page 34):

$$P_{YFingertip}Max - P_{YFingertip}Min = 75.5mm - 52mm = 23.5mm \qquad (3.20)$$

The nylon tendon cable passes through a hole in the finger at 3mm from the centre of the PIP joint to allow easy bending of the finger; the tendon wire connects the SMA actuator to the articulated finger. The SMA actuator is positioned on the forearm.

Heating the Nickel-Titanium wire by Joule's effect, with a specific amount of electric current, causes its contraction which then coils the tendon wire, connected to the MP of the finger, as shown in Figure 3.11, producing an angular motion of the PIP joint. Steel springs are inserted in between each joint to bring the finger's components back when the SMA wire is cooled.

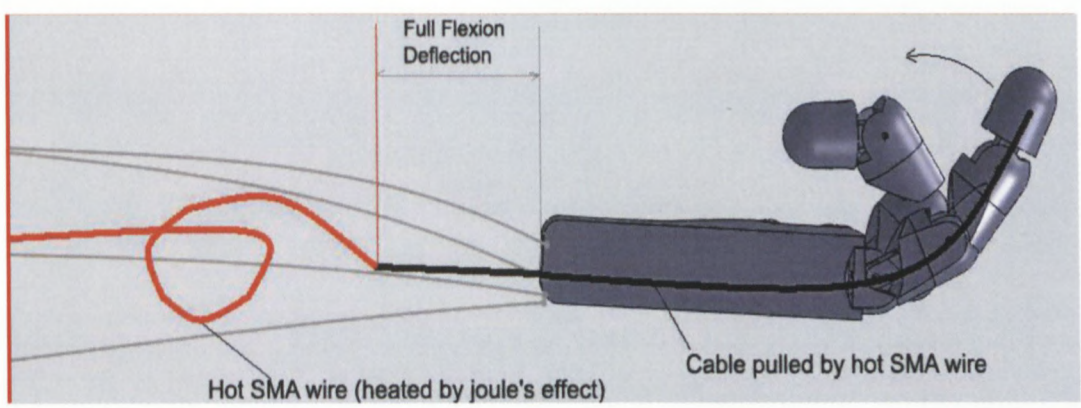

Figure 3.11: Cutaway drawing of the actuation mechanism (SolidWorks, Release 2010)

3.7 Electrical Characterisation

The basic principle of actuation--"an SMA wire shortens or contracts in length when an electric current flows through it"-- means SMA wire changes shape when heated but recovers its shape when cooled.

Actuating Nickel-Titanium wires can be done by direct electric heating using a low voltage power supply.

The standard circuit is shown in Figure 3.12 below:

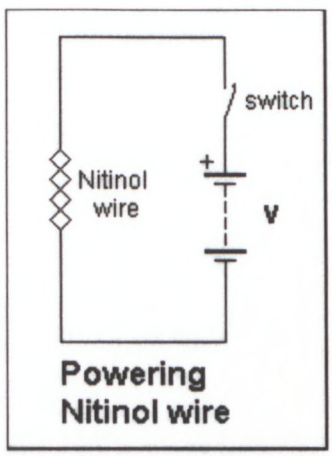

Figure 3.12: Standard actuation circuit

Alternating Current (AC) presents sinusoidal fluctuations which can evenly heat the SMA wire. Direct Current (DC) has constant current and voltage (no sinusoidal fluctuations).

Direct Current is then required for precise current and voltage; it preserves the long life cycle of SMA wires.

Figure 3.13 below shows a DC supplied circuit for actuating the fingers of the prosthetic hand. Each variable resistance, R, is a Nickel-Titanium wire incorporated in the forearm.

Each artificial muscle (Nickel-Titanium alloy wire) is controlled by a switch, S. When 'ON', the switch allows the current to cross the wire (muscle), the SMA wire heats, the artificial muscle shrinks, dragging the string of connection to the finger; thus the finger clenches.

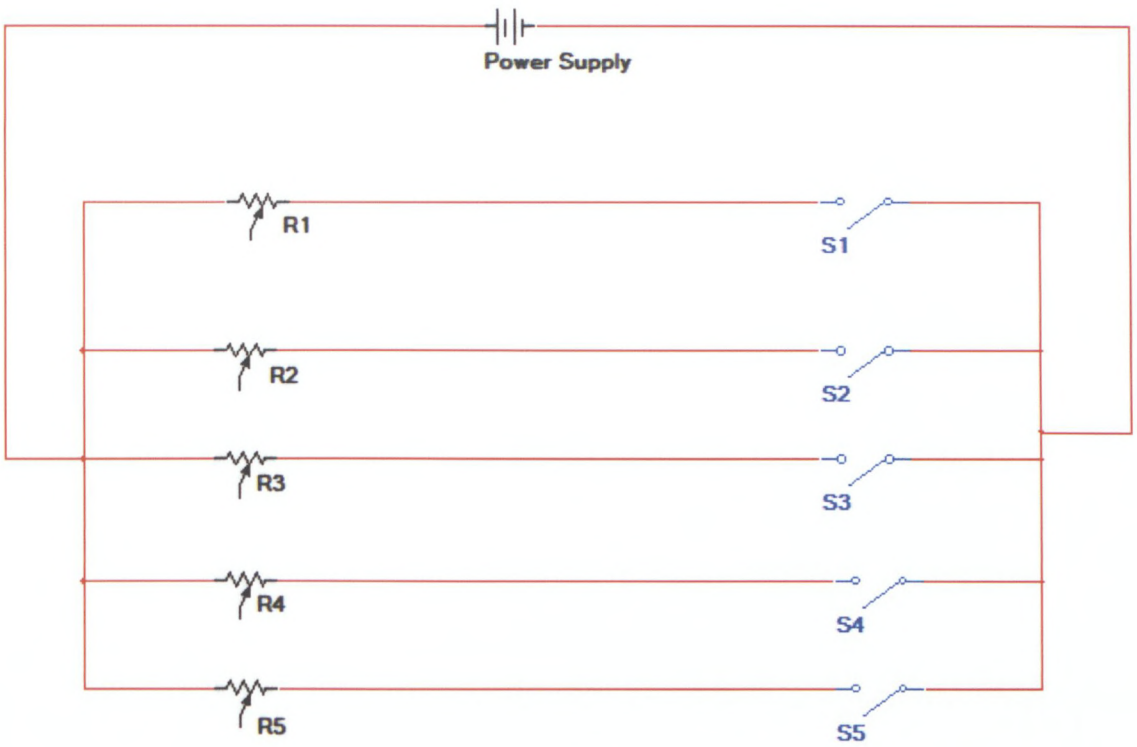

Figure 3.13: Proposed Electric Circuit of Actuation

3.7.1 Dimensions of Artificial Muscles

Dimensioning SMA wires to perform a given linear actuation requires determining their electrical resistance. The resistance of a given resistor or conductor grows with the length of the conductor for a specific material resistivity, and decreases with an increase in cross-sectional area. The resistance (R) of a conductor of uniform cross section, therefore, can be calculated as

$$R = \rho \frac{L}{A} \tag{3.21}$$

Where (L) is the length of the conductor, measured in meters [m], A is the cross-section area of the conductor measured in square metres [m²], and **ρ** is the electrical resistivity (also called specific electrical resistance) of the material, measured in ohm-metres (Ω·m).

In the case of Nickel-Titanium wires with the following dimensions: Length= 70mm; diameter= 1mm.

We can calculate the cross-section of the wire:

$$A = \pi \frac{D^2}{4} = \pi \frac{0.001^2}{4} = 7.9x10^{-7} m^2 \tag{3.22}$$

Nickel-Titanium wire has two different temperature depending phases, thus two different electrical resistivities[1].

$$\rho_{Martensite} = 80x10^{-8}\Omega m \quad (3.23)$$

$$\rho_{Austenite} = 100x10^{-8}\Omega m \quad (3.24)$$

At room temperature, $\rho_0 = \rho_{Martensite}$, the electrical resistance is calculated using relations (3.21), (3.22), and (3.23) as:

$$R = \rho\frac{L}{A} = 80\text{x}10^{-8}\frac{0.07}{7.9\text{x}10^{-7}} = 7.1\text{x}10^{-2}\Omega \quad (3.25)$$

In the case of this study, experiments have been conducted on the Nickel-Titanium wires used as artificial muscles (actuators) with the same dimensions in terms of length and diameter.

Experiments conducted in the laboratory, demonstrated that for Nickel-Titanium wires of such size (70mm long and 1mm of diameter), the transformation Martensite-Austenite started when applying a voltage of 1.5V. By increasing the voltage from 1.5V up to 10V, the actuation speed increases considerably. However, increasing the voltage above 10V, the material overheats and loses its shape memory effect.

Therefore, the experiments were conducted in the voltage range of 1.5 – 5 – 10V.

The heat induced in the Nickel-Titanium element increases its temperature above the transformation temperature. Phase transformation occurs and the actuation stroke is obtained. However, as the phase transformation occurs and the material is strained, the resistance of the material alters significantly.

Waram (1993) also showed that the change in resistance means that the flow of electric current in the wire does not remain constant as time evolves. It also means that the power dissipated across the SMA element does not remain constant as the time evolves. As a result, the heat is not induced uniformly in the SMA element.

Connecting all Nickel-Titanium wires in parallel decreases the value of the total resistance of the circuit. This connection results in a high peak of electric current required to perform actuation.

For the purpose of producing simultaneous gestures (fist, two or three fingers bent at the same time), the series parallel circuit below was constructed.

[1]: Technical Characteristics of Flexinol Actuator Wires F1140Rev H Page 2

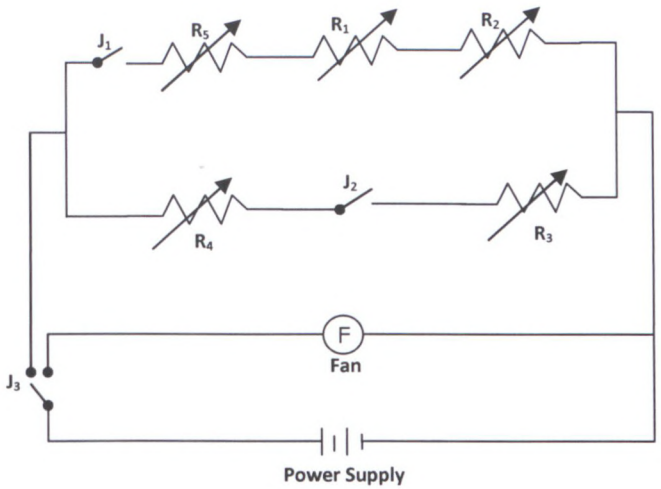

Figure 3.14: Series-parallel actuation circuit

In Fig 3.14, three resistances--R_1, R_2, and R_5--are mounted in a series along with the switch J_1, while the switch J_2 is mounted between R_3 and R_4. The bipolar switch, J_3, connects the power supply to the cooler fan or to the actuation circuit. A fan F is used to improve the speed of the relaxation time (cooling time).

Table 3.4: Equivalent resistance of the series-parallel

Switch engaged	Number of Fingers Actuated	Equivalent resistance (R_{eq})	Power consumption ($P = V^2/R_{eq}$)		Actuation
J_1	3	$R_{eq} = \sum_{i=1}^{3} R_i = 0.213\Omega$	@1.5V	**10.5W**	**Gesture one**
			@5V	**117.3W**	
			@10V	**469.4W**	
J_2	2	$R_{eq} = \sum_{i=1}^{2} R_i = 0.142\Omega$	@1.5V	**15.8W**	**Gesture two**
			@5V	**176.1W**	
			@10V	**704.2W**	
J_1 & J_2	5	$R_{eq} = (\frac{1}{0.213} + \frac{1}{0.142})^{-1} = 0.085\Omega$	@1.5V	**26.4W**	**Gesture three (fist)**
			@5V	**294.1W**	
			@10V	**1176.4W**	
J_3	None	— — —			**The fan is on**

Table 3.4 represents a scenario of three switches J_1, J_2 and J_3 connected to Nickel-Titanium actuators. When each is engaged or when engaged simultaneously, the table above showed different equivalent resistances depending on the connection (series, parallel or combined series-parallel). By application of a range different

voltages (1.5, 5 and 10V), the power dissipated across Nickel-Titanium elements is calculated. According to the above values of power consumption and from experimental observations, a supply of voltage of 1.5V helps to prevent overheating and extend the life cycles of the actuators.

3.8 Cooling Fan

The contraction of Nickel-Titanium is due to heating and the relaxation solely to cooling. Cooling Nickel-Titanium wires is greatly affected by heat sinking and design features. The wire contracts and relaxes at higher temperatures; accordingly, the temperature differential between ambient or room temperature and the wire temperature is greater and correspondingly the wire will drop below the transition temperature faster in response to the faster rate of heat loss.

Forced Air cooling (fan) helps to improve the speed of the relaxation time (cooling time).

Cooling Fan Performance[2]:

- Trademark: HPIC
- Type: CPU cooler
- Input Voltage: 12V DC
- Frame size: 40x40x10.5mm
- Impeller type: 10 blades
- Power: 1.44W
- Speed: 38RPM
- Motor: 4poles brushless DC
- Coil: single winding
- Air pressure: 0.40 mmH_20
- Airflow: 21.2CFM [Cubic Feet per Minute] (≈0.6m^3/min.)
- Air velocity: 580LFM [Linear Feet per Minute] (≈2.95m/s)
- Noise level: 13dBA
- Net weight: 19g

Figure 3.15: Cooling fan

([2]) : http://www.high-pace.com/products01-1.asp (downloaded on 2012-10-22)

3.9 Finger's Contraction Force

The finger bending force is the force necessary to pull on the nylon wire (artificial tendon) in order to bend completely the finger as shown on figure 3.16 below.

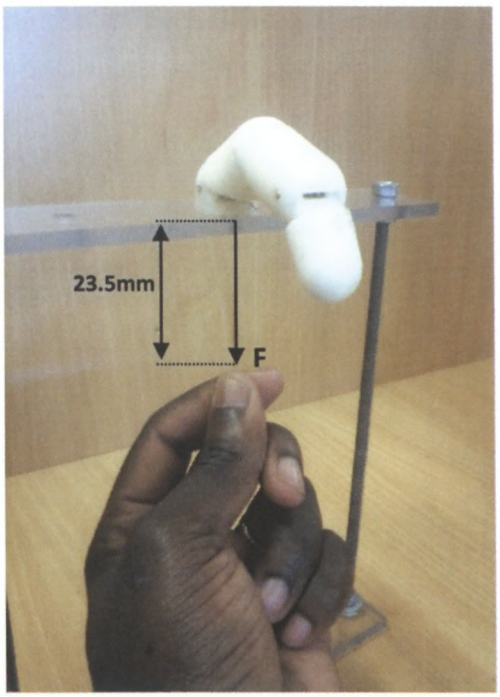

Fig. 3.16: Bending force

This force is also called 'restoring force', as it tends to restore the system to equilibrium; when cooling, the SMA spring wire straightens out and this restoring force straightens the fingers to vertical position.

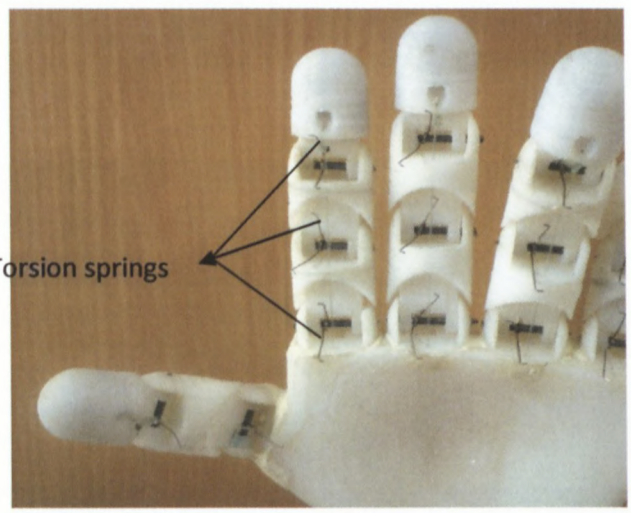

Fig 3.17a Springs inserted between joints

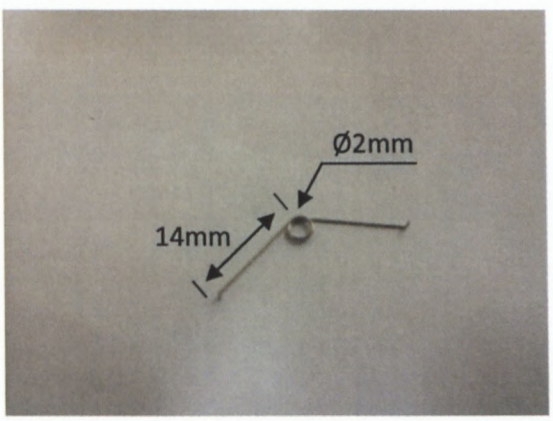

Fig 3.17b Torsion spring dimensions

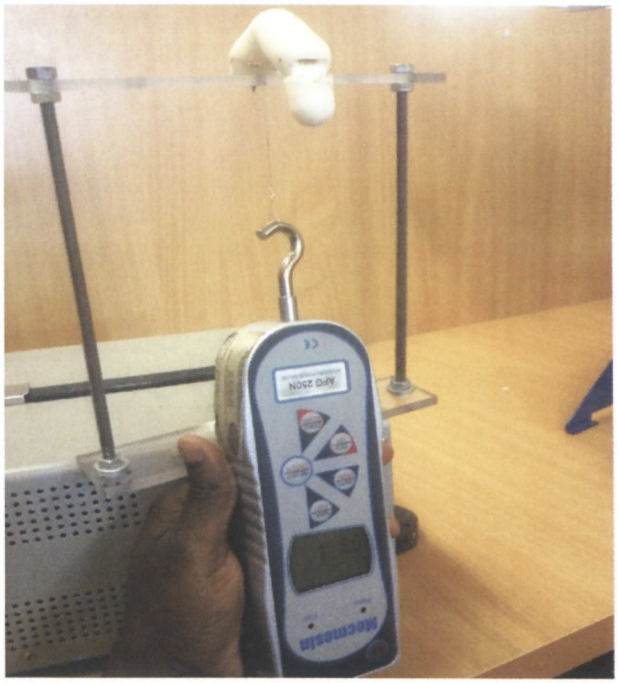

Fig. 3.18 Finger Bending Force (1.05N)

The finger bending force is the total force necessary to bend each finger; which includes the stiffness of each torsion spring inserted in the joints of the finger (the restoring force).

Four of the fingers have 3 torsion springs (the thumb has two); the total stiffness of the springs can be determined by applying the Hook's law as follows:

$$F = K.x \tag{3.26}$$

F: Finger Bending Force [N]

K: stiffness of the whole finger which has three torsion springs [N/m]

x: elongation: 23.5mm (see Fig. 3.16) [m].

$$K = \frac{F}{x} = \frac{1.05}{0.0235} = 4.5N/m \tag{3.27}$$

The stiffness of each torsion spring is one third of the total stiffness.

$$k' = \frac{K}{3} = \frac{4.5}{3} = 1.5N/m \tag{3.28}$$

The net finger contraction force was measured as shown on Fig. 3. 19a below

Fig 3.19a: Contraction force of each finger (3.80N)

Fig3.19b: Contraction of the finger until it bends completely

Fig. 3.19b shows that, when the finger is completely bent, there is no more contraction force because the SMA wire has completely coiled and cannot go further than it has been trained to remember that shape.

The Table 3.5 and Fig 3.19c below show the evolution of the contraction force.

Table 3.5: Evolution of the Contraction force per unit of time

Time (s)	0	5	10	15	20	25	30	35	40	45
Force (N)	0	1.8	2.5	3.8	2.1	0.8	0.45	0.45	0.4	0.45

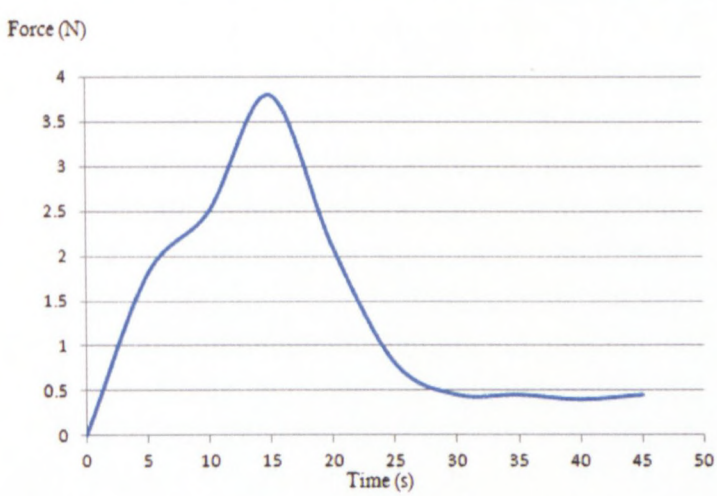

Fig. 19.c: Graph of contraction force

In fact, at 0 second, the finger is straightened; 5 seconds later, the middle phalanx starts bending; and after 10 seconds, the distal and proximal phalanxes follow the bending movement. After 15 seconds, the finger is bent and the SMA wire is almost fully coiled. From 25 seconds and beyond, the SMA wire has "remembered" its spring-coiled shape and does not pull any farther; the force gauge shows 0.4N which is the total weight of the collar shaft, the grub screw, the insulated pin terminal and the crocodile clamp attached to the SMA wire.

3.10 SMA Wires Pulling Force

The SMA wires pulling force is the contraction force developed by the SMA wire (when heated and changes into spring shape) without taking into account the springs' restoring force.

Lerdelé (2002) showed that the transition temperatures are related to the stress in the SMA wires through

$$T_{Af} = T_{Af}^{0} + \frac{\sigma}{C} \qquad (3.29)$$

$$T_{Ms} = T_{Ms}^{0} + \frac{\sigma}{C} \qquad (3.30)$$

In these equations, T_{Af} and T_{Ms} are respectively the temperature at the end of the Austenite transformation, and the temperature of start the Martensite transformation. They both correspond to the actuated state of the samples. Thus the stress σ is the total recovery force produced by the wires. In order to estimate the stress, we may do a reverse engineering procedure.

To contract the artificial muscle of the Nickel-Titanium by the application of a 1.5V electric tension, a resulting current of 2.4A has been measured (see Figure 3.20 on page 47 of this thesis).

The equation (3.29) shows the transition temperatures are related to the stress in the SMA wire through

$$T_{Af} = T_{Af}^{0} + \frac{\sigma}{C} \qquad \text{(Confer 3.29)}$$

T_{Af}^{0} is the austenite finish temperature without load; in this case, due to smaller temperature increase (small gap between martensite and austenite), it is close to the room temperature (23.5^{0}C: highest starting temperature on Fig 3.26 on page 57).

T_{Af} is the highest temperature reached during experimentations (41.7^{0}C); see Figure 3.26 on page 57 of this thesis.

C is the stress influence coefficient for Austenite: $C = -0.35MPa/K$ (Lagoudas *et al.*, 2003:8).

The stress is deducted from the equation (3.29).

$$\sigma = \mathrm{C}(\mathrm{T_{Af}} - \mathrm{T_{Af}^0}) = -6.405 \times 10^6 \mathrm{N/m^2} \quad (3.31)$$

In continuum mechanics, the stress measures the internal forces $\boldsymbol{F}$ acting within a deformable body per section unit,

$$\sigma = \frac{F}{A} \quad (3.32)$$

$\boldsymbol{A}$ is the cross section area of Nickel-Titanium wires

$$F = \sigma x A = -6.405\mathrm{x}10^6 \times 7.9 \times 10^{-7} = -5.06\mathrm{N} \quad (3.33)$$

The negative sign indicates that the force exerted by the spring is in direct opposition to the direction of displacement. This is the compression force.

Experimentally, this result is verified by mounting the artificial muscle of Nickel-Titanium wire on a special test bed; the digital force gauge displays the reading of the amount of force generated by the SMA wire heated by Joule's effect with the DC power supply.

Experiment set-up:

- a DC power supply [0 – 30V, 3A max];
- a digital force gauge [0 – 200N]; and
- a test bed to set the Nickel-Titanium actuator.

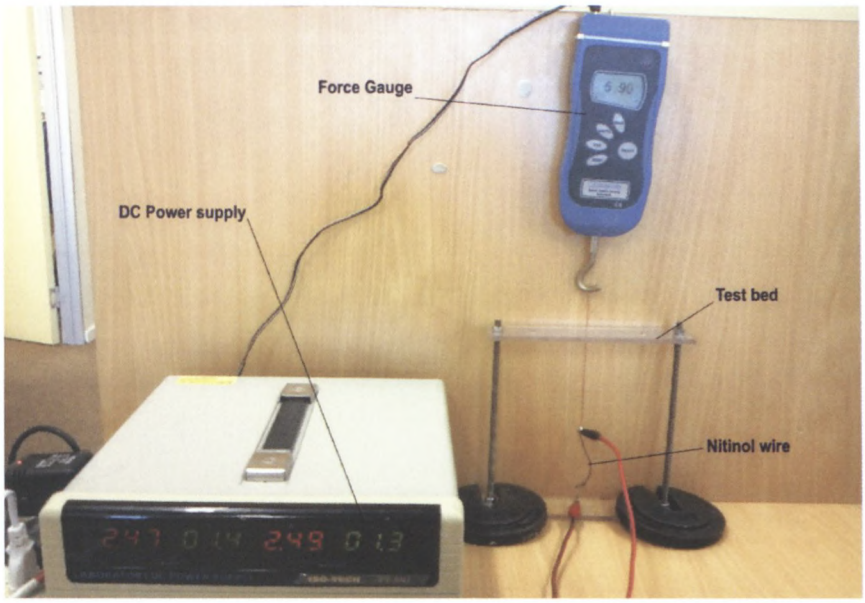

Figure 3:20: Experimental measurement of SMA pulling force (Adaptronics AMTL Lab)

Experimentally, as shown in Figure 3:20, the SMA pulling force measured was 5.90N.

The discrepancy between the absolute values of the analytical and the experimental measurements is due to the fact that analytical calculations use values (room temperature measured by the manufacturer [Dynalloy Inc.] (27^{0}C at normal conditions of temperature and pressure) differs from the room temperature (23^{0}C) measured in the Adaptronics AMTL Laboratory during the period experiments were conducted: winter 2010).

The above pulling force is exerted equally by each finger of the hand as each finger is connected to a Nickel-Titanium actuator of equal size.

3.11 Thermo-Mechanics Considerations

When heated, the deformation of a Shape Memory Alloy wire is a function of temperature, stress and Martensite phase fraction (Philander, 2005:60):

$$d = d_A + \xi_{M_+}(d_{M_+} - d_A) + \xi_{M_-}(d_{M_-} - d_A) \qquad (3.34)$$

Where, d_{M_+},d_{M_-},ξ_{M_+},ξ_{M_-}: are the deformation of the specimen at twinned and de-twinned Martensite, and phase fraction at twinned and de-twinned Martensite respectively, and d_A: the original length.

Relation (3.34) can also be considered as the load-deformation relation complemented by the system of non-linear ordinary differential equations for the martensitic phase fractions.

The reverse transformation equation proposed by Liang (1990) describing the phase transformation from Martensite to Austenite (heating) is:

$$\xi = \frac{\xi_M}{2}\cos[a_A(T - A_s) + b_A\sigma] + 1 \qquad (3.35)$$

ξ: Martensite fraction which has a value of 1 (for Martensite phase) and 0 (for Austenite phase);

ξ_M: is the minimum Martensite fraction the wire reached during the cooling;

$a_A = \frac{\pi}{A_f - A_s}\ (^0C^{-1})$ is a curve-fitting parameter, T is the temperature of the wire, σ is the wire's stress, A_s is the Austenite phase start temperature, A_f is the Austenite phase final temperature, $b_A = \frac{a_A}{c_A}$ and c_A are curve-fitting parameters.

The forward transformation equation proposed by Liang (1990), describing the phase transformation from Martensite to Austenite (cooling) is:

$$\xi = \frac{1-\xi_A}{2}\cos[a_M(T - M_f) + b_M\sigma] + \frac{1+\xi_A}{2} \qquad (3.36)$$

Where ξ_A is the minimum Martensite fraction obtained during heating, $a_M = \frac{\pi}{M_s - M_f}$: is a curve-fitting parameter, M_s is the Martensite phase start temperature, M_f is the Martensite phase final temperature, $b_M = \frac{-a_M}{c_M}$ and c_M are curve-fitting parameters.

3.12 Motion Control Unit

The prototype hand actuated by Nickel-Titanium wires is controlled by a Motion Control Unit (see Fig 3.21 & 22) made of a set of switches operated in order to communicate different gestures to the hand.

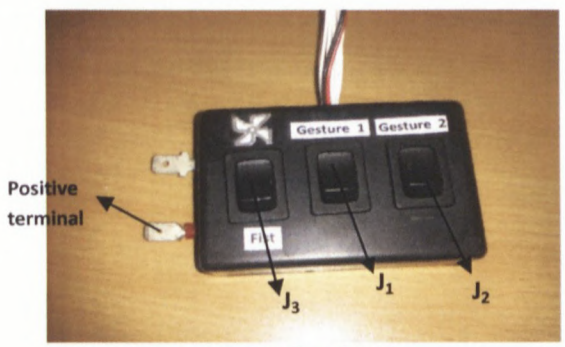

Figure 3.21: Control box

Figure 3.22: Connexions inside of the control box (only wires connected to switches)

3.12.1 Logic of Actuation

The flowchart is a pictorial representation of the actuation system showing the step-by-step process of a gesture as shown in figure 3.23.

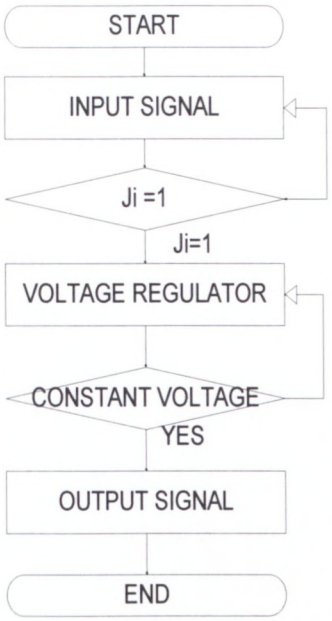

Figure 3.23: Flowchart of the actuation process

INPUT SIGNAL: Turning "ON" or "OFF" the switches Ji {i=1,.. 3}.

DECISION: Si=1 is the decision; if a switch Ji {i=1... 3} is on "ON" position, this means Si=1, the decision is "YES", and then the information is transmitted to the next step. If Si=0, the switch Si is at "OFF" position, the decision is then "NO" and the process returns to INPUT SIGNAL.

VOLTAGE REGULATOR: At this step of the process, the signal is sent to tension regulator which maintains constant the voltage inside the actuation circuit.

CONSTANT VOLTAGE: The decision is "YES" if the voltage released by the regulator is constant, and then the process progresses.

OUTPUT SIGNAL: The output signal is the final actuation of the finger due to a constant voltage along the Nickel-Titanium wire.

Taking into consideration equations found in different modules (mechanical, electrical and thermal), we can link them in an algorithm structure, in order to emphasise the actuation process.

A computational algorithm is developed to effectively solve the above system of differential and algebraic equations and used for the numerical study of stress-induced transformations. Both stationary solutions for each loading step and non-stationary solutions (kinetic loading) are considered.

Philander (2005) has presented a simplistic model of development of a computational design tool for uses in the design of SMA actuator systems. In his model, the solution algorithm starts off by calculating the nodal displacements of a given structural system being subjected to an externally applied load, a load which can be either dependent or independent of time. These displacements are then used to determine the strains.

Based on Philander's (2005) approach concerning computational design tools to simulate the behaviour of Nickel-Titanium SMAs, we can write the structure plan which can be easily rewritten using MATLAB® R2010a (Release 2010).

3.12.2 Solution Algorithm

The solution algorithm to determine the force of the Nickel-Titanium actuators is expressed in the following structured plan:

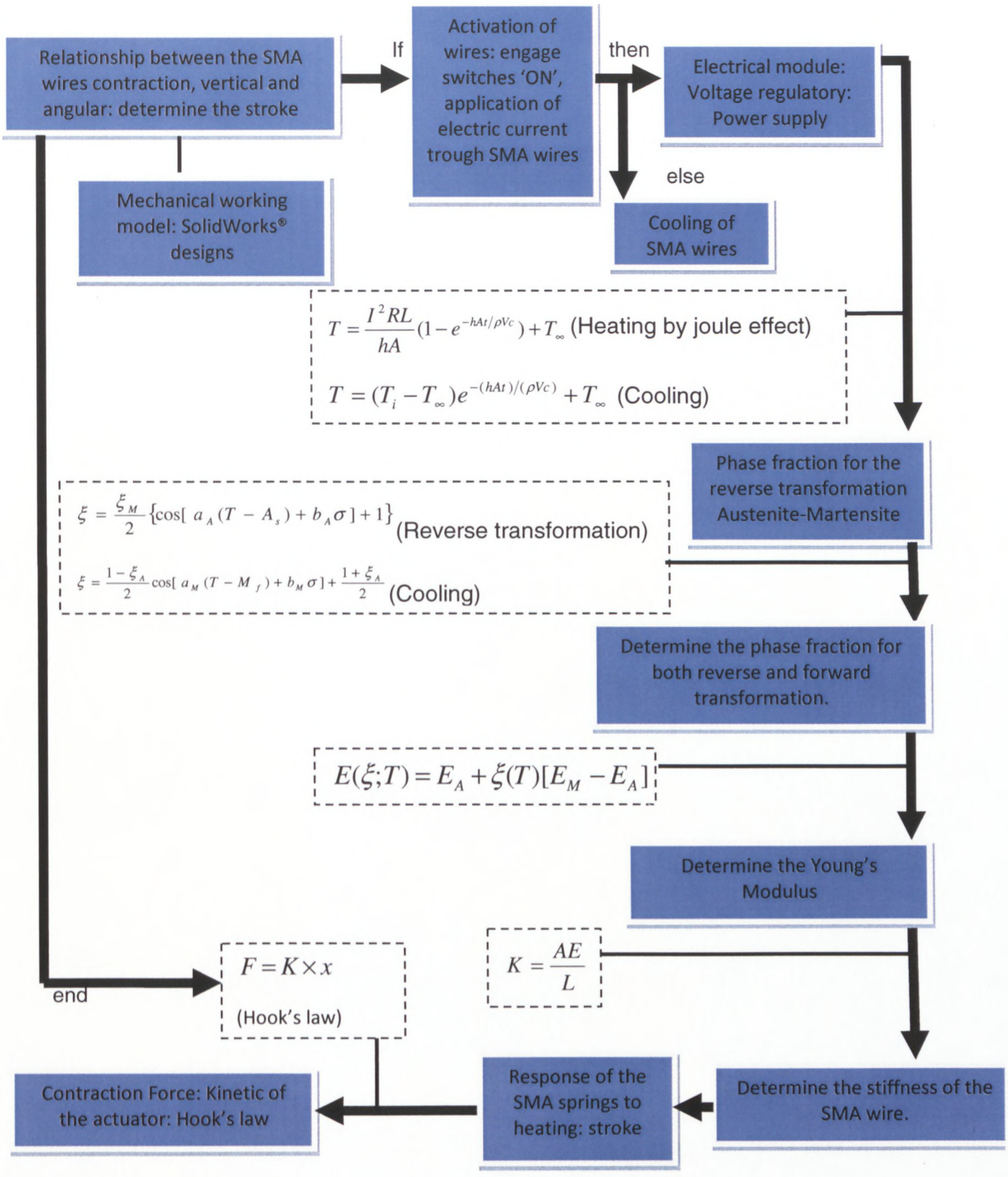

3.12.3 MATLAB® Script of the Algorithm of Actuation

Table 3.5 describes the actuation algorithm script. This algorithm, run with Matlab®, shows each sequence of the actuation of the hand from the switch to the grasping force generation with three different gestures.

Table 3.5: Script of the algorithm of actuation

```
if J==1
% a switch is engaged ON
disp('S is ON');
else
% a switch is not engaged: OFF position
disp('S is OFF');
end;
for n=1:3, k=1:1/3;
if I==V/(k*R)
% constant voltage: direct current
solve('I=(V*((n*pi*(D^2))/(4*ls)))');
else
% non-constant voltage
disp('danger: can overheat SMA wires');
end;
if I==sqrt(P/R)
% heating the SMA wire by Joule's effect
solve('T=(I*R*L*(1-exp((-h*A*t)/(rho*V*c)))/(h*A))+Troom')
% determine the phase transformation for the reverse
% transformation
solve('ksi=(0.5*KsiM*cos(aM*(T-As)+bA*sigma))+1');
else
% cooling of SMA wire
solve('T=((Ti-Troom)*exp((-h*A*t)/(rho*V*c)))+Troom')
```

```
% determine the phase transformation for the forward
%transformation
solve('Ksi=0.5*(1-ksiA)*cos(aM*(T-Mf)+(bM*sigma))+0.5*(1+ksiA)');
end;
for x=0:n;
if K==A*(E/L)
% determine the Young Modulus of the SMA wire
disp('F=k*x');
%Hook's law to determine the stroke of the actuator
%x is the deflexion of the SMA wire and k is the stiffness
end;
end;
end
```

Where: Ls=L_s; pi= π; rho= ρ; Troom=T_∞; KsiA=ξ_A; KsiM=ξ_M; bA=b_A; aM=a_M; sigma= σ; Mf=M_f

In this section, we showed the development of a computational design tool to simulate the behaviour of Nickel-Titanium SMAs, a design tool specifically suited to design actuators consisting of Nickel-Titanium SMAs that harness the Shape Memory Effect for their operation. The framework of this tool is written in the Language of MATLAB®. The computational framework of this tool consists of a calibrated constitutive model to simulate the complex material responses exhibited by SMAs.

3.13 Micromechanical and Phenomenological Models of the Heating and Cooling Process

Lagoudas *et al.* (2003) developed two approaches for constitutive modelling of SMAs. The first is the 'direct approach': the evolution laws are obtained by either considering transformation micro-mechanisms (Tanaka, 1986:251-263) or secondly, by directly matching experimental results (i.e. 'phenomenological approach') drawn by Liang (1990). The first approach uses the thermodynamic approach, starting with the construction of a free energy and then, by utilising a dissipation potential in conjunction with the Second Law of Thermodynamics, the evolution laws for the

internal state variables, (i.e., the volume fraction of the various forms of Martensite are derived).

In the thermodynamic approach developed by Lagoudas *et al.* (2003), the Second Law of Thermodynamics applies constraints to material constitution, but these constraints are usually weak. Hence, if a constitutive model does not violate the thermodynamic constraints, it can usually also be derived from the thermodynamic approach. A three-dimensional constitutive model was developed by Liang (1990) which was based on the First and Second Law of Thermodynamics and was defined by three parameters: 1) the equivalent strain, 2) the absolute temperature, and 3) the Martensitic fraction. They discovered that the constitutive equations were non-linear and therefore required large computational effort.

In this study, the phenomenological models developed by Tanaka (1986) and later refined by Liang (1990) are utilised to describe the behaviour of the SMAs. These models are based on the experimental characterisation of SMAs and hence are phenomenological. In this section, the phenomenological behaviours of the heating and cooling process of SMAs wires actuating an articulated finger are investigated.

3.13.1 Micromechanical Model

The constitutive behaviour of Nickel-Titanium as an SMA can be calculated by applying this micromechanical model numerically. The micromechanical model is based on calculations and formulae presented in the previous section (thermal module), showing that it is possible to predict the heating trend for the SMA wire with the following relation:

$$T = \frac{I^2 RL}{hA}\left(1 - e^{-hAt/\ddot{\rho}Vc}\right) + T_{\infty} \qquad (3.\ 37)$$

where $\mathbf{T}$ is the estimated temperature; $\mathbf{I}$ is the applied current; $\boldsymbol{R}$ is the wire resistance; $\mathbf{V}$ is the volume of the wire; $\ddot{\boldsymbol{\rho}}$ is the density; $\mathbf{h}$ is the convection coefficient; c is the specific heat; $\mathbf{A}$ is the surface area of the wire; $\mathbf{T}_{\infty}$ is the ambient temperature; and $\mathbf{t}$ is the time.

Cooling from activation temperature to room temperature under free convection conditions was also analysed. The equation used to predict the cooling temperature of the SMA wire is given below:

$$T = (T_i - T_\infty)e^{-(hAt)/(\ddot{\rho}Vc)} + T_\infty \quad (3.38)$$

T_i is the surface temperature.

The heating and cooling relations are exponential functions.

Liang (1990) showed that the heating relation is a natural exponential function. The general form of natural exponential functions is given by:

$$y(t) = Ae^{-Ct} + B \quad (3.39)$$

Where A: the coefficient of scale factor, B: the y-offset coefficient, and C: the exponent coefficient.

We can deduce the following from the heating relation:

$$A = \frac{I^2RL}{hA} \quad (3.40)$$

$$B = T_\infty \quad (3.41)$$

$$C = {}^{-hA}/_{\rho Vc} \quad (3.42)$$

Liang (1990) also showed that the cooling process follows the inverse exponential function with the general expression given by

$$y(t) = A(1 - e^{-Ct}) + B \quad (3.43)$$

Deducing from the cooling relation, we have:

$$A = T_i - T_\infty \quad (3.44)$$

$$B = T_\infty \quad (3.45)$$

$$C = {}^{-hA}/_{\rho Vc} \quad (3.46)$$

3.13.2 Phenomenological Model

The phenomenological model is an experimental approach to determine the SMAs parameters of response to both heating and cooling. The below series of experiments are intended to determine the heating and cooling equations through algebraic functions using the curve-fitting software DataStudio® 1.9.8 (Release 2007).

3.13.3 Material Tested

Commercially available Nickel-Titanium wires of 1mm diameter, 70mm length, were used in these experiments. The material was purchased from the supplier Dynalloy, Inc. USA.

3.13.4 Experimental Set-up

The experiment has been conducted on one finger mounted on a support, or a test bed, such as shown in Figure 3.24 below.

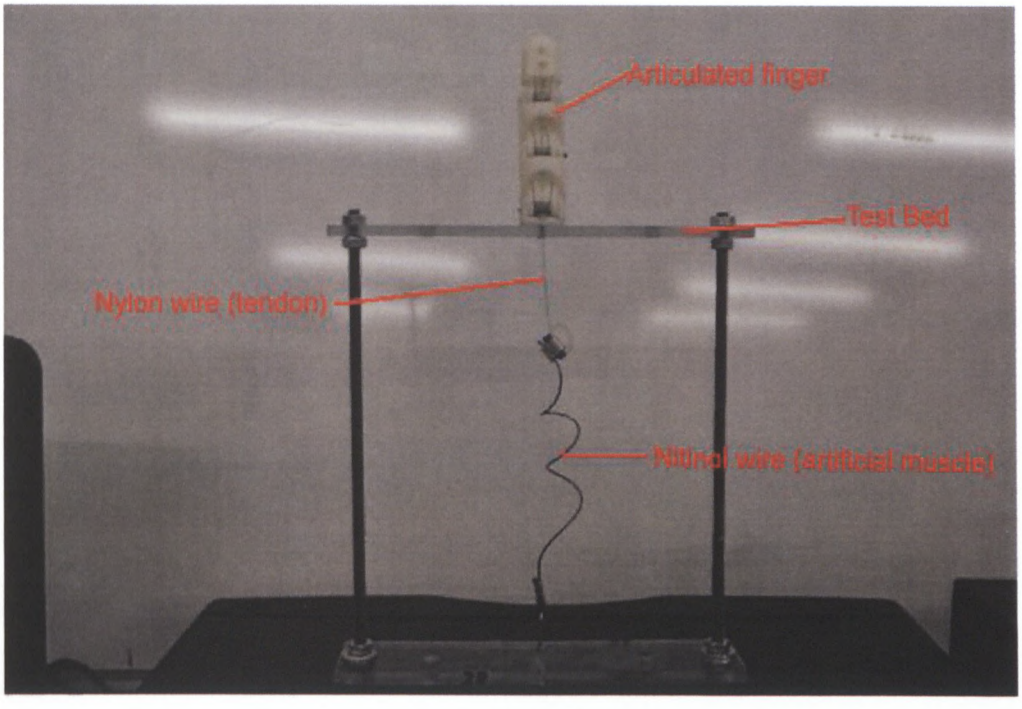

Figure 3.24: Test bed set-up

As all fingers are connected to Nickel-Titanium actuators of the same size, this experiment has been conducted on one finger, thus the result will be the same for all other fingers.

The measurements were made with the following apparatus:

1. a data logger GLX (XplorerGLX): portable graphing data logger, for real-time data visualisation, graphing, collection and analysis (sampling rate: 50 kHz maximum, calculation engine: 50 MHz FPU: real-time graphing and instant calculations from Floating Point Processor) interacting with a computer using the software DataStudio® 1.9.8 (Release 2007);
2. a computer to visualise and read values measured and curves plotted;
3. a thermometer: non-contact infrared sensor (Range: -30 to 900^{0}C); and

4. a power supply (Input: 220/240V, 50Hz ~, output: 3-15V/ 18A DC).

The experiment set-up is seen in Figure 3.25 below:

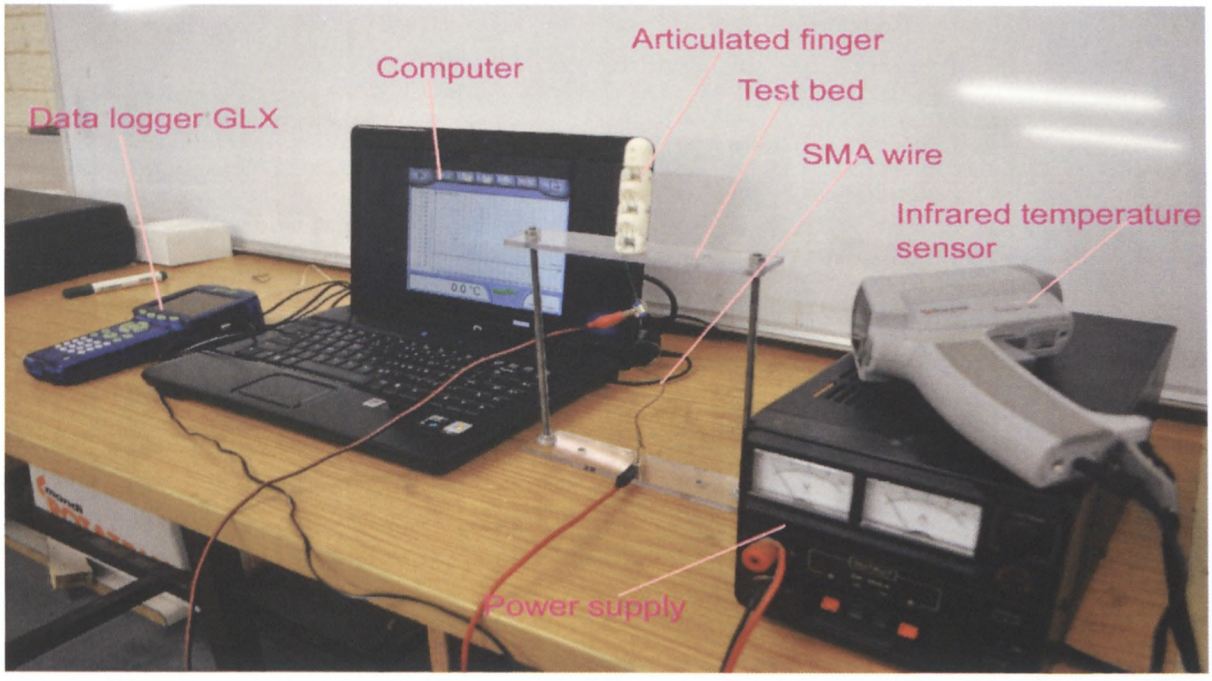

Figure 3.25: Lab equipment set-up (Adaptronics AMTL)

Measurements have been conducted on the above-mentioned SMA wire specimen in order to determine the heating and cooling graph; from this graph, the heating and cooling relations will be deduced.

3.13.5 Heating and Cooling Parameters

Fifteen tests have been run at different voltages (five tests @1.5V, five tests @5V and five others @10V) for 100 seconds each. For each run, we will determine the parameters for heating and cooling relations (A, B, C).

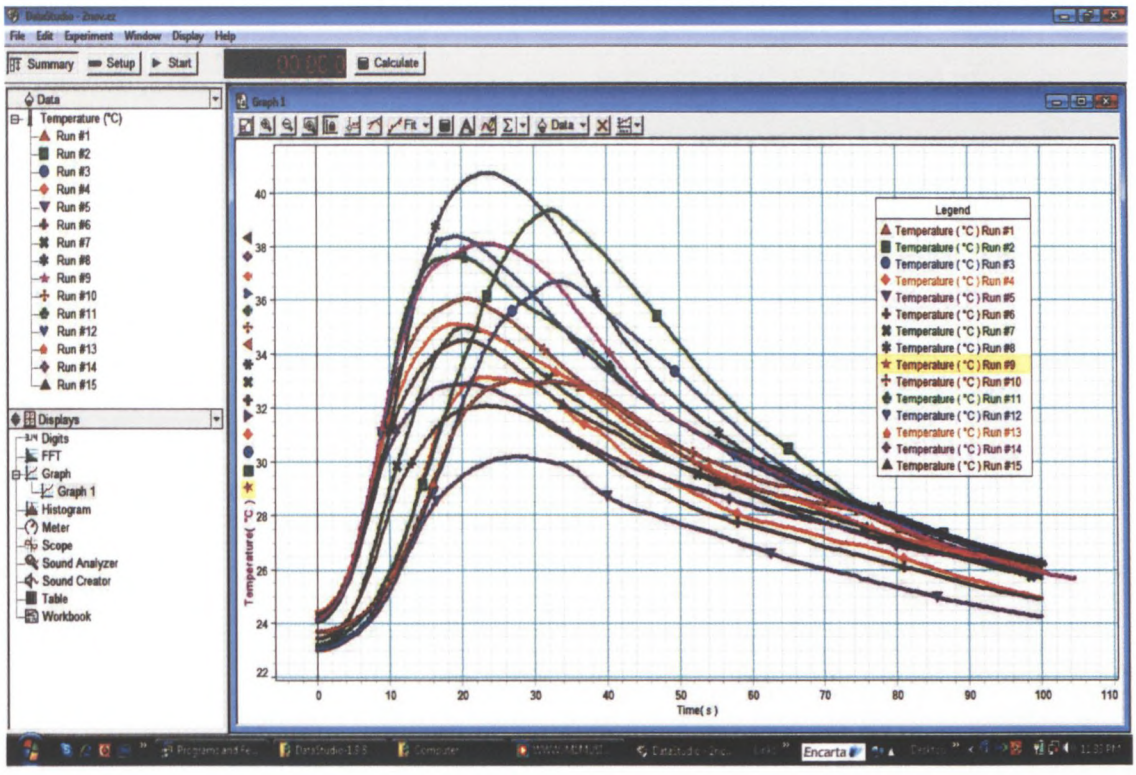

Figure 3.26: Overview of heating curves with DataStudio® 1.9.8 (Release 2007)

The heating and cooling parameters are found by curve-fitting each plotted curve. Figures 3.27 and 3.28 below show respectively the heating and cooling parameters for the first test run. Results of the other 14 tests can be found in appendix B.

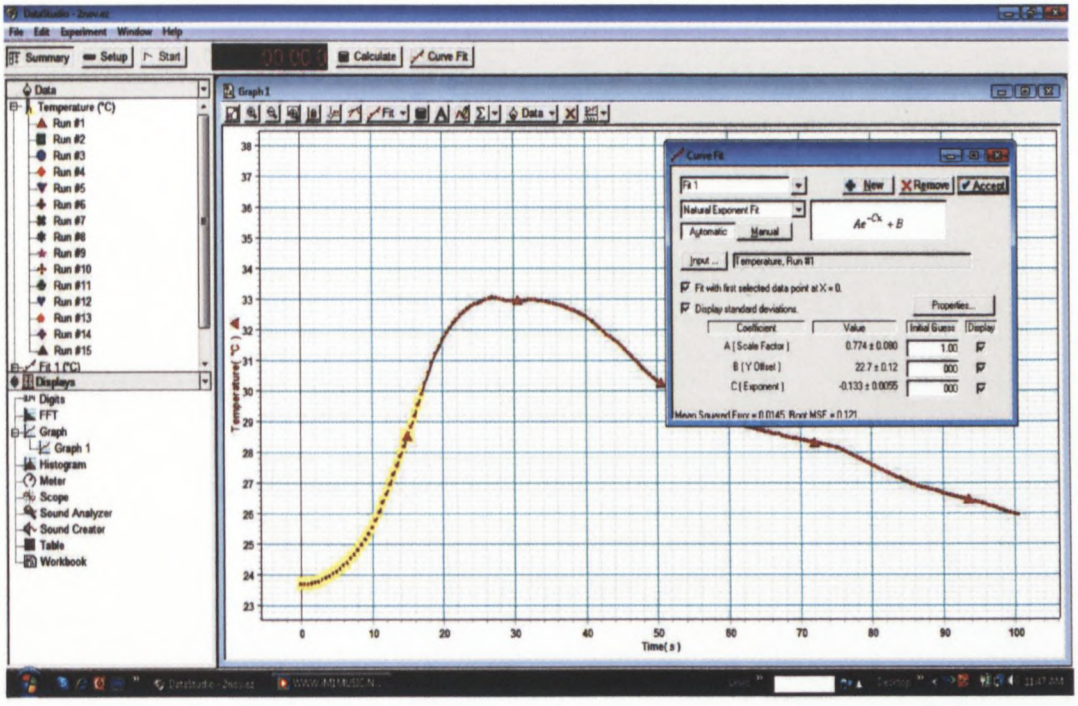

Figure 3.27: Heating curve-fit with DataStudio® 1.9.8 (Release 2007)

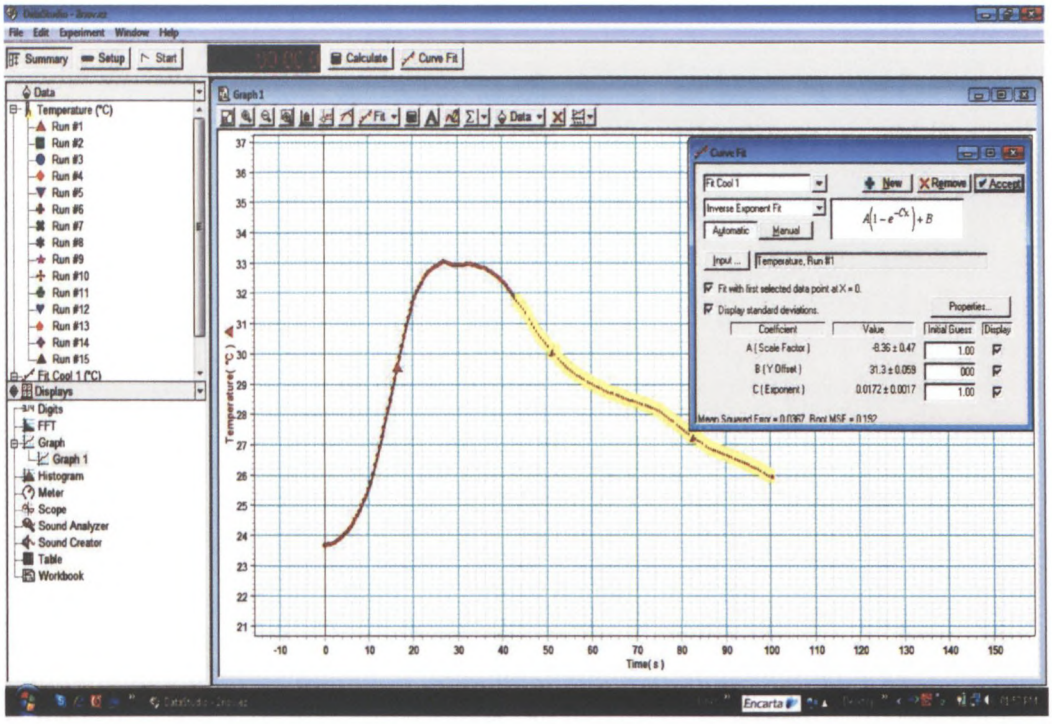

Figure 3.28: Cooling curve-fit with DataStudio® 1.9.8 (Release 2007)

The data logger GLX calculated the parameters for heating and cooling relations by curve-fit functions. After finding the average of each parameter (A, B and C) the phenomenal heating and cooling functions can be recorded (Figures 3.25 and 3.26).

Heating test results:

Table 3.6: Heating process results

Voltage	Test Number	Coefficient of scale factor A	Y-offset coefficient B	Exponent coefficient C
1.5V (2.5A)	Run #1	0.774	22.7	0.1330
	Run #2	1.960	20.8	0.0969
	Run #3	1.950	20.8	0.0891
	Run #4	0.661	22.1	0.1650
	Run #5	0.731	22.1	0.1420
5V (3A)	Run #6	0.739	22.5	0.2060
	Run #7	2.330	20.4	0.1270
	Run #8	3.100	20.7	0.1200
	Run #9	2.990	20.7	0.1370
	Run #10	2.580	21.3	0.1460
10V (4A)	Run #11	2.340	21.3	0.1560
	Run #12	2.660	21.1	0.1460
	Run #13	2.290	21.8	0.1500
	Run #14	1.820	22.1	0.1620
	Run #15	2.300	21.7	0.1440

Cooling test results:

Table 3.7: Cooling process results

Voltage	Test Number	Coefficient of scale factor A	Y-offset coefficient B	Exponent coefficient C
1.5V (2.5A)	Run #1	-8.360	31.3	0.0172
	Run #2	-13.50	37.5	0.0316
	Run #3	-11.40	35.1	0.0281
	Run #4	-8.14	30.7	0.0192
	Run #5	-8.86	28.8	0.0120
5V (3A)	Run #6	-7.36	30.7	0.0199
	Run #7	-9.33	32.5	0.0193
	Run #8	-11.00	36.3	0.0355
	Run #9	-11.20	34.4	0.0229
	Run #10	-12.80	33.0	0.0126
10V (4A)	Run #11	-13.80	35.3	0.0166
	Run #12	-11.10	35.4	0.0380
	Run #13	-9.28	33.0	0.0214
	Run #14	-7.68	31.5	0.0184
	Run #15	-9.44	32.5	0.0181

Considering the data in the above table, we can calculate the average value of each coefficient:

Table 3.8: Heating and cooling results

Voltage	Heating			Cooling		
	Average Coefficient of scale factor A	Average Y-offset coefficient B	Average Exponent coefficient C	Average Coefficient of scale factor A	Average Y-offset coefficient B	Average Exponent coefficient C
1.5V(2.5A)	1.215	21.70	0.1252	-10.052	32.68	0.0216
5V (3A)	2.348	21.12	0.1472	-10.432	33.38	0.0220
10V (4A)	2.282	21.60	0.1516	-10.260	33.54	0.0225

Thus, from the above table, the average equations of heating and cooling processes can be written as follow:

$$T_{1.5V,heat} = 1.215e^{0.1252t} + 21.7 \quad (3.47)$$

$$T_{5V,heat} = 2.348e^{0.1472t} + 21.12 \quad (3.48)$$

$$T_{10V,heat} = 2.2282e^{0.1516t} + 21.6 \quad (3.49)$$

$$T_{1.5V,cool} = -10.052(1 - e^{-0.0216t}) + 32.68 \quad (3.50)$$

$$T_{5V,cool} = -10.432(1 - e^{-0.0220t}) + 33.38 \quad (3.51)$$

(3.52)

These functions are visualised with Matlab® as followed:

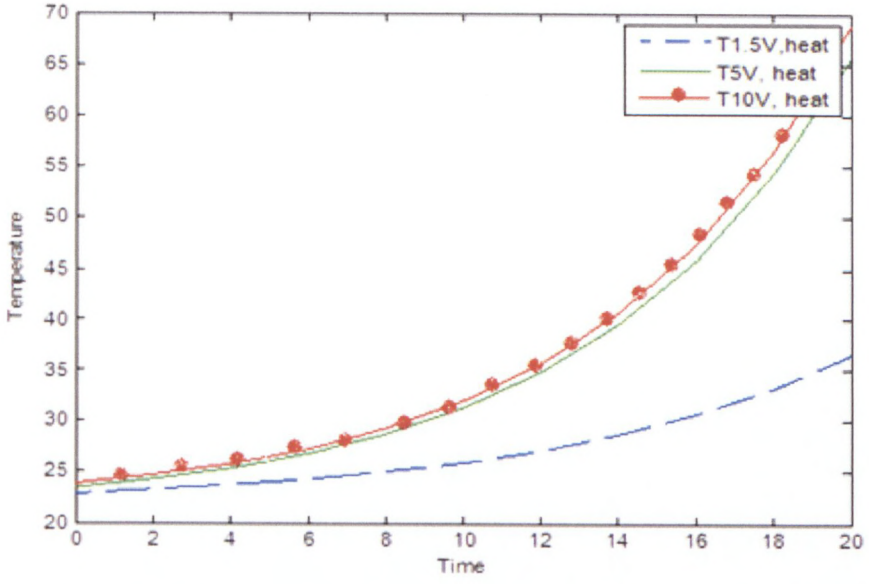

Figure 3.29: Heating curves at different voltages (Temperature in ^{0}C, Time in second)

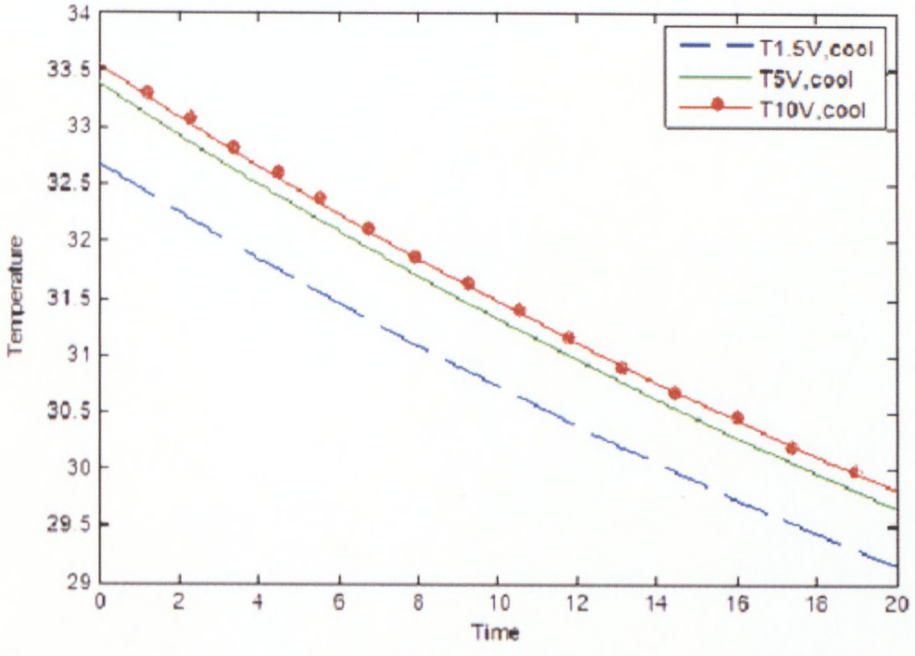

Figure 3.30: Cooling curves at different voltages (Temperature in ^{0}C, Time in second)

3.14 Summary

A model of the Nickel-Titanium actuators has been developed that includes the change in free length of the wires due to phase transformation. By using this model, Nickel-Titanium wires can be finely designed according to the force and displacement requirements. This greatly expands the positive potential for Nickel-Titanium actuators. Normally, actuators need gears or transmissions to match the impedance of the load, frequently making the actuator system bulky and cumbersome. But Nickel-Titanium actuators can be tuned to match the load by changing the shape and the annealing temperature of the wires.

The speed response of the actuators varies depending on the electric current applied to the SMA wires.

The average pull force exerted by each artificial muscle is 5.90N (necessary to hold an object with sufficient grasping force), with an average stroke of 23.5mm (necessary to bend the finger completely). As all fingers are connected to Nickel-Titanium actuators of the same size, this experiment has been conducted on one finger, thus the result will be the same for all other fingers.

Chapter Four

Rapid Prototype Manufacturing of the Artificial Hand

4.1 Introduction

In this chapter, we describe the 'Rapid Prototyping' (RP) process of efficiently designing and modelling the SMA actuated hand, a 'Rapidly Prototyped' hand with five fingers connected to a palm and forearm. Four fingers are composed of three connected cylindrical links except the thumb which has two links, and each finger is to be attached to the palm by modifying spherical joints. Finally, this chapter delineates the procedures for operating the SMA actuated hand, and present an anatomical comparison to the human hand.

4.2 Rapid Prototyping Techniques

Rapid prototyping techniques are modern techniques of building a full-scale of a working model for study, testing or display in order to save time of modifications of drawings to the original shape based on a Computer Aided Design (CAD) model of the item.

The prototype to manufacture is first designed as a CAD model using SolidWorks (details of drawing are found in Appendix A on page 79); this helps to check the substantiation of product designs (motion simulations, collision analysis, and early detection of design errors).

The Adaptronics AMTL (Adaptronics Advanced Manufacturing Technology Laboratory) at the Cape Peninsula University of Technology is equipped with Rapid Prototyping Manufacturing Machines: a Laminated Object Manufacturing Machine; a 3D printer dimensions SST (Soluble Support Technology); a Z-Corp Printer 310 Plus; and CNC Machines.

A professional 3D Dimensions SST printer was used to build the prototype parts for this project.

The Rapid Prototyping process begins with the development of CAD solid models, made for this project using SolidWorks, a CAD software package. Upon completion, the solid model is converted under SLT file, and then exported to the 3D Dimensions SST printer for fabrication, as shown in Figure 4.1.

Figure 4.1: 3D Dimensions SST 1200 Printer (Adaptronics AMTL)

4.3 Rapidly Prototyped Artificial Hand

One of the crucial steps in the fabricating of an artificial hand prototype is the successful fabrication of the joints. Therefore, an important design consideration in this robotic hand prototype is to adhere to the same range of motion and size similar

to that of an average human hand. Furthermore, no lubrication is needed because the material used for building the assembly joints, Acrylonitrile Butadiene Styrene (ABS) plastics, allows for good finger mobility because of proper joint clearances. Even so, while the joints move freely with little friction, it is certainly possible that over time some wearing may occur and consequently, metal inserts may be necessary for future joints. However, to date, this has not been a problem and no maintenance is required. The lifetime of the material of the prototype hand is anticipated to be similar to that of traditional plastic parts.

4.3.1 Fabrication Materials

Solid models are exported to the 3D printer Dimension SST which impresses models into ABS plastics, a thermoplastic with chemical formula: $(C_8H_8)_x \cdot (C_4H_6)_y \cdot (C_3H_3N)_z$. ABS plastics can be used between –25 and 60°C as its mechanical properties vary with temperature (Harper, 1975:1-3).

The most important mechanical properties of ABS plastics are its impact resistance and toughness. Table 4.1 below shows thermo-mechanical properties of ABS plastics.

Table 4.1 Mechanical properties of ABS plastic (Harper, 1975:62)

Properties of ABS plastic (P400)	
Elastic Modulus	2.10^9 N/m^2
Poisson's Ratio	0.394 N/A
Shear Modulus	3189.10^5 N/m^2
Density	1020 kg/m^3
Tensile Strength	3.10^7 N/m^2
Thermal Expansion Coefficient in X	5.2e-005/K
Thermal Conductivity	0.2256 W/(m.K)
Specific Heat	1386 J/(kg.K)
Melting point	105^{0}C

4.3.2 3D Models Printing

The Dimension SST 1200 3D Printer uses a Fused Deposition Modelling (FDM) process to render 3Dimensional models in ABS plastic. The sources for these models are .STL files--exported from most major 3D modelling applications--which is a format used by stereo-lithography software to generate information needed to produce 3D models on the 3D Dimensions SST.

Figures 4.2, 4.3, 4.4, 4.5 and 4.6 show settings of the printing parameters (i.e. build orientation of layers, views and scale).

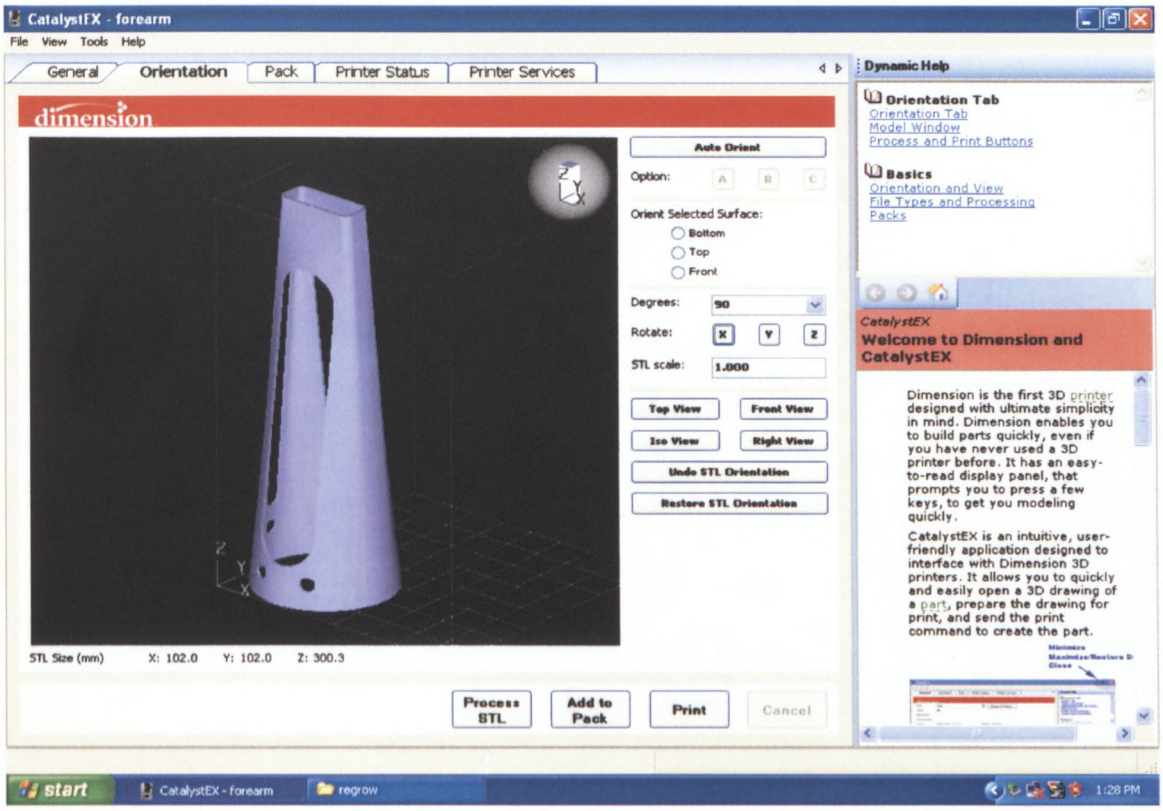

Figure 4.2: Printing process on the 3D printer Dimension SST

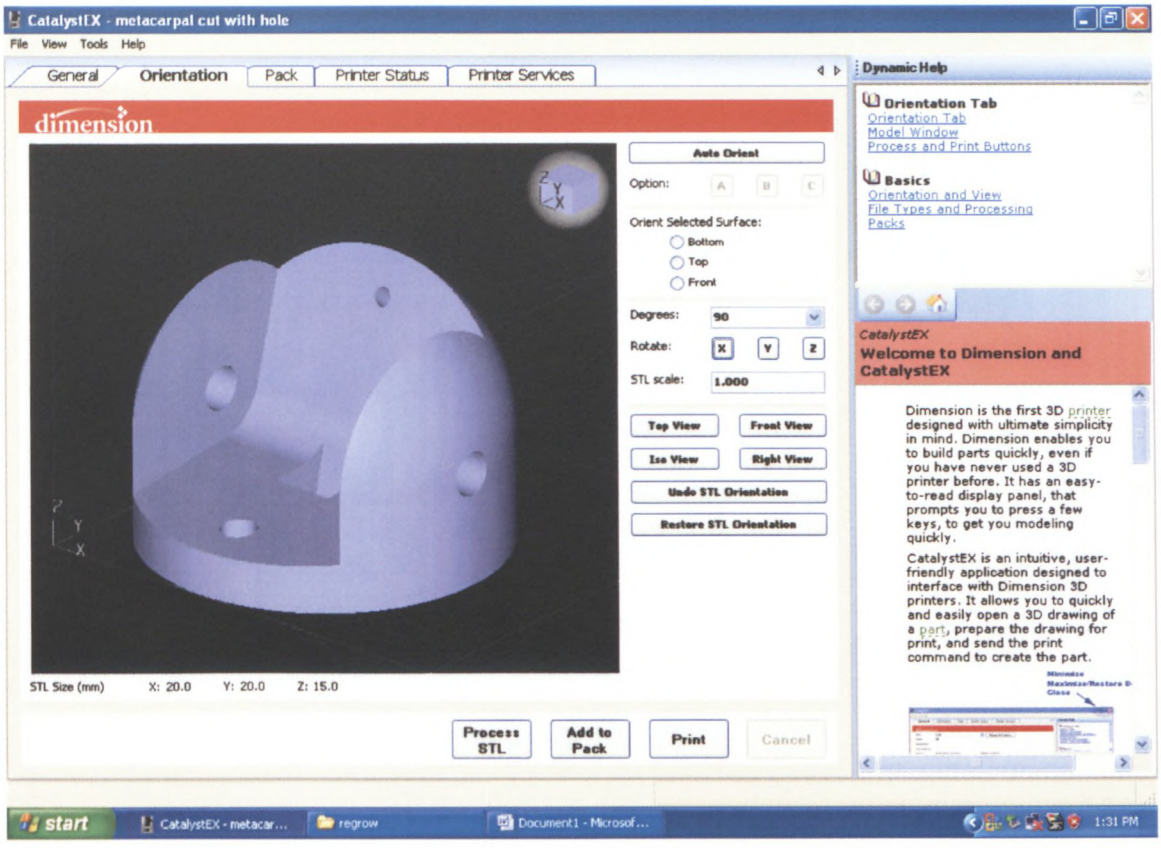

Figure 4.3 View of the MCP joint before printing

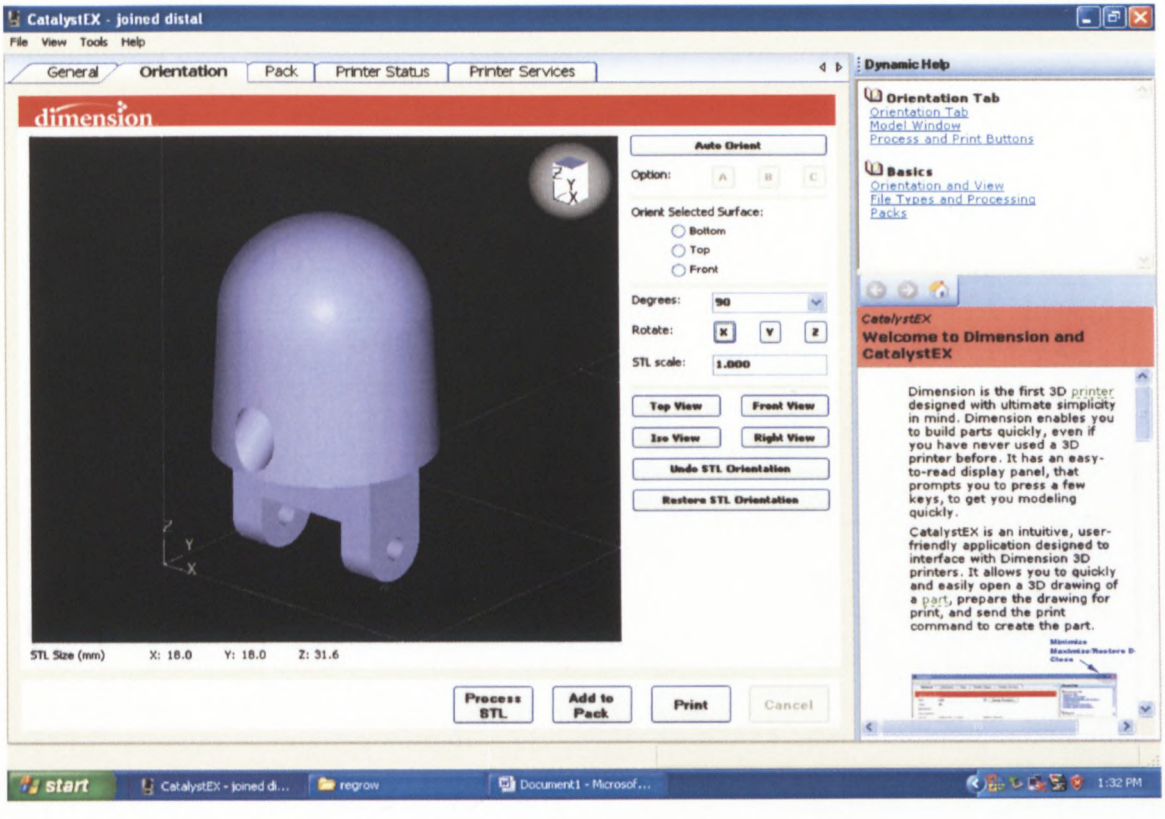

Figure 4.4: View of the Distal joint before printing

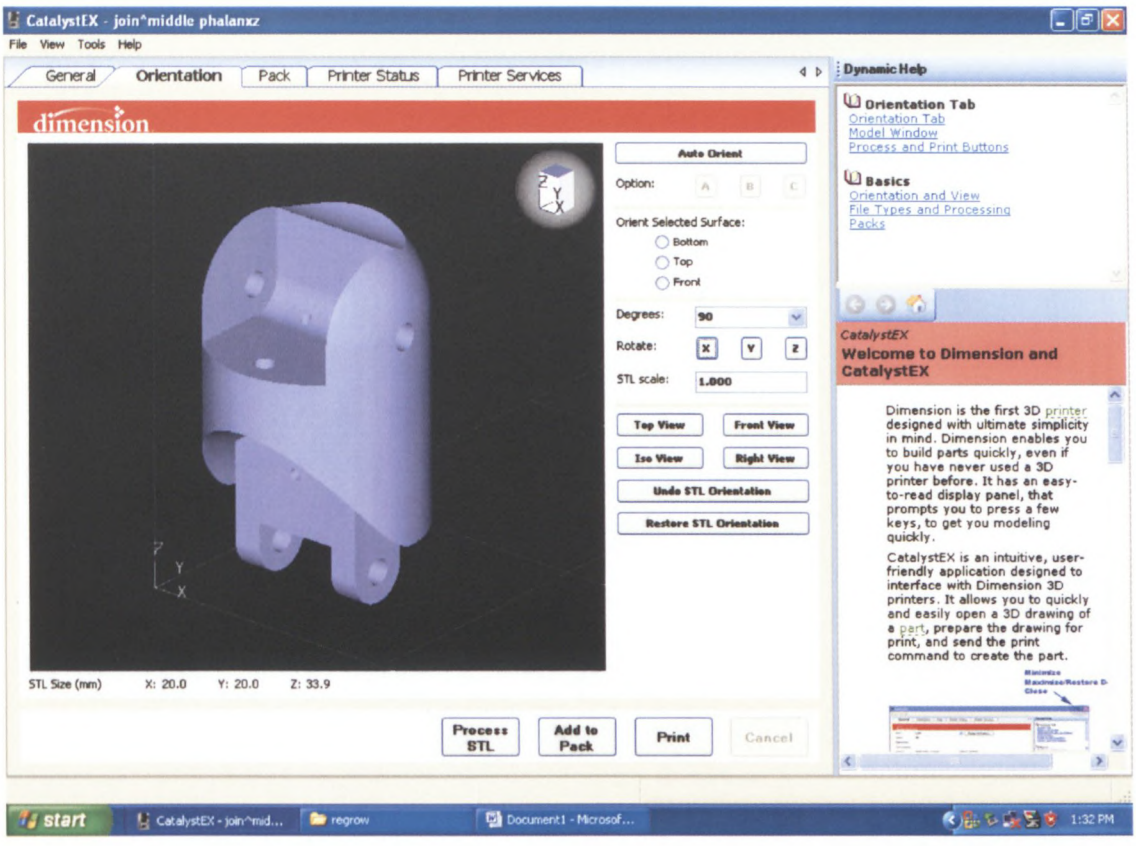

Figure 4.5: View of the middle phalanx joint before printing

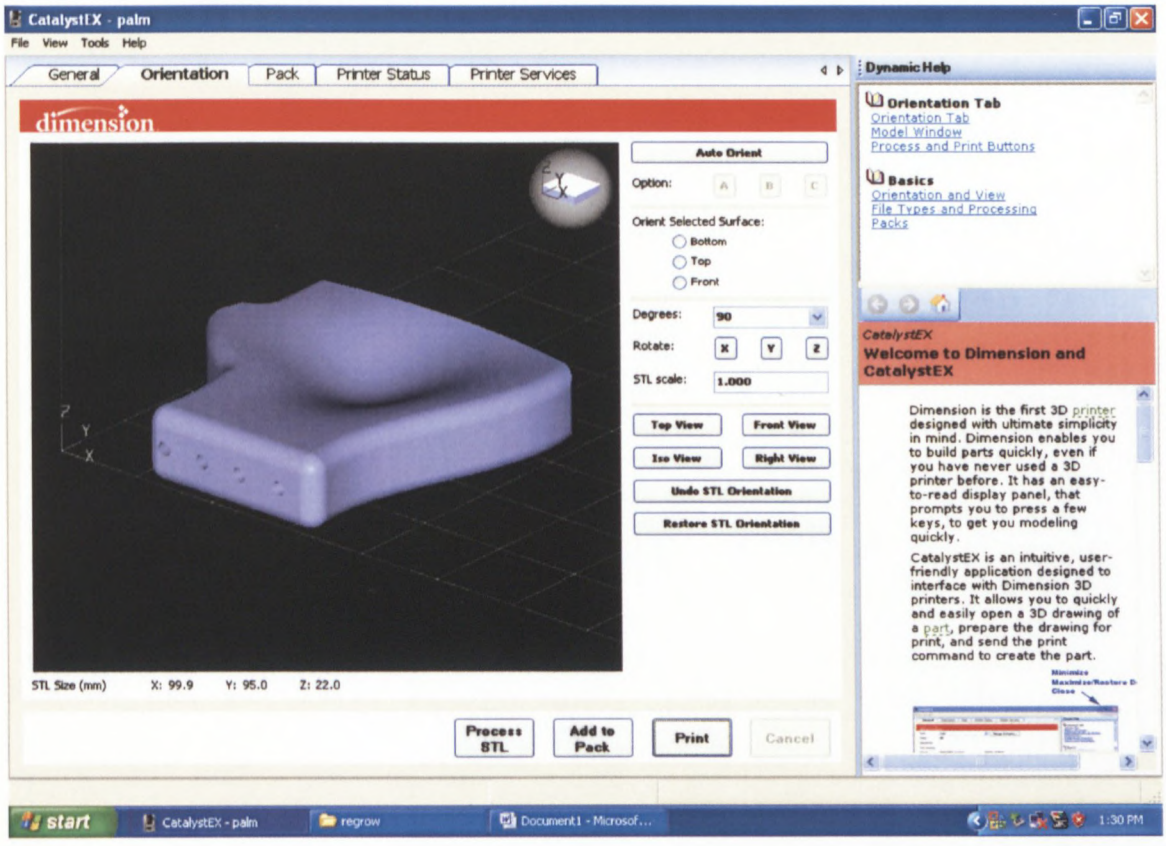

Figure 4.6: View of the palm before printing

After hours of printing, contingent upon on the size and shape of individual models, the models made of ABS plastic are placed into an SST Station to remove the support material. An SST Station is an agitation system that utilises hot water and a soap bath (soluble concentrate P400SC) in a sink to automatically wash away the support structures (see Figure 4.7).

Figure 4.7: SST Station sink for washing away the support material from the palm

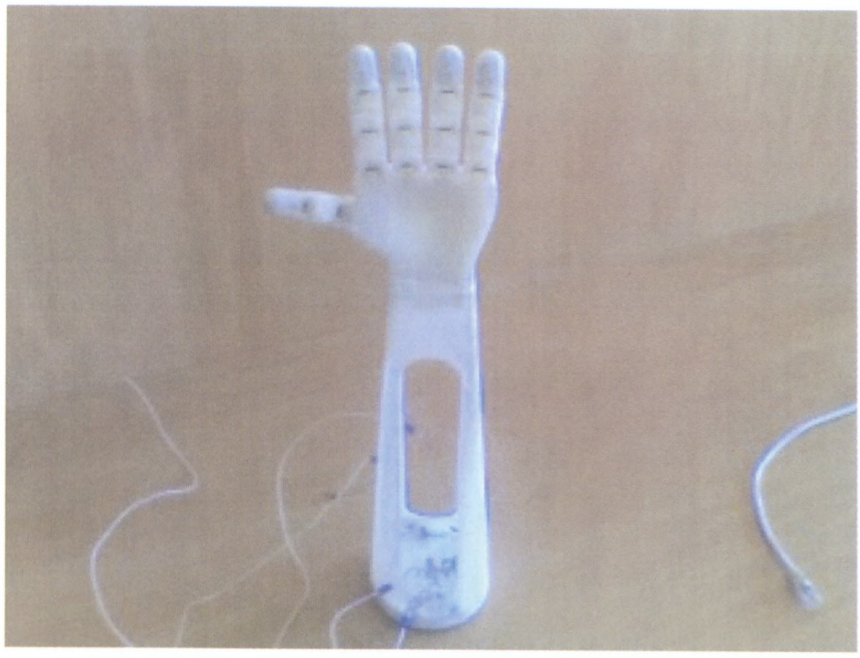

Figure 4.8: View of the whole hand assembled after printing

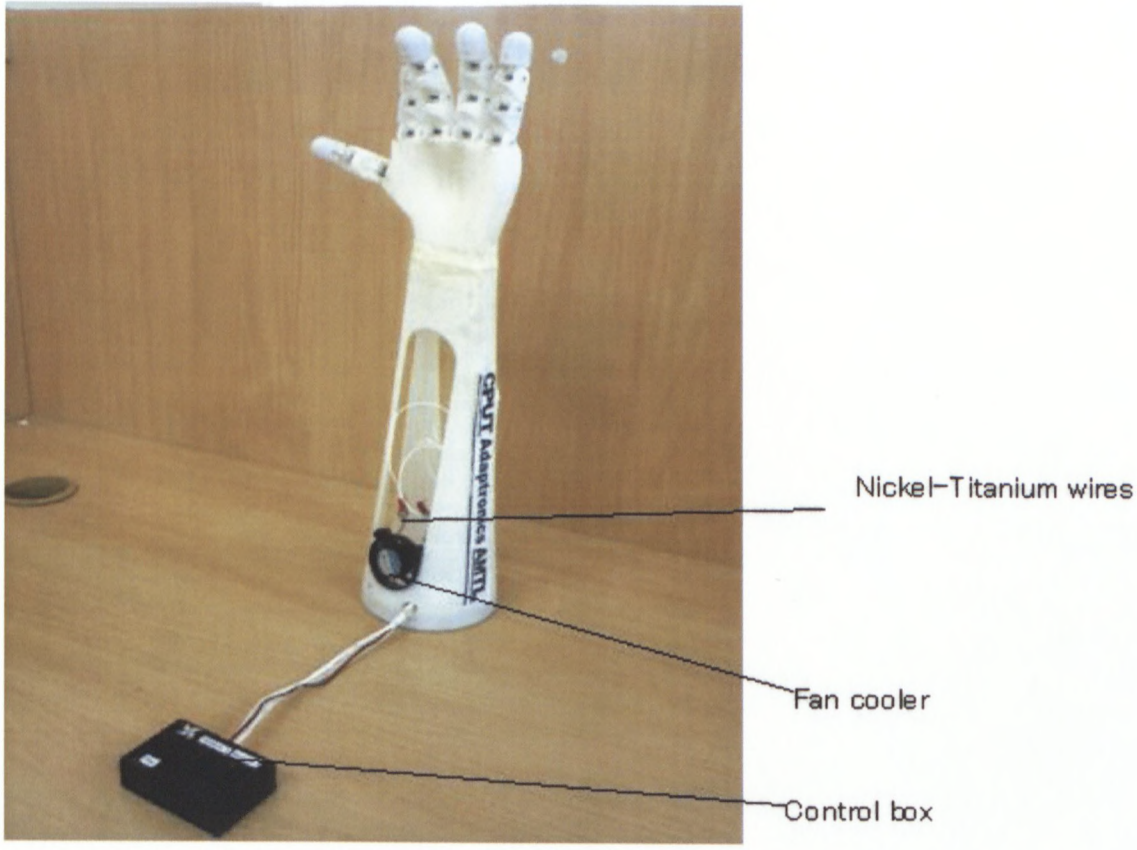

Figure 4.9: View of the whole hand

Figure 4 11 below shows the integration of the fan and actuators inside the forearm.

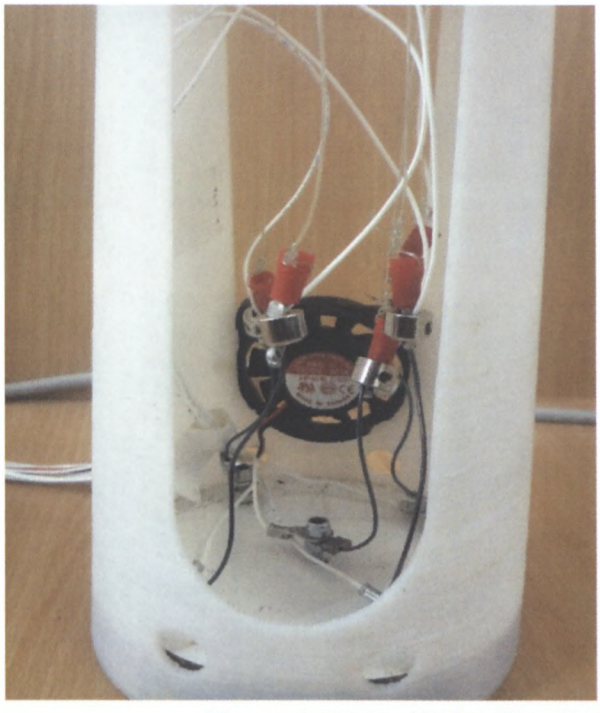

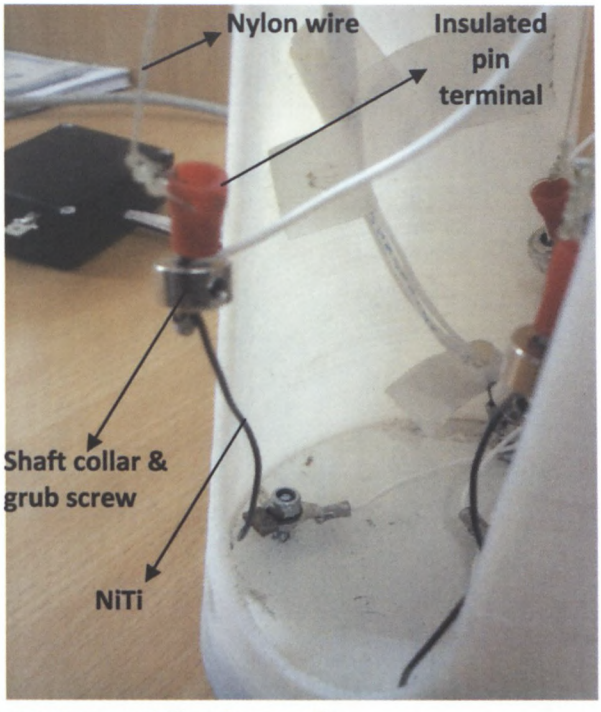

Figure 4.10&11: Nickel-Titanium actuators and Fan integration

4.4 Operating Procedure

A combination of electric voltages supplied to each muscle enables the actuation the shape memory alloy hand, mimicking the desired gesture of a human hand.

The fingers of the hand can move independently, according to need. Either one finger can bend or all fingers can bend uniformly to grip and grab an object.

The combination of each switch, either at ON or OFF, works as a matrix of five elements (switches) in a variety of either ON or OFF combinations, in different orders and arrangements, resulting in countless gestures.

Figures 4.11 & 12: Gesture of the hand (all fingers bent)

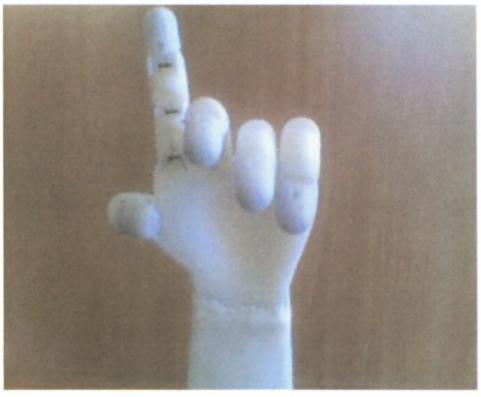

Figures 4.13 & 14: Human-like gestures

4.5 Anthropometric Comparison of the Artificial Hand vs. the Actual Human Hand

Table 4.2 establishes an anthropometric comparison of the artificial hand vs. the actual human hand.

Table 4.2: Anthropometric measurement comparison between the human hand and SMA actuated hand

Measures of comparison	Human hand	SMA actuated hand
Number of articulated parts	>30	15
Number of fingers	5	5
Number of finger joints	3	3
Motion ability of fingers	Sequential and uniform motion	Sequential motion
Actuators	muscles, tendons	SMA wires, Nylon strings and the springs in the joints
Location of actuators	Muscles in the forearm, tendons in the hand	SMA wires in the forearm, Nylon strings in the hand
Noise level (dB)	0	0
Components of fingers	Distal phalanx, middle phalanx and proximal phalanx	Distal phalanx, middle phalanx and proximal phalanx

Chapter Five

Conclusion

5.1 Summary

The work presented in this document encompasses the task of developing a prototype of an artificial hand using Nickel-Titanium wires as fingers' actuators. SMAs were chosen for two primary reasons: firstly, they have a high energy density compared to other materials. Nickel-Titanium has been chosen as suitable actuator based on:

- Tight places utilisation– Nickel-Titanium actuator wires are smaller by far than alternatives. At least 1000 times smaller than solenoids for the same work done;

- Design simplification– Nickel-Titanium actuator wires can often be used "as is", eliminating gearboxes, housings, bearings, and so on. Their flexible forgiving performance is easier to work with;

- In corrosive environments– Nickel-Titanium actuator wires' high corrosion resistance really pays off;

- For noise levels reduction– Nickel-Titanium actuator wires' movement by molecular restructuring is acoustically quiet;

- Lower costs – Nickel-Titanium actuator wires are inexpensive and cost less to use in many applications and;

- Actuation longevity: At stresses below 103MPa, permanent strain will remain less than 0.5% strain even after hundreds of thousands of cycles. At 138MPa, 1% permanent strain will occur after 100,000 cycles.

These above listed facts justify the choice of Nickel-Titanium actuators

This work entailed the manufacture of a 5-fingered artificial hand, dexterously and anatomically similar to a human hand, with SMA as artificial muscles. Industrially, this device may be used for the following applications, among others: space aeronautics (remote controlled manipulator arm mounted on an unmanned rover for space exploration); oceanography (undersea exploration); military (bomb defusing arm mounted on a remote controlled rover); and nuclear (radioactive environment manipulation). The goal was to develop a bio-mimetic, ultra-lightweight hand, with a sufficient number of degrees-of-freedom to enable the application of substantial forces on each finger. Additional design requirements included fast fabrication times, noiseless operation and easy replacement of components.

Finally, Rapid Prototyping techniques are used to print the 3D model of the hand into ABS plastics allowing for the fabrication of the hand in a very short time. Because of the speed and ease of this type of manufacturing, replacing one malfunctioning part, or even a complete hand, is quite executable. As a result of these ABS plastics, the weight of the hand is reduced and the bulkiness common to other artificial hands is reduced, and in fact, virtually eliminated.

5.2 Contribution

Even though the applications of such an artificial hand for robotics and prosthetic uses are quite different, the mechanical design for both is similar. This work has followed an anatomical approach of actuation based on artificial muscles mounted to a forearm, triggering nylon strings to actuate fingers.

Many researchers have investigated the use of Nickel-Titanium (straight long wires) as actuators, but in reducing the length of wires by a pre-training process which allows the actuators to adopt the spring shape when contracting, this study has been unique in the sense that the studies of others have been based on investigations of long wires that contract by heat treatment without previous training.

5.3 Recommendations

This project was based on the application of SMAs to perform actuation of fingers for a prototype of an artificial hand. The actuation system was assisted by a set of switches operated manually.

Future work will involve the performance of power supply autonomy, actuation control commands, the minimisation of the actuation time for both bending and straightening of fingers and an artificial resin skin to cover the entire hand with bones shaped joints can be envisaged.

REFERENCES

Atkins, D.J., Heard, D.C.Y. & Donovan, W.H. 1996, "Epidemiologic overview of individuals with upper-limb loss and their reported research priorities", *Journal of Prosthetics and Orthotics*, Vol. 8, no. 1, pp. 2-11.

Banks, J.L. 2001, *Design and Control of an Anthropomorphic Robotic Finger with Multi-point Tactile Sensation*, Technical Report, AITR–2001–005, MIT Artificial Limb Lab, Massachusetts Institute of Technology, Department of Electrical Engineering and Computer Science, Boston, MA.

Brinson, L.C. 1993, "One-dimensional constitutive behaviour of shape memory alloys: thermo-mechanical derivation with non-constant material functions and redefined martensite internal variable". *Journal of Intelligent Materials Systems and Structures,* vol.4, pp. 229–242.

Britt M., Ellen L. & Thomas H. "The History of Prosthetic Devices". [Online] downloaded on March 10th 2010. http://www.unc.edu/~mbritt/Prosthetics%20History%20Webpage%20-%20Phys24.html.

Carroll, K. & Edelstein, J.E. (eds). 2006, *Prosthetics and patient management: a comprehensive clinical approach.* SLACK Incorporated, New Jersey, pp. 79–266.

Elahinia, M.H. & Ahmadian, M. 2005, "An enhanced SMA phenomenological model: The shortcomings of the existing models*". Journal of Smart Materials and Structures.* Vol. 14, pp. 1297-1308.

Guey, B.L. 2009, *An Intelligent Prosthetic Hand Using Hybrid Actuation and Myoelectric Control.* PhD thesis, School of Mechanical Engineering, University of Leeds. United Kingdom.

Harper, C.A. 1975, *Handbook of plastic and elastomers*, McGraw-Hill, New York, pp. 1-3, 1-62, 2-42, 3-1.

Incropera, F.P. & DeWitt, D.P. 2001, *Fundamentals of Heat and Mass Transfer*, 5th ed. Wiley, New York, NY.

Kargov, A., Pylatiuk, C., Martin, J., Schulz, S. & D¨oderlein L.A. 2004, "Comparison of the grip force distribution in natural hands and in prosthetic hands", *Disability and Rehabilitation*, Taylor & Francis Ltd., UK, Vol. 12 no.26, pp. 705–711.

Kargov, A., Werner, T., Pylatiuk, C. & Schulz, S. 2008, "Development of a miniaturised hydraulic actuation system for artificial hands", *Sensors and Actuators, A: Physical,* Vol. 141, no. 2, pp. 548-557.

Kyberd, P.J. 2004, Research and the Future in Myoelectric Prosthetics, in Ashok Muzumdar (ed.), *Powered Upper Limb Prostheses: Control, Implementation and Clinical Application*, Springer, Berlin, pp. 175–190.

Lagoudas D.C. & Shu S.G. 1997, "Modeling flexible beam actuated by shape memory alloy wires", *Journal of Smart Materials and Structures*, Vol. 6, pp. 256-277.

Lagoudas D.C., Webb, G.V. & Kulkarni, M. 1999, "Adaptive shape control for an SMA-actuated aerofoil rib structure*". In Proceedings of IMCE '99, ASME International Mechanical Engineering congress and Exposition, November 14-19, 1999*, Nashville, Tennessee. USA.

Lagoudas D.C., Zhonghe B., Qidwai A.M. & Entchev. P.B. 2003, SMA_UM: User Material Subroutine for Thermomechanical Constitutive Model of Shape Memory Alloys. Department Aerospace Engineering Texas A&M University, College Station, TX, pp. 8.

Lagoudas, D.C., Zhonghe, B., Muhammad, A.Q. & Pavlin, B.E. 2003, *SMA_UM: User Material Subroutine for Thermomechanical Constitutive Model of Shape Memory Alloys*, Department of Space Engineering, Texas A&M University, pp. 8-12.

Lederlé, S. 2002, *Issue of the design of shape memory alloy actuators.* Master of Science thesis, Massachusetts Institute of Technology, Department of Aeronautics and Astronautics, USA.

Liang, C. 1990, *The constitutive modelling of shape memory alloys.* PhD thesis Virginia Tech, Blacksburg, VA.

Philander, O. 2005, *The Development of a Computational Design Tool for uses in the design of Actuator Systems consisting of NiTi Shape Memory Alloy Wires Harnessing the Shape Memory Effect.* Doctor of Technology thesis, Peninsula Technikon, South Africa.

Schuerch, H.U. 1968, *Certain Physical Properties and Applications of Nitinol.* Report No. ARC-R-280 prepared under contract NAS7-426 Mod 2 Astro-Research Corporation at the

National Aeronautics and Space Administration NASA, Santa Barbara, California, USA, pp. 6-7, 8-9.

Shaw, J.A. 1997, *Material Instability In a Nickel-Titanium Shape Memory Alloy*, EMRL Report, Austen. Vol. 3, no. 97, pp. 2-18, 25.

Smith, S.A. & Hodgson, D.E. 2003, "Shape Setting Nitinol*". Proceedings from the Materials & Processes for Medical Devices Conference. 8-10 September 2003*, Anaheim, CA, USA.

Tanaka, Y. 1986, *A thermomechanical sketch of shape memory effects: One-dimensional tensile behaviour.* Res. Mechanica, Vol.18, pp. 251-263.

Thompson, S.A. 2000, "An overview of Nickel-Titanium alloys used in dentistry". *International Endodontic Journal, Vol.* 33, pp. 297-310.

Wang, F.E., Pickart S.J. & Alperin H.A. 1972, "Mechanism of the TiNi martensitic transformation and the crystal structures of TiNi-II and TiNi-III phases". *Journal of Applied Physics,* Vol. 43, pp. 97–112.

Waram, T.C. 1993, *Actuator design using Shape memory alloys.* Technical report, Mondotronics, Inc.

Warwick, K., Gasson, M., Hutt, B., Goodhew, I., Kyberd, P., Andrews, B., Teddy, P. & Shad, A. 2003, "The Application of Implant Technology for Cybernetic Systems", *Archives of Neurology*, Vol. 10, no. 60, pp. 1369-1373.

Warwick, K., Gasson, M., Hutt, B., Goodhew, I., Kyberd, P., Schulzrinne, H. & Wu, X. 2004, "Thought Communication and Control: A First Step using Radiotelegraphy", *IEE Proceedings on Communications*, Vol. 3, no. 151, pp. 185-189.

Warwick, K., Hutt, B., Gasson, M. & Goodhew, I. 2005, "An attempt to extend human sensory capabilities by means of implant technology", *Proceedings IEEE International Conference on Systems, Man and Cybernetics*, Hawaii, Vol. 10, no. 2, pp.1663-1668.

Warwick, K., Kyberd, P., Murgia, A., Gasson, M., Tjerks, T., Metcalf, C., Chappell, P., Lawson, S. & Barnhill, T. 2009, "Case studies to demonstrate the range of applications of the Southampton Hand Assessment Procedure", *British Journal of Occupational Therapy*, Vol. 5 no. 72, pp. 212-218.

Zhang, X.D., Liang C., & C.A. Rogers. 1987, "Modelling of two-way shape memory effect". *Journal of Intelligent Material Systems and structure,* Vol. 8, no. 4, pp. 353-362.

Nelson, D. L., "Tendon Laceration Page", [Online] Available: http://www.davidlnelson.md/Tendon_laceration.htm. Downloaded on March 15th, 2010.

Dynalloy price Guide: [Downloaded on March 15th, 2010] http://www.dynalloy.com/PriceGuide.php

Technical Characteristics of Flexinol Actuator Wires F1140Rev H [Online] Available: http://www.dynalloy.com/Technical_Characteristics_-_TCF1140.pdf [Downloaded on March 15th, 2010]

Appendix A

Drawings Design Datum

Appendix A regroups drawings details and design measurements of different parts of the prototype.

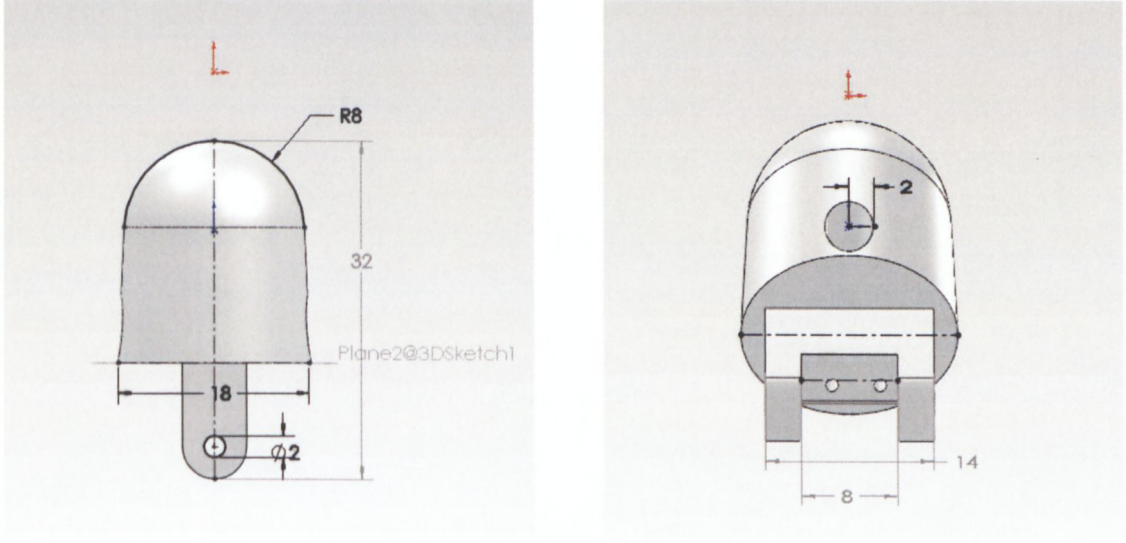

Figure A. 1& 2: Distal outer dimensions

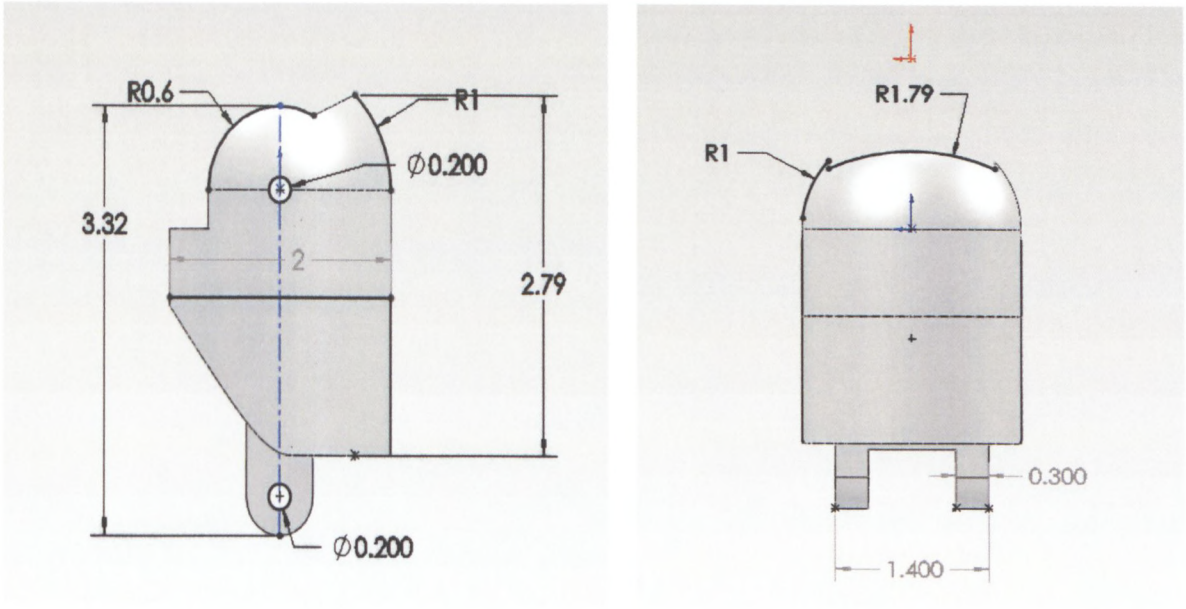

Figure A. 3&4: Proximal phalanx and Middle phalanx dimensions

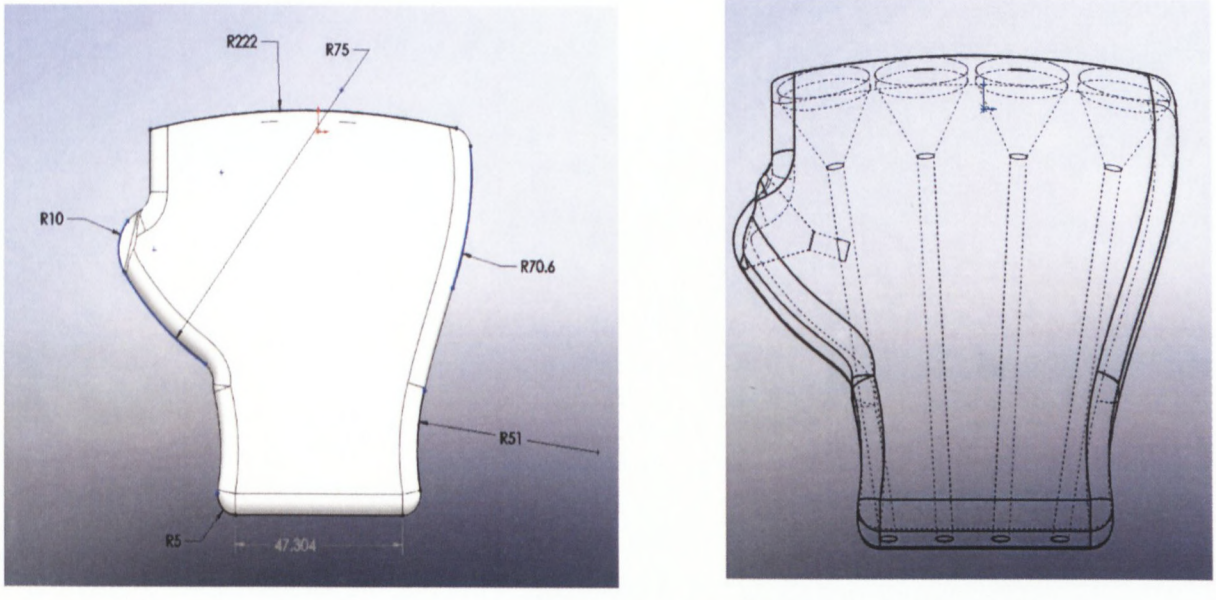

Figure A. 5&6: Palm dimensions and tubulation

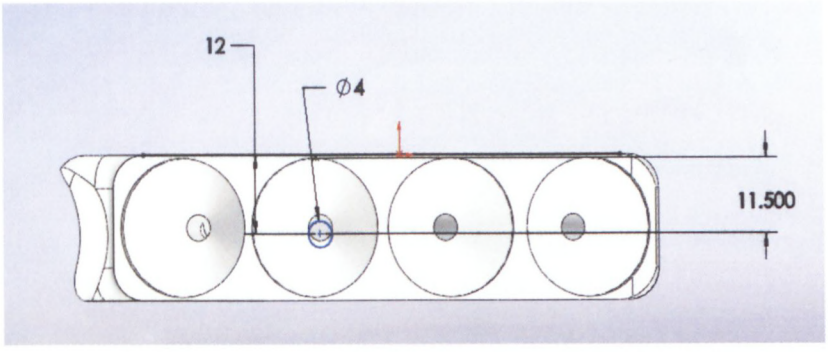

Figure A. 7: Palm top view dimensions

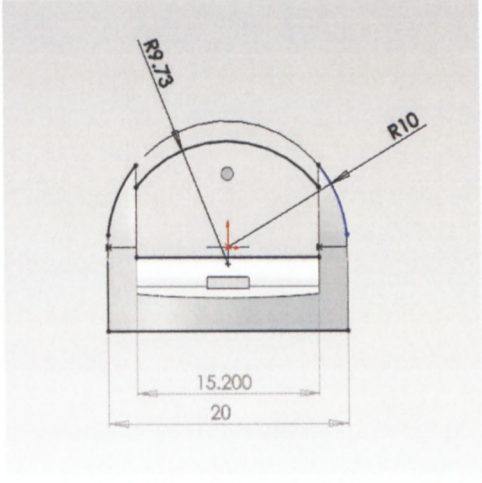

Figure A. 8: MCP phalanx dimensions

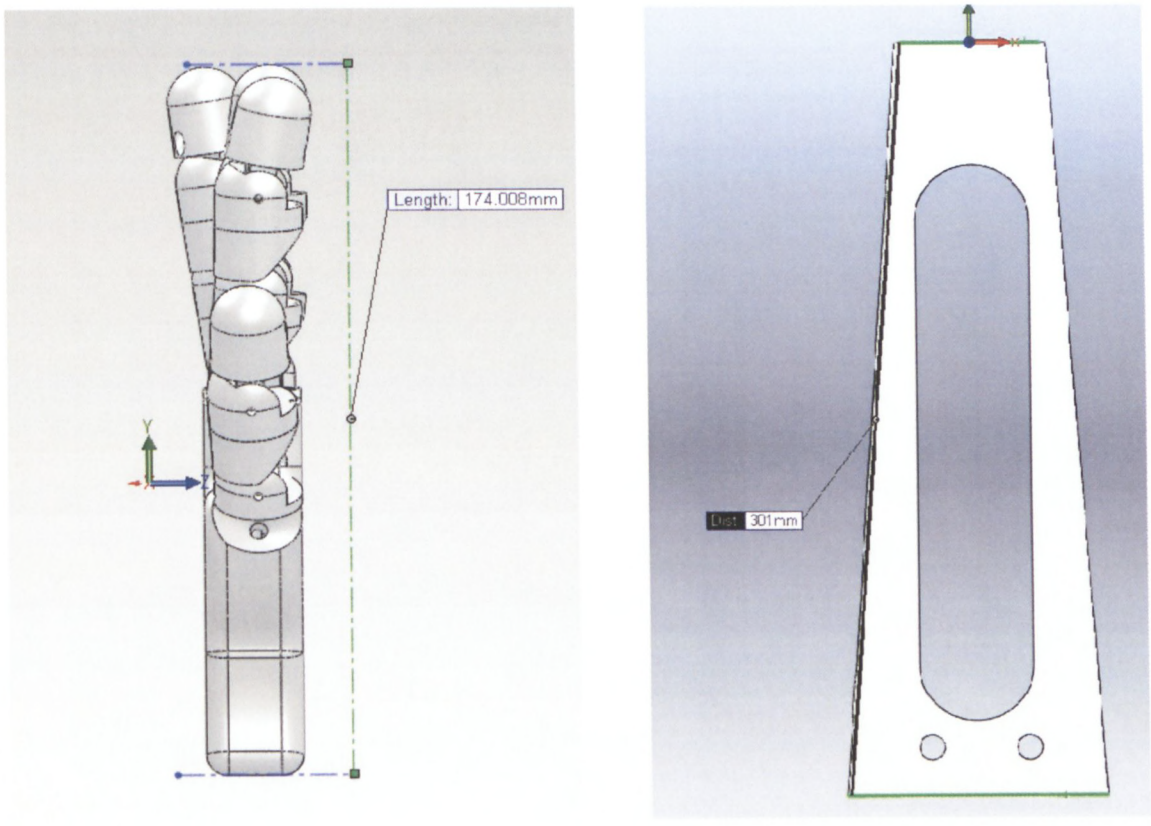

Figure A. 9&10: Hand assembly and forearm dimensions

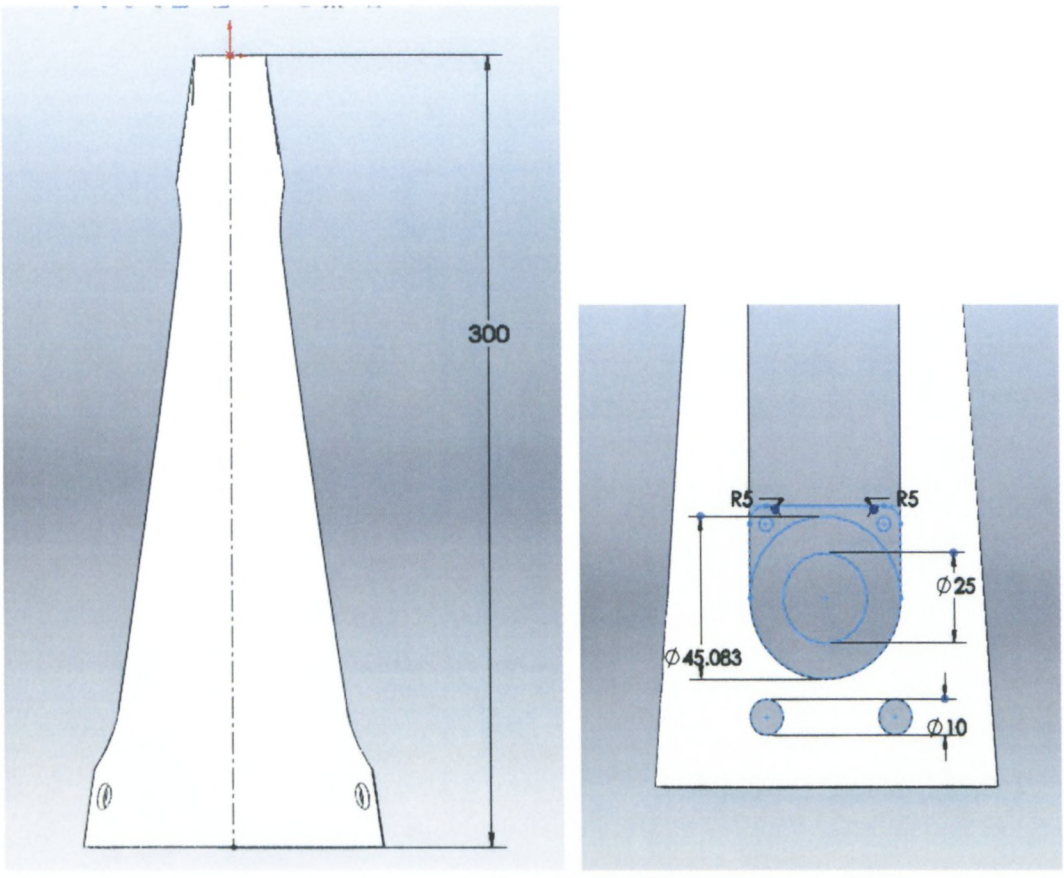

Figure A. 11&12: Forearm size and cooling fan emplacement dimensions

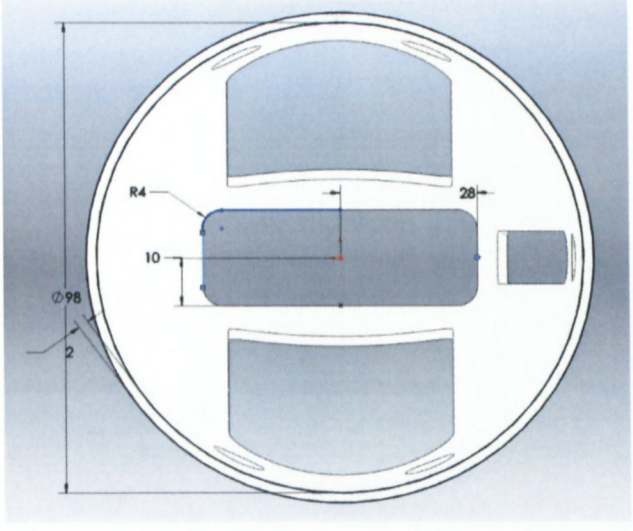

Figure A. 13: Forearm bottom view dimensions

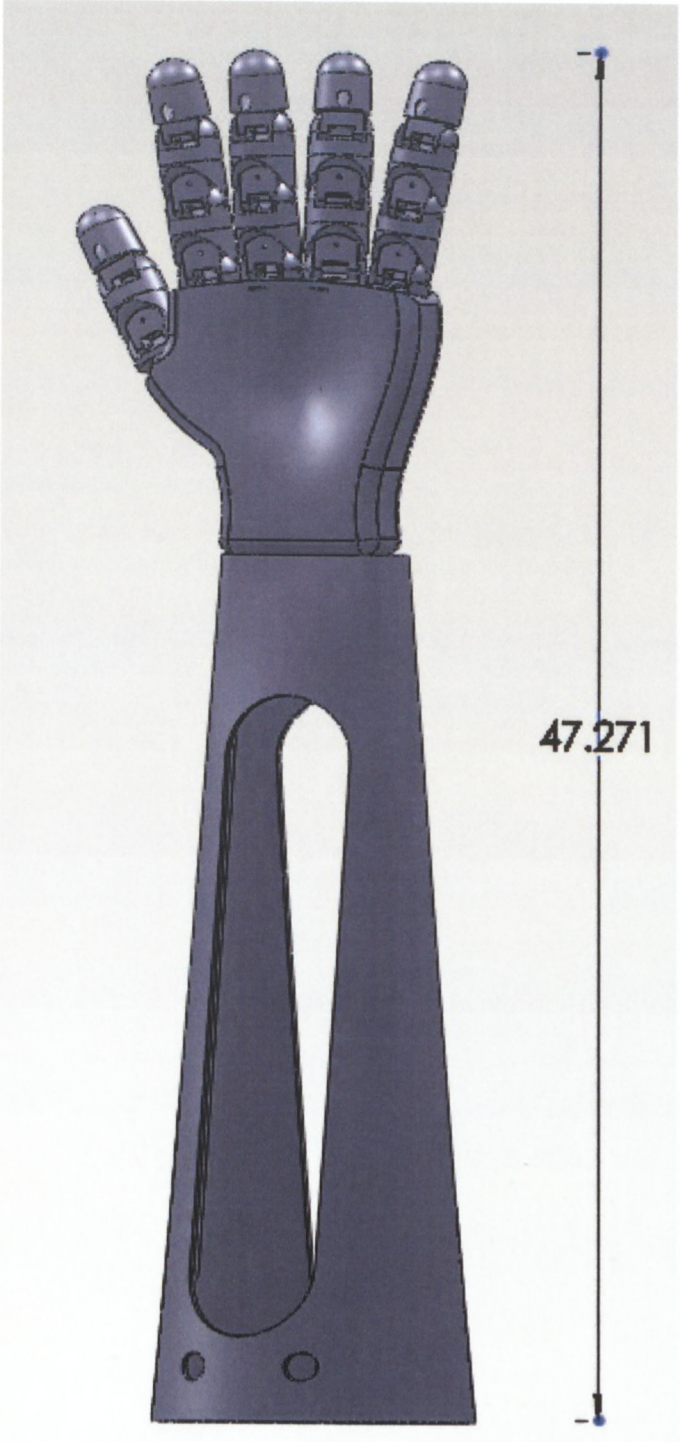

Figure A. 14: Overall assembly length

Appendix B

Heating and Cooling Curve-fitting Parameters as discussed in Chapter Three

The heating and cooling curve-fitting parameters (the coefficient of scale factor , the Y-offset coefficient , and the exponent coefficient) are found by curve-fitting each plotted curve with DataStudio® 1.9.8 (Release 2007).

1. Heating parameters

Run #2:

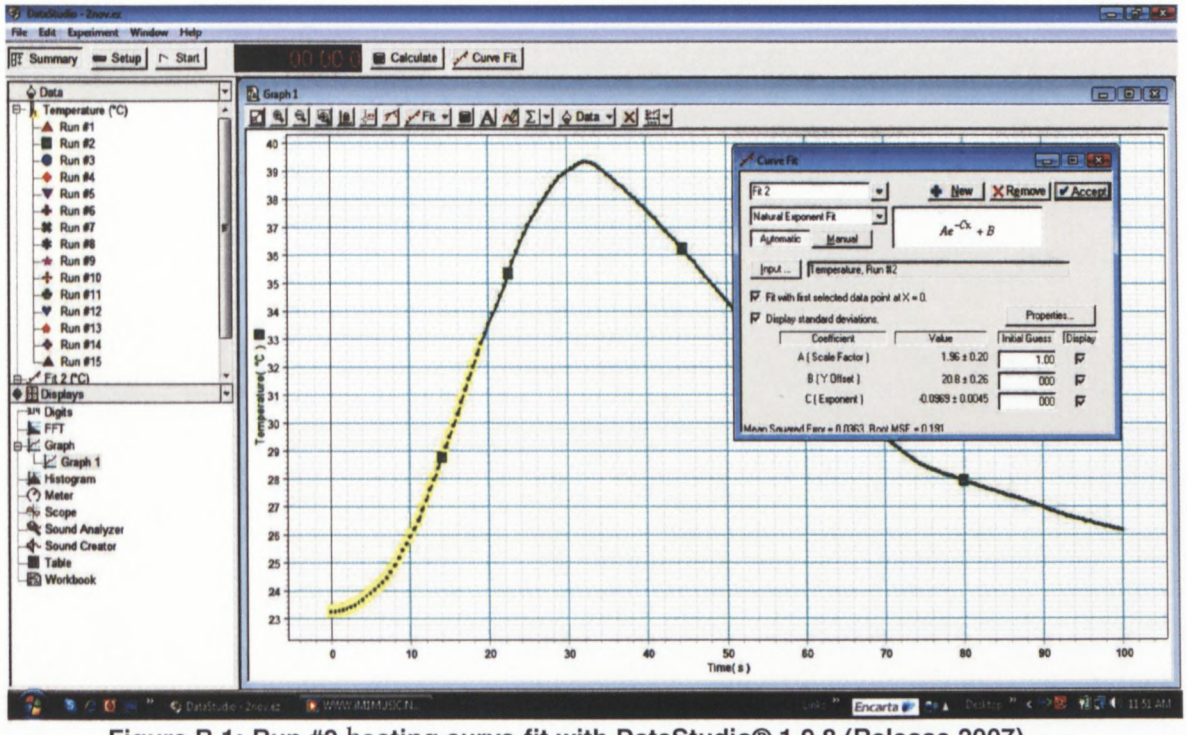

Figure B.1: Run #2 heating curve-fit with DataStudio® 1.9.8 (Release 2007)

Run #3:

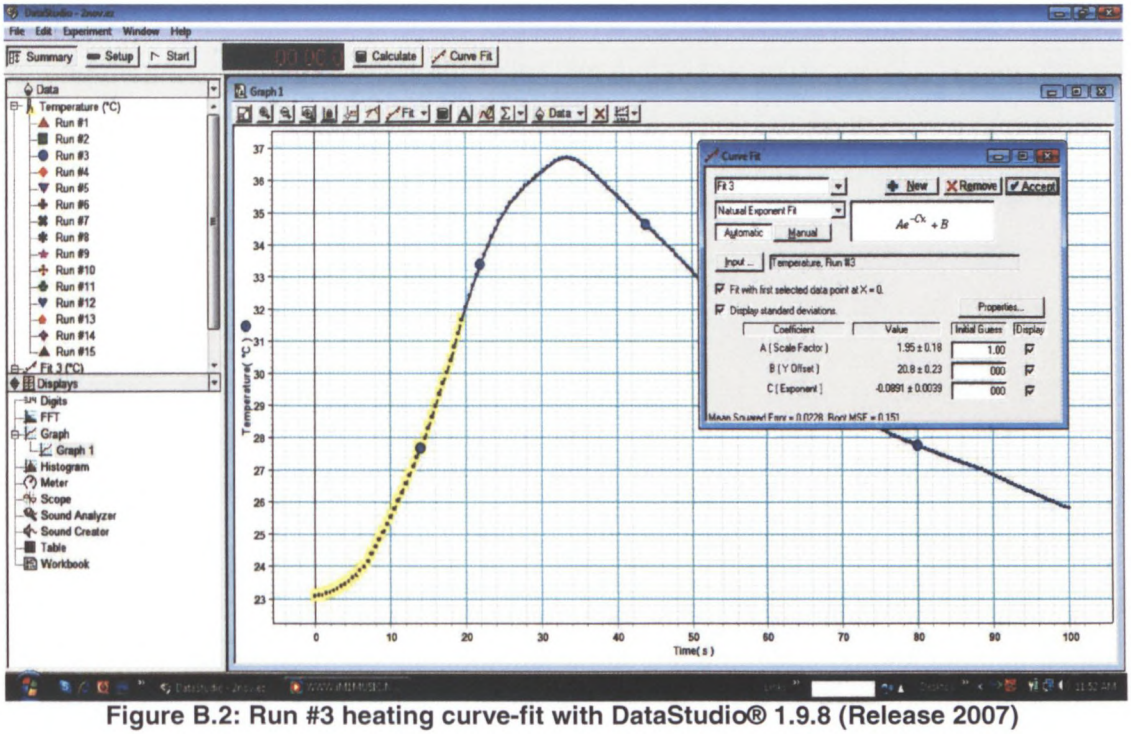

Figure B.2: Run #3 heating curve-fit with DataStudio® 1.9.8 (Release 2007)

Run #4:

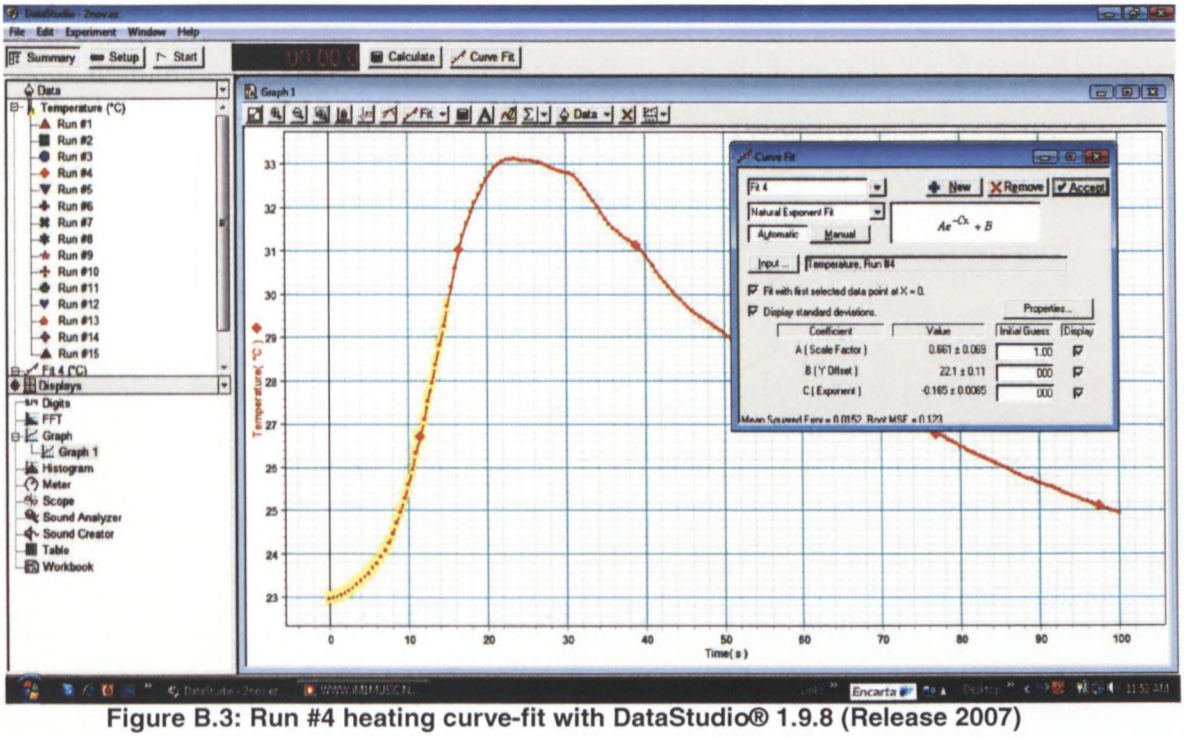

Figure B.3: Run #4 heating curve-fit with DataStudio® 1.9.8 (Release 2007)

Run #5:

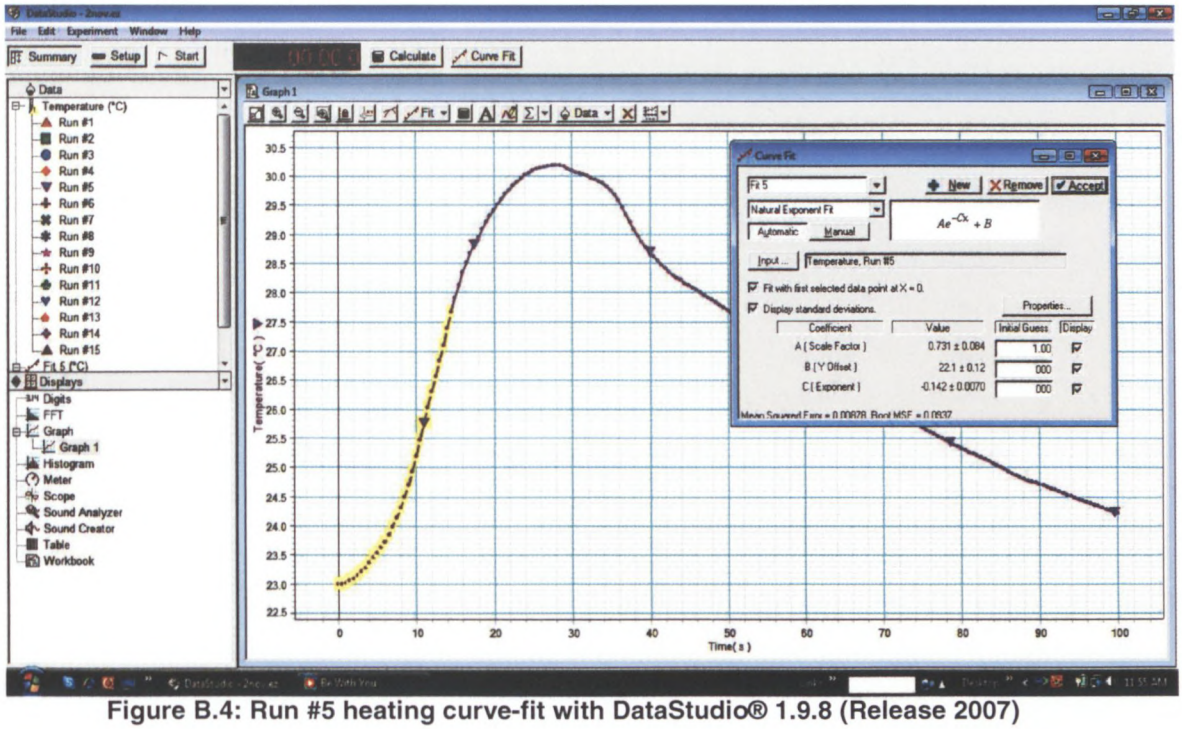

Figure B.4: Run #5 heating curve-fit with DataStudio® 1.9.8 (Release 2007)

Run #6:

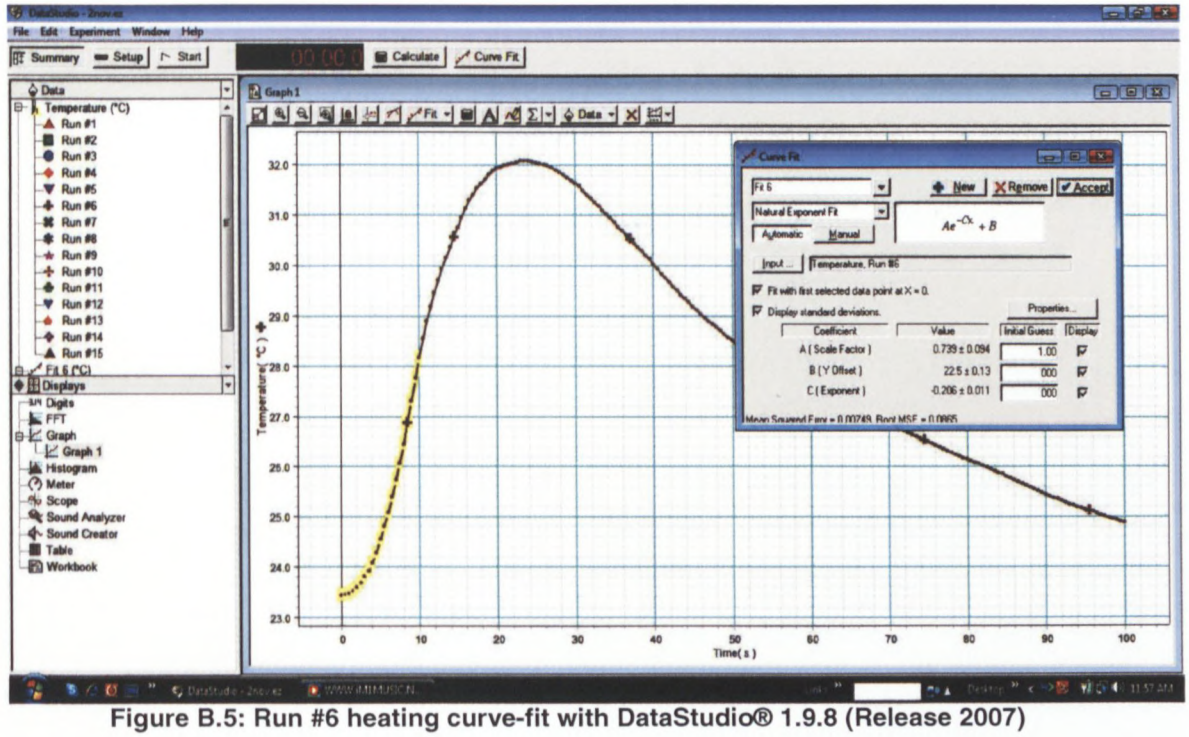

Figure B.5: Run #6 heating curve-fit with DataStudio® 1.9.8 (Release 2007)

Run #7:

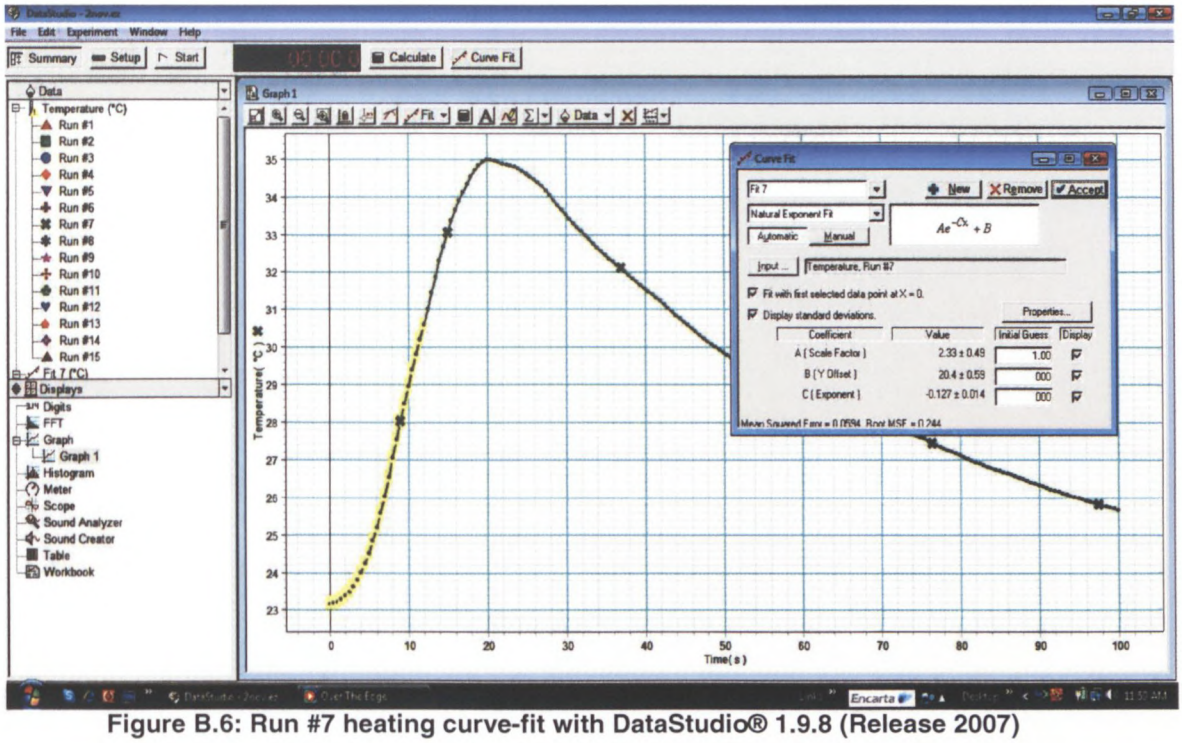

Figure B.6: Run #7 heating curve-fit with DataStudio® 1.9.8 (Release 2007)

Run #8:

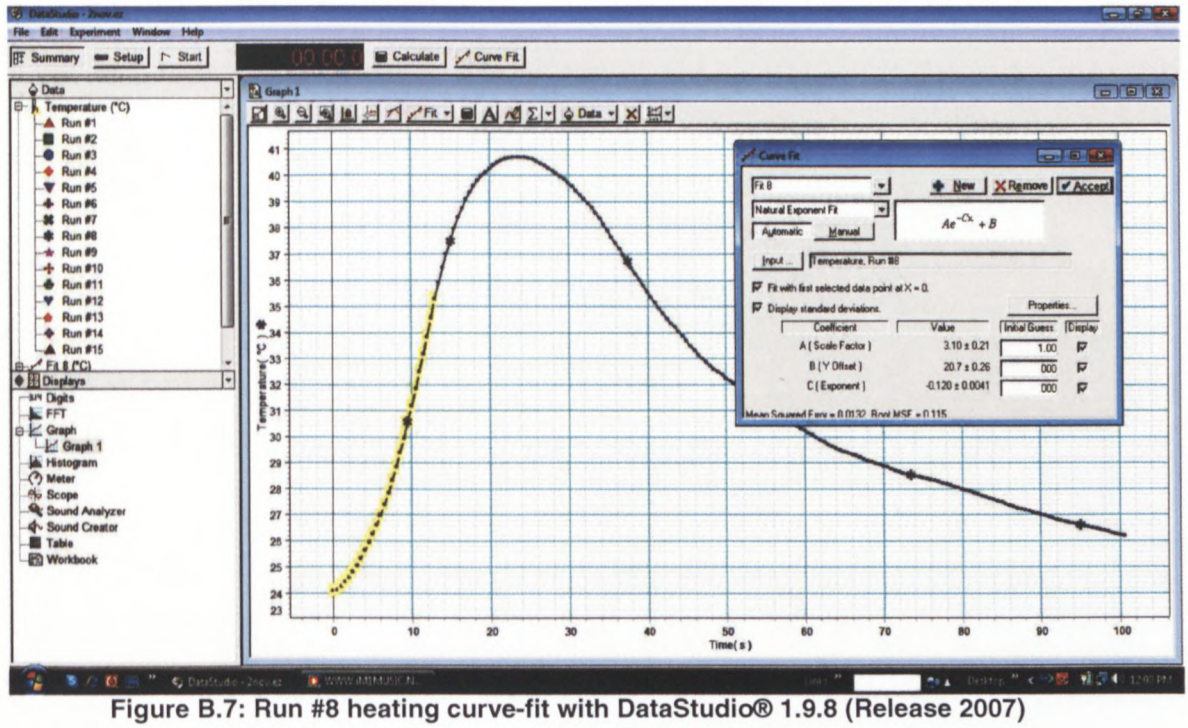

Figure B.7: Run #8 heating curve-fit with DataStudio® 1.9.8 (Release 2007)

Run #9:

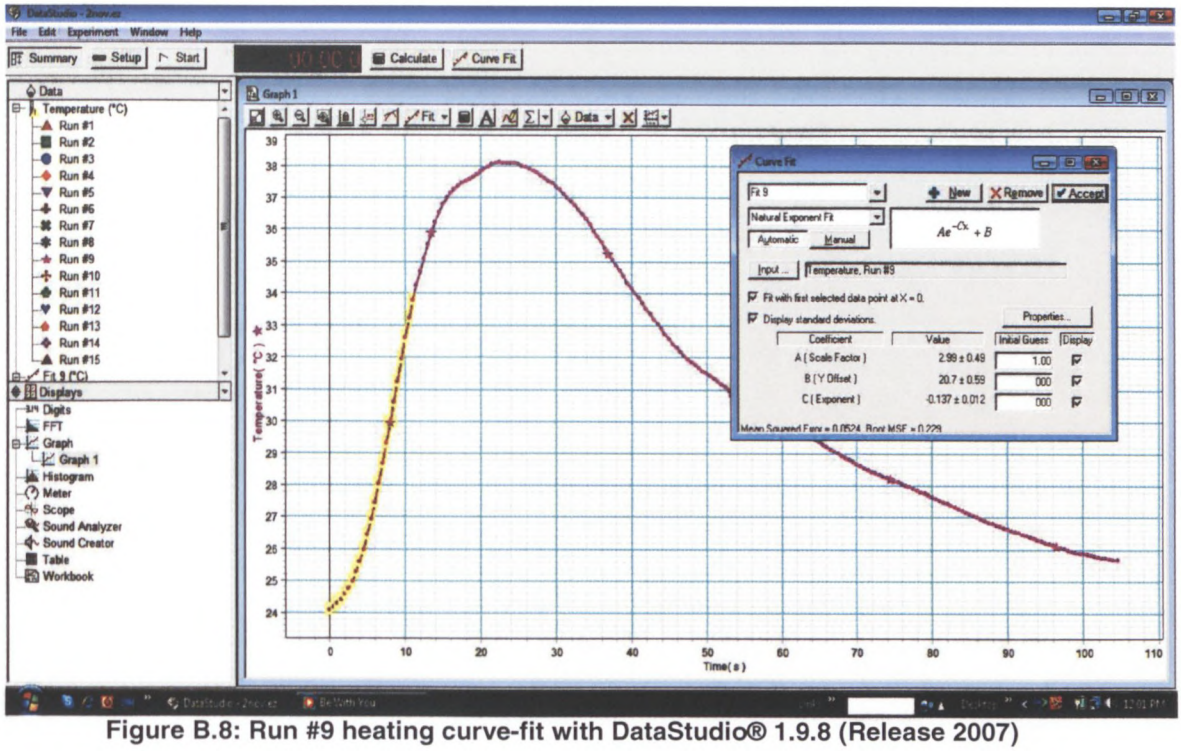

Figure B.8: Run #9 heating curve-fit with DataStudio® 1.9.8 (Release 2007)

Run #10:

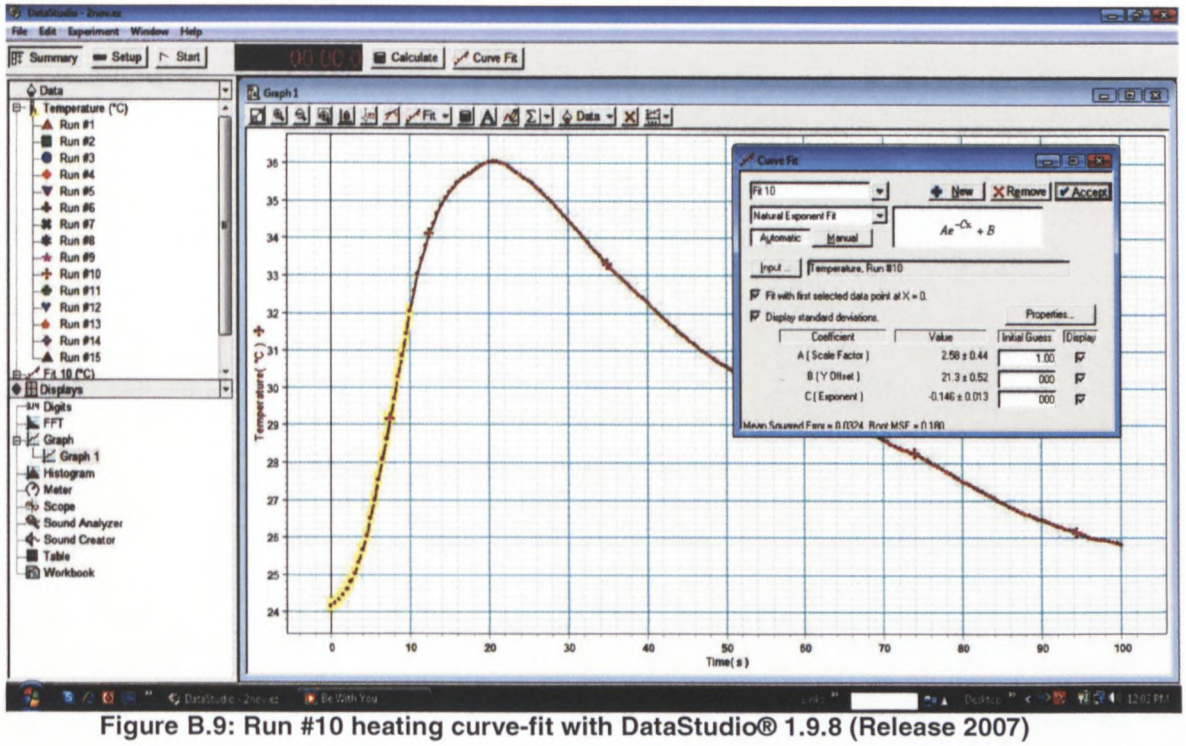

Figure B.9: Run #10 heating curve-fit with DataStudio® 1.9.8 (Release 2007)

Run #11:

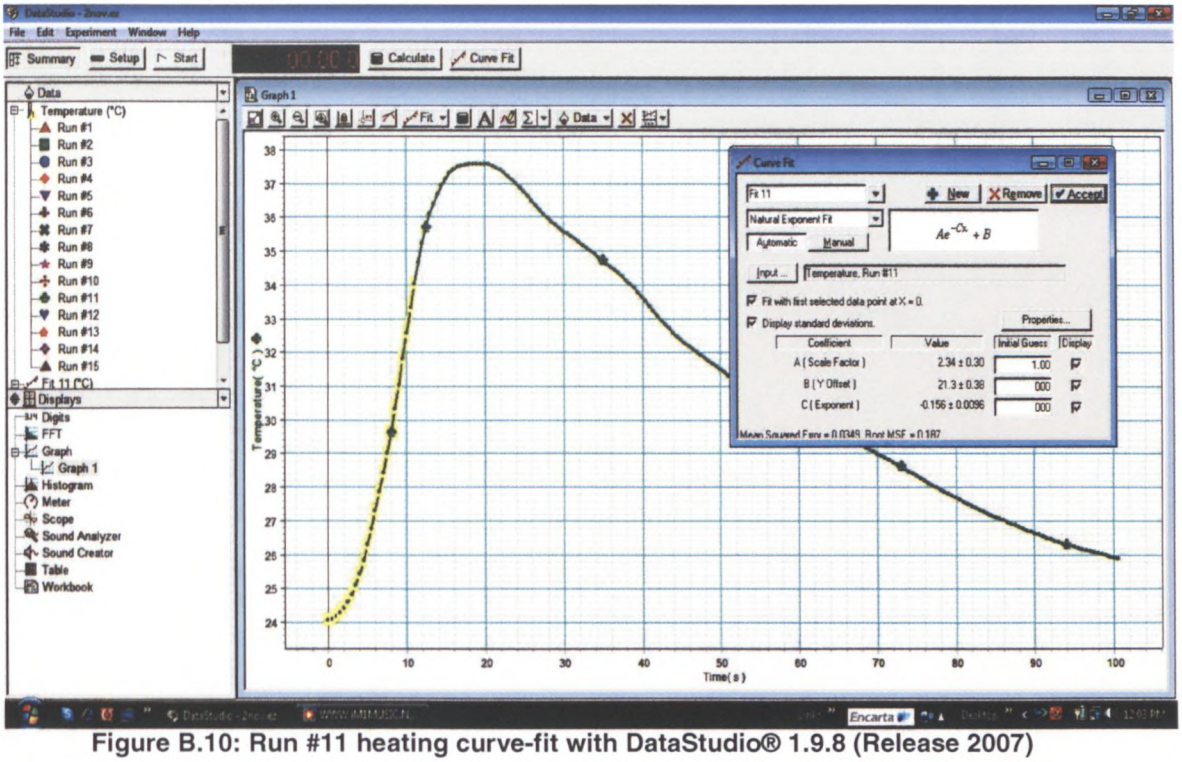

Figure B.10: Run #11 heating curve-fit with DataStudio® 1.9.8 (Release 2007)

Run #12:

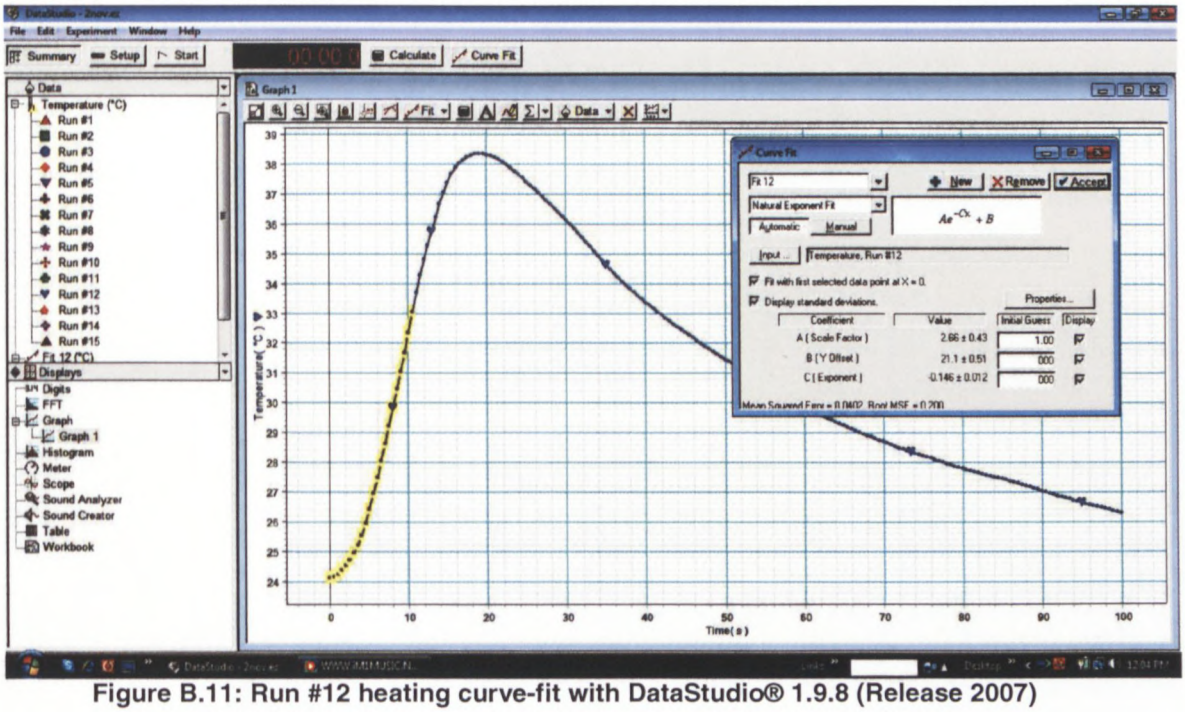

Figure B.11: Run #12 heating curve-fit with DataStudio® 1.9.8 (Release 2007)

Run #13:

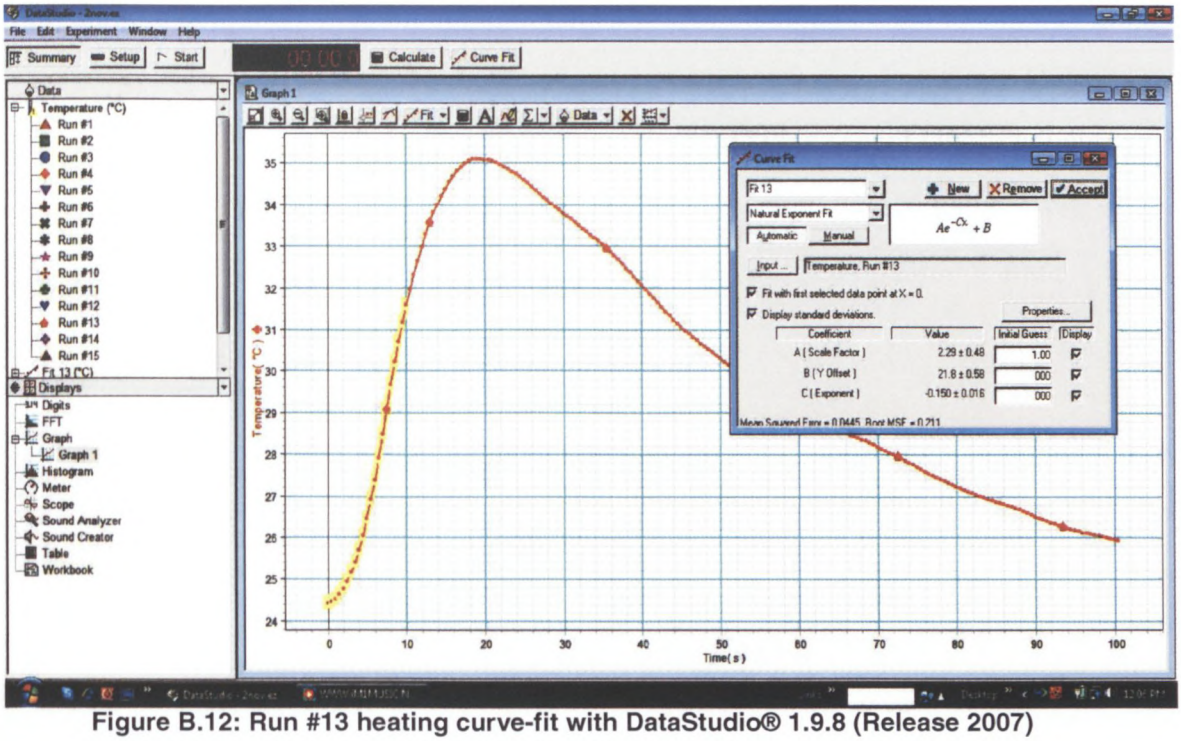

Figure B.12: Run #13 heating curve-fit with DataStudio® 1.9.8 (Release 2007)

Run #14:

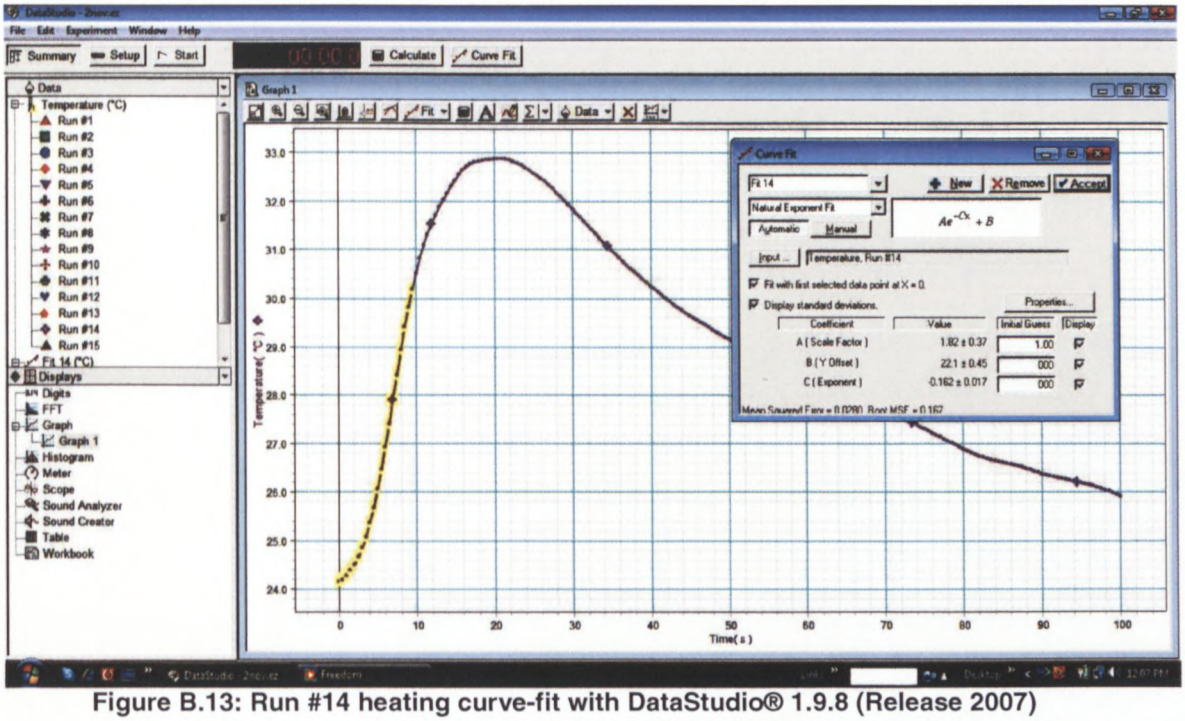

Figure B.13: Run #14 heating curve-fit with DataStudio® 1.9.8 (Release 2007)

Run #15:

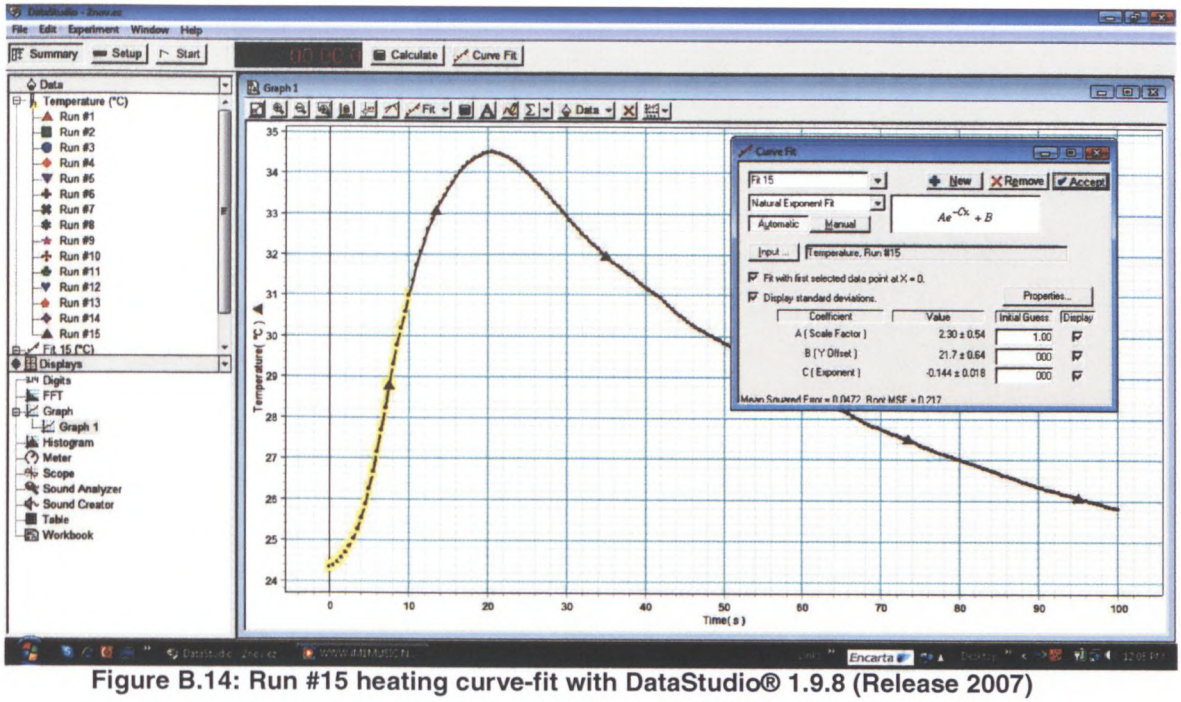

Figure B.14: Run #15 heating curve-fit with DataStudio® 1.9.8 (Release 2007)

2. Cooling parameters

Run #1:

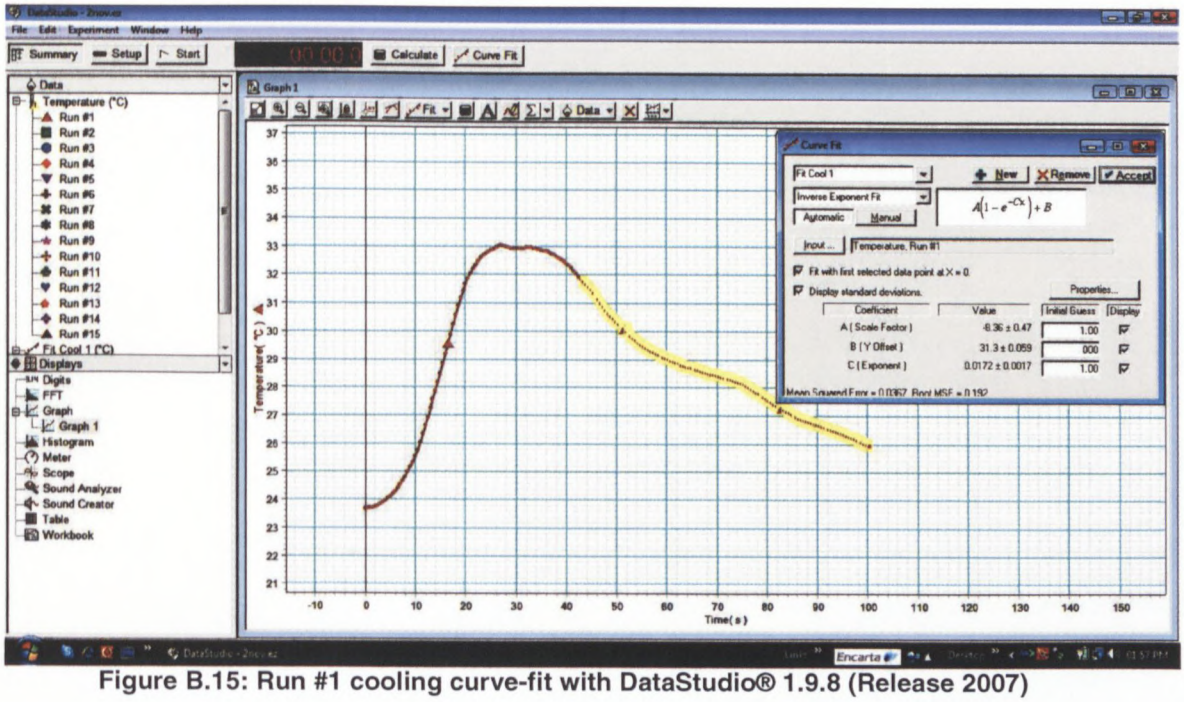

Figure B.15: Run #1 cooling curve-fit with DataStudio® 1.9.8 (Release 2007)

Run #2:

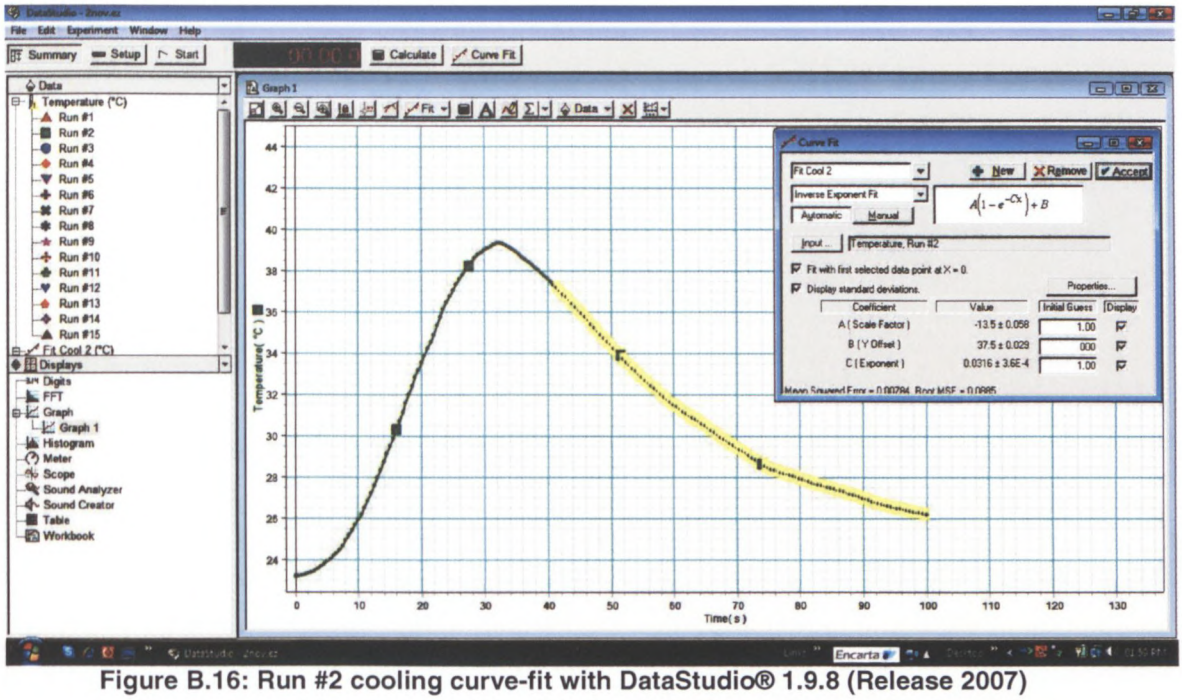

Figure B.16: Run #2 cooling curve-fit with DataStudio® 1.9.8 (Release 2007)

Run #3:

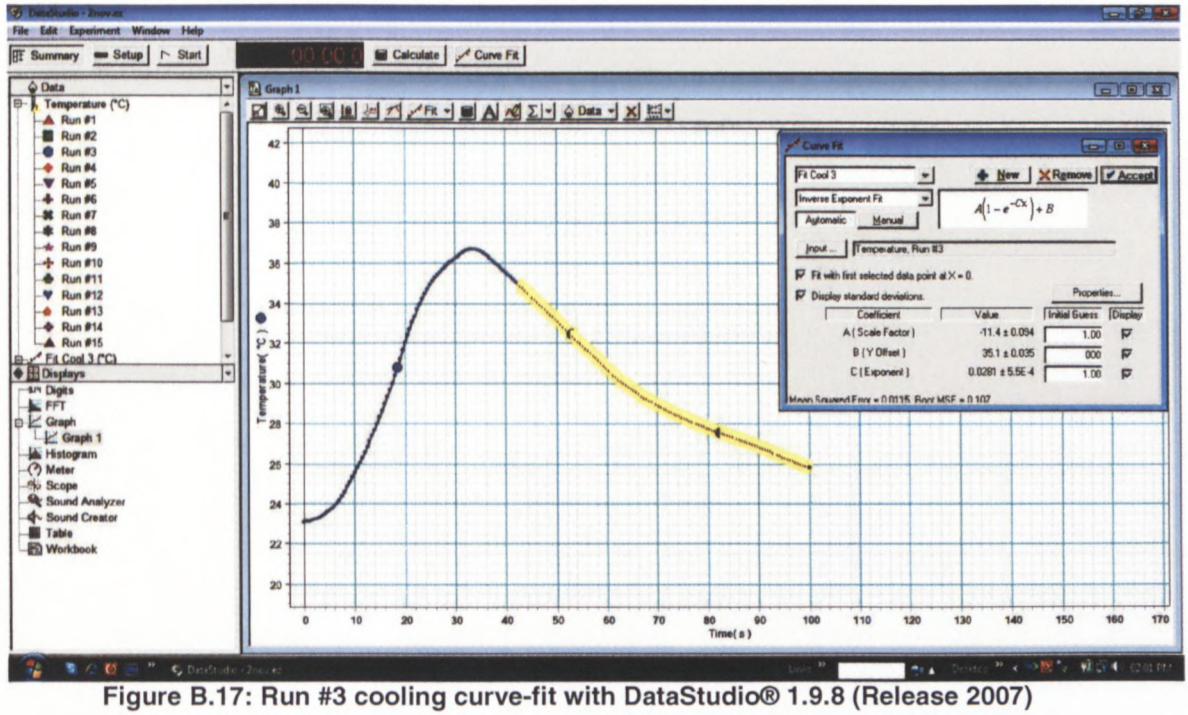

Figure B.17: Run #3 cooling curve-fit with DataStudio® 1.9.8 (Release 2007)

Run #4:

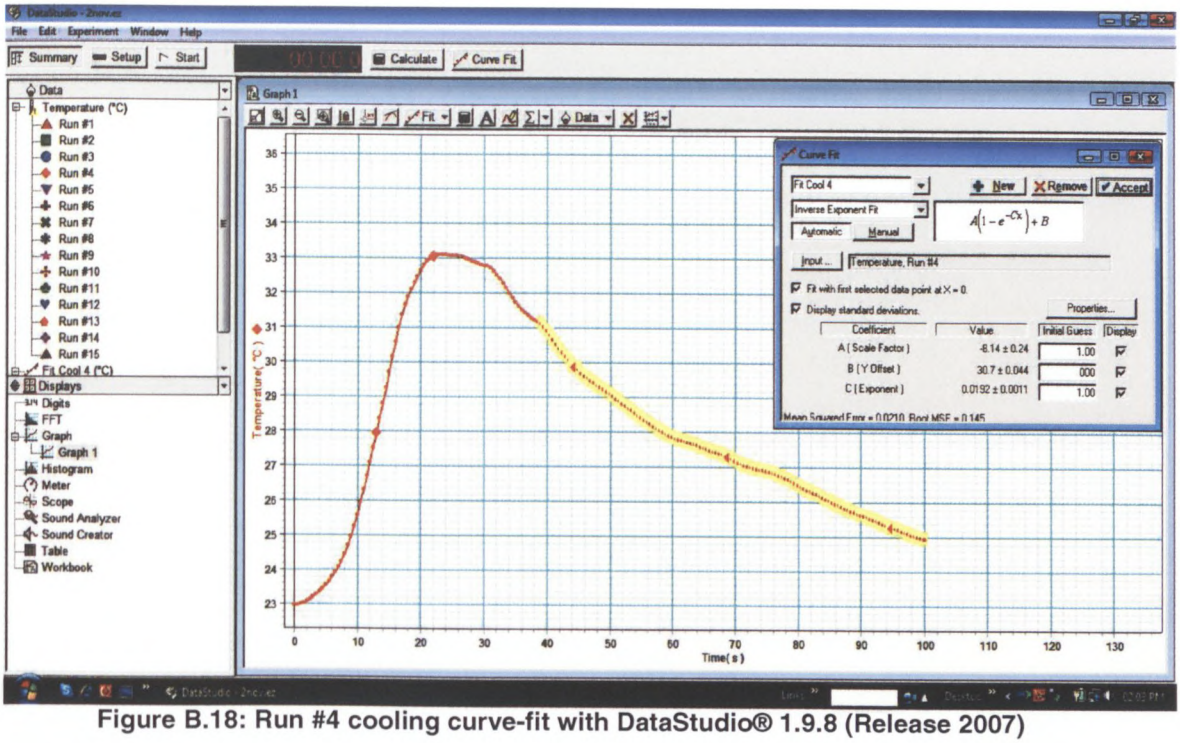

Figure B.18: Run #4 cooling curve-fit with DataStudio® 1.9.8 (Release 2007)

Run #5:

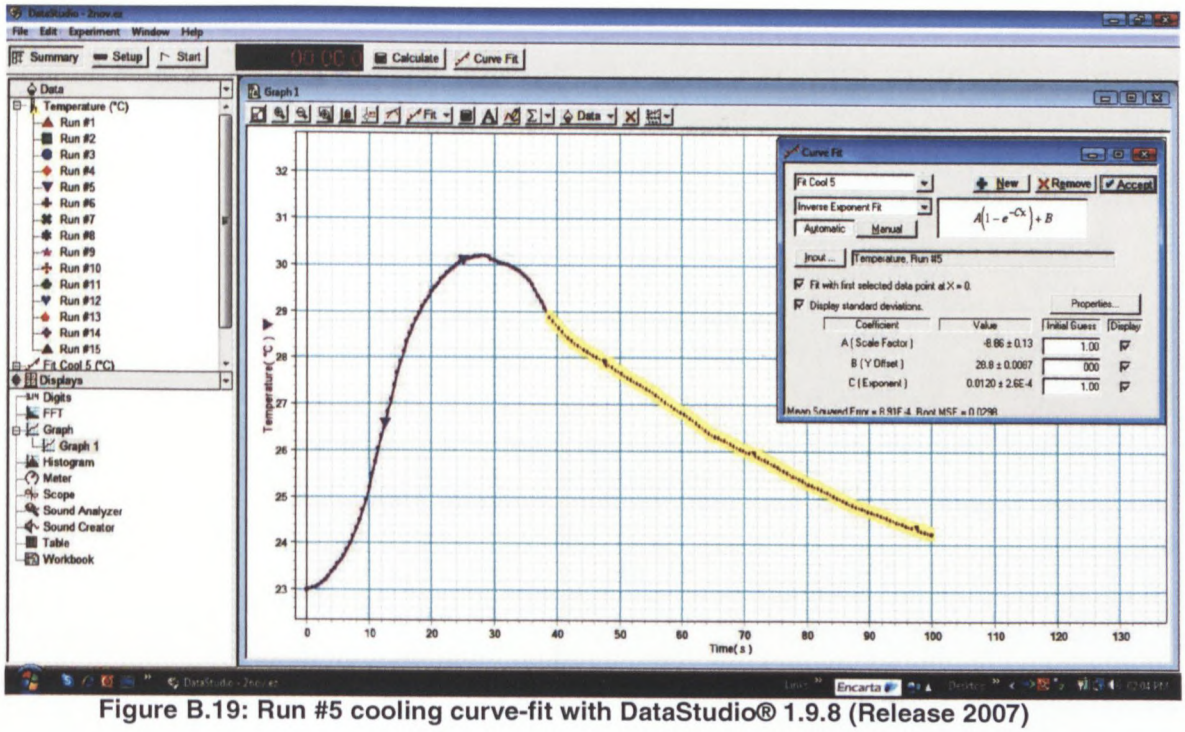

Figure B.19: Run #5 cooling curve-fit with DataStudio® 1.9.8 (Release 2007)

Run #6:

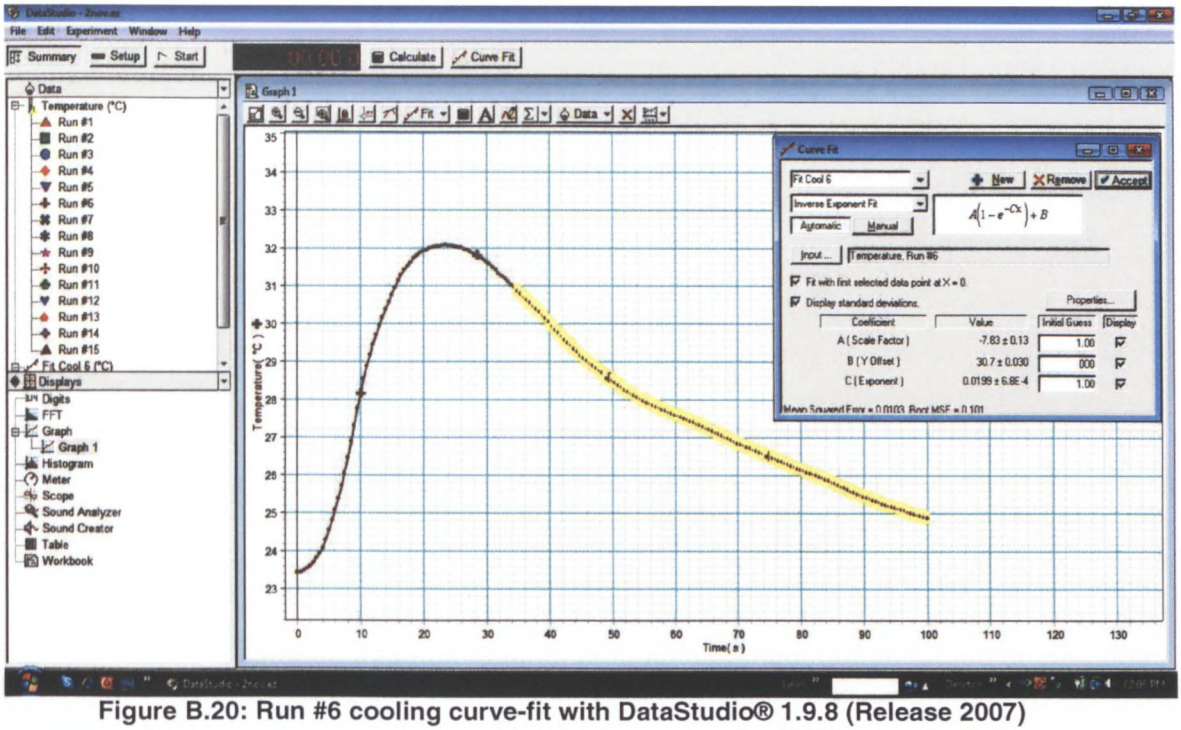

Figure B.20: Run #6 cooling curve-fit with DataStudio® 1.9.8 (Release 2007)

Run #7:

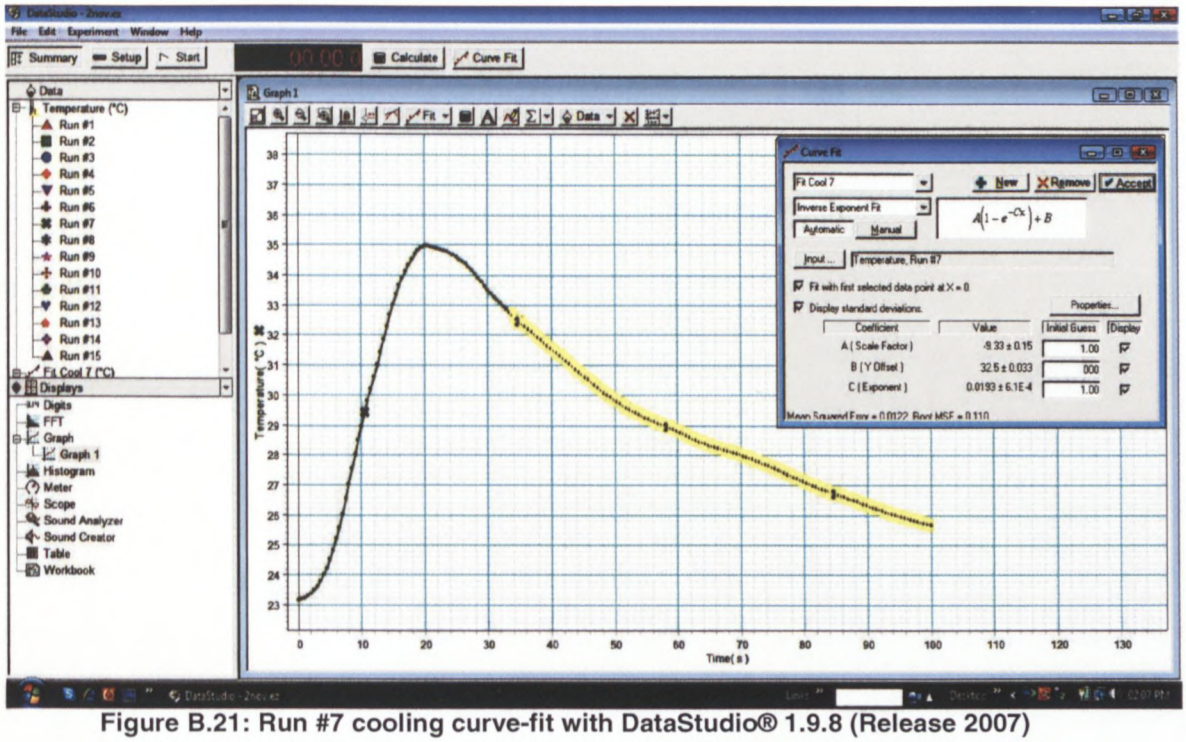

Figure B.21: Run #7 cooling curve-fit with DataStudio® 1.9.8 (Release 2007)

Run #8:

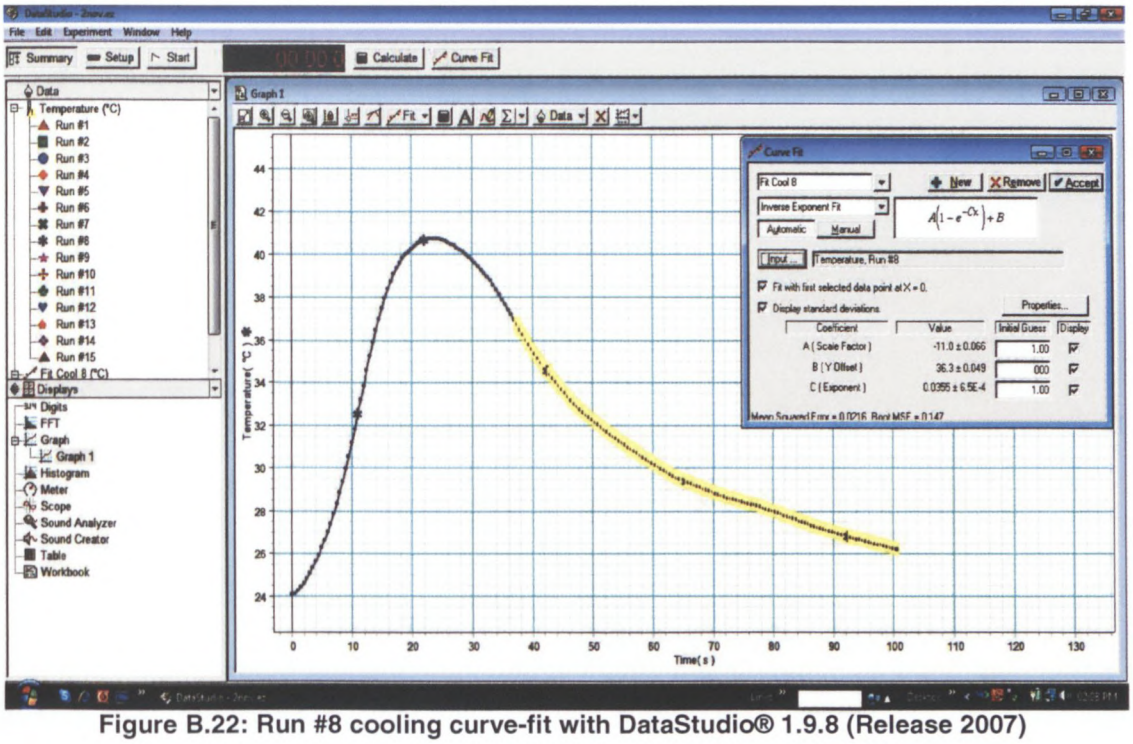

Figure B.22: Run #8 cooling curve-fit with DataStudio® 1.9.8 (Release 2007)

Run #9:

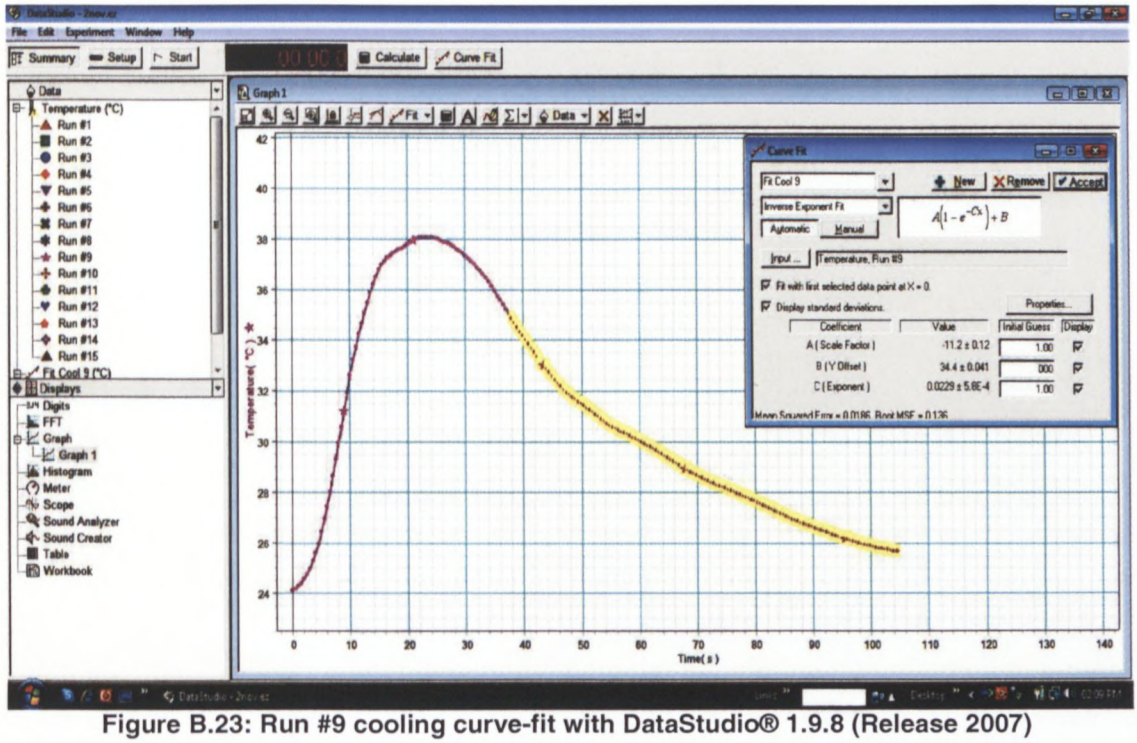

Figure B.23: Run #9 cooling curve-fit with DataStudio® 1.9.8 (Release 2007)

Run #10:

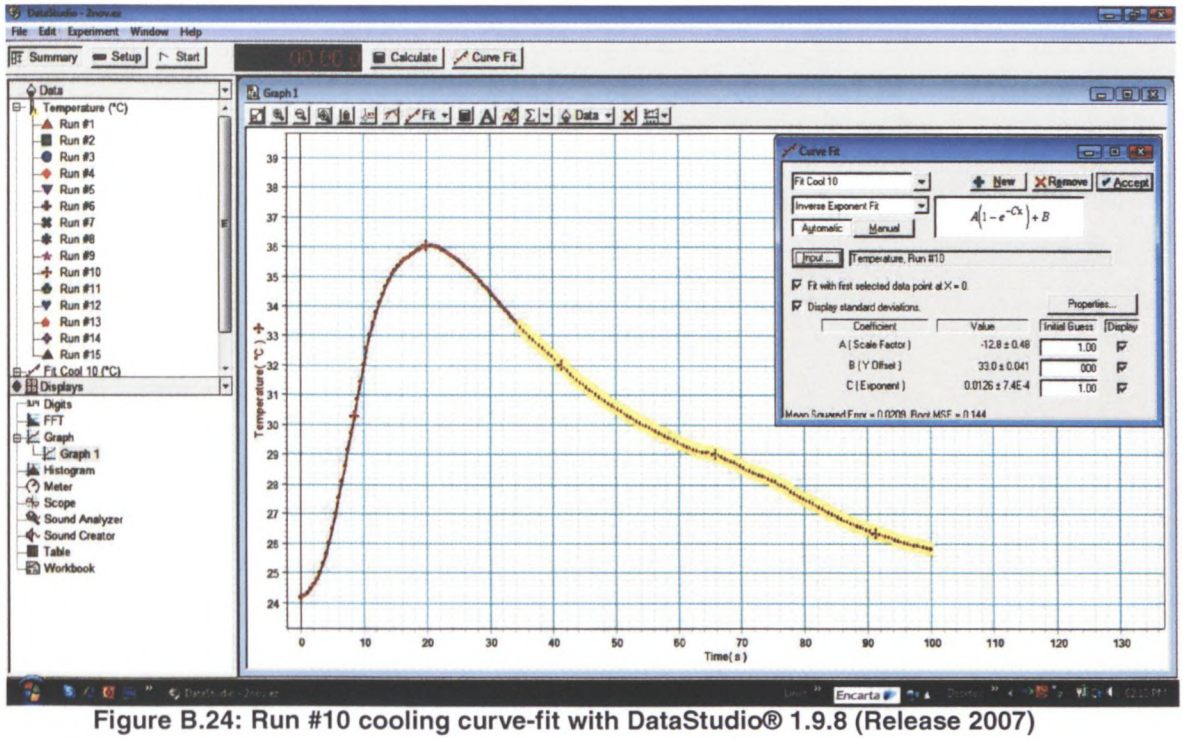

Figure B.24: Run #10 cooling curve-fit with DataStudio® 1.9.8 (Release 2007)

Run #11:

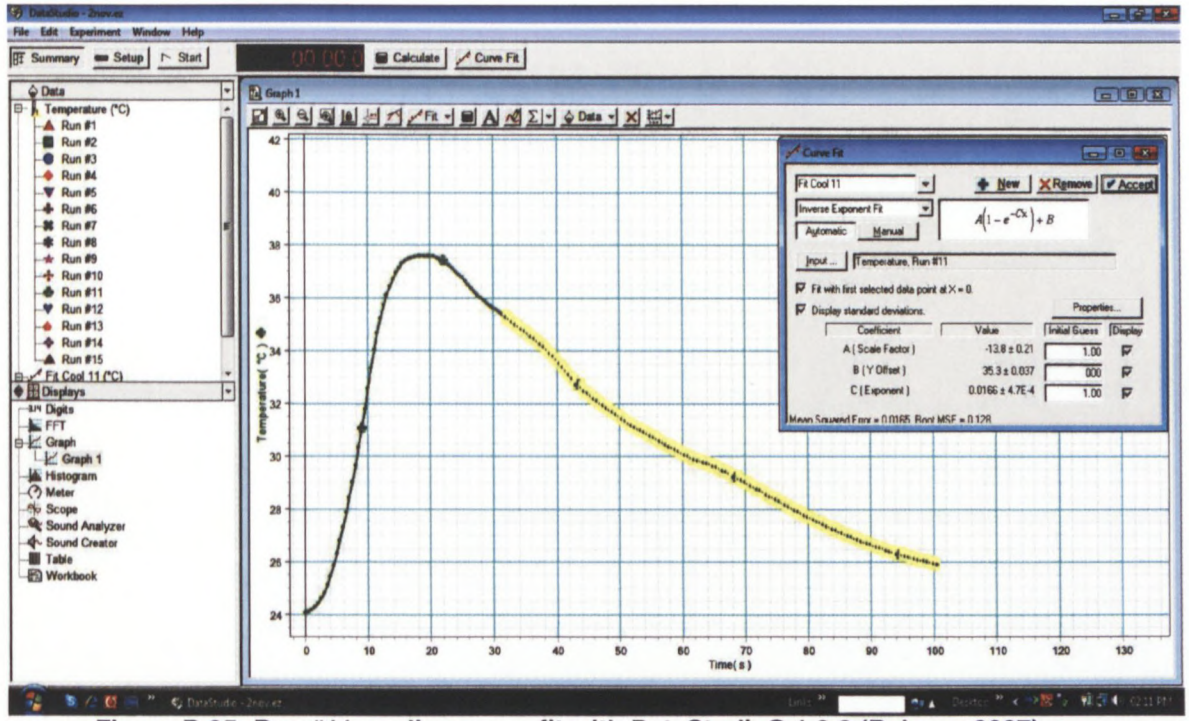

Figure B.25: Run #11 cooling curve-fit with DataStudio® 1.9.8 (Release 2007)

Run #12:

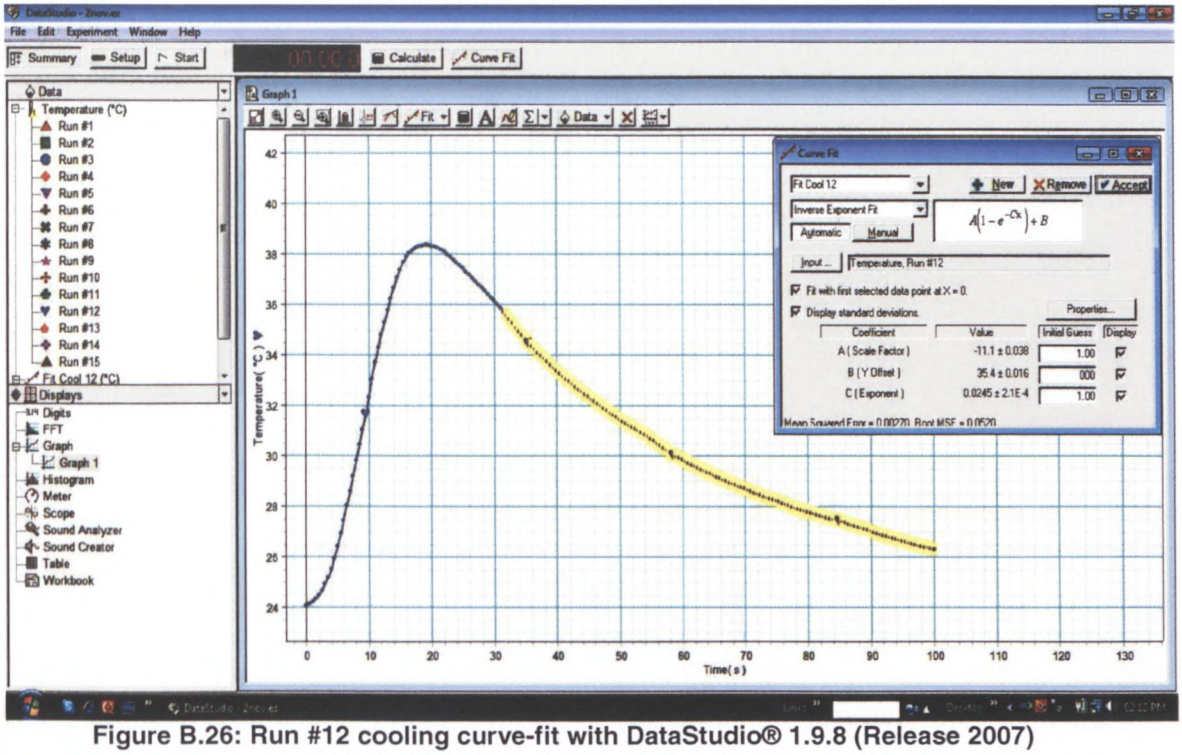

Figure B.26: Run #12 cooling curve-fit with DataStudio® 1.9.8 (Release 2007)

Run #13:

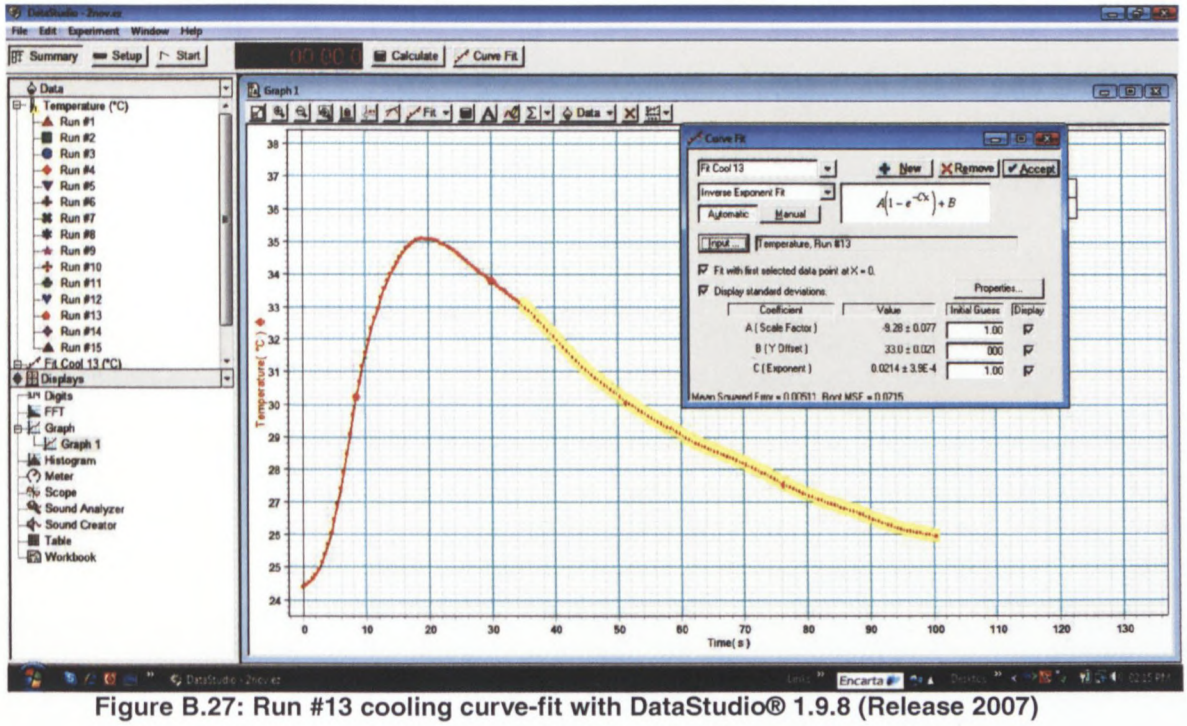

Figure B.27: Run #13 cooling curve-fit with DataStudio® 1.9.8 (Release 2007)

Run #14:

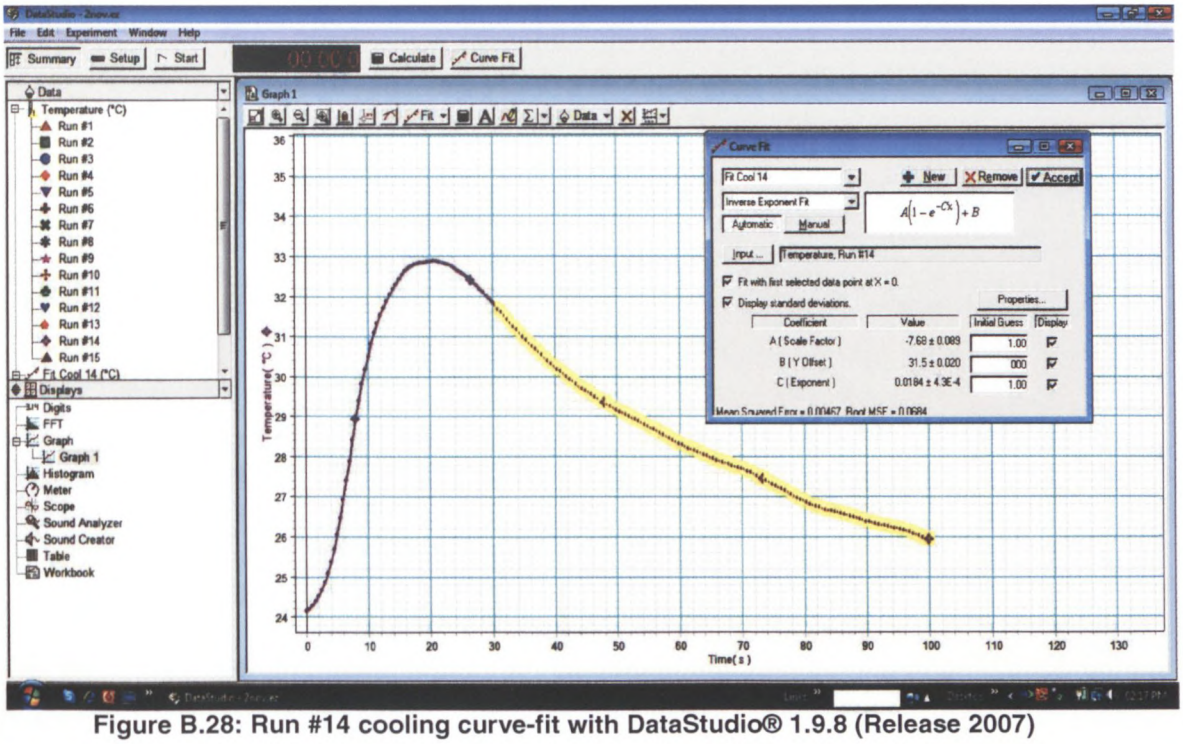

Figure B.28: Run #14 cooling curve-fit with DataStudio® 1.9.8 (Release 2007)

Run #15:

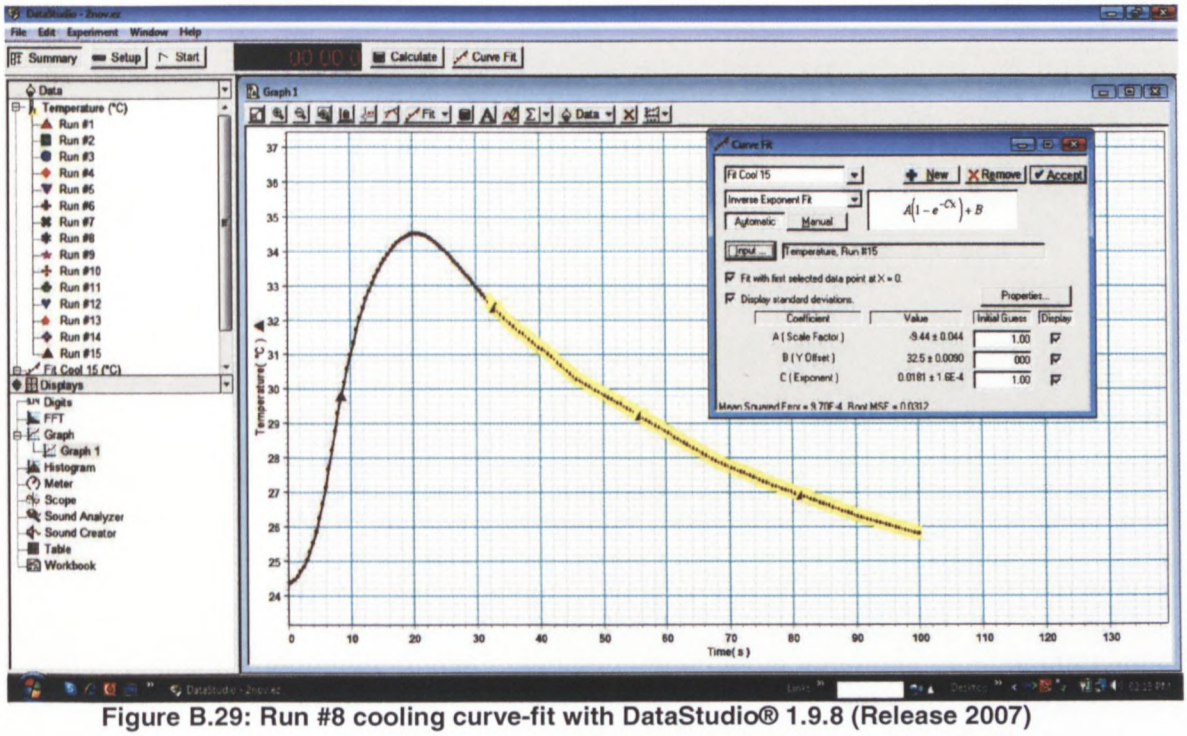

Figure B.29: Run #8 cooling curve-fit with DataStudio® 1.9.8 (Release 2007)